

# **Investigations on the phase II metabolism of propranolol and hydroxypropranolols**

**Inaugural-Dissertation  
to obtain the academic degree  
Doctor rerum naturalium (Dr. rer. nat.)**

**submitted to the Department of Biology, Chemistry, Pharmacy  
of Freie Universität Berlin**

**by  
Fan Yang  
2023**

Research of the present study was conducted from 2018 until 2023 under the supervision of Prof. Dr. Maria Kristina Parr at the Institute of Pharmacy of the Freie Universität Berlin in collaboration with Prof. Dr. Matthias Bureik at Tianjin University, China.

1<sup>st</sup> Reviewer: Prof. Dr. Maria Kristina Parr

2<sup>nd</sup> Reviewer: Prof. Dr. Matthias Bureik

Date of defense: 07.12.2023

I hereby declare that this dissertation was written and prepared by me independently. Furthermore, no sources and aids other than those indicated have been used. Intellectual property of other authors has been marked accordingly. I also declare that I have not submitted the dissertation in this or any other form to any other institution as a dissertation.

# ACKNOWLEDGEMENT

First of all, I would like to thank Prof. Dr. Maria Kristina Parr for giving me this invaluable opportunity to work in her lab, and for the captivating topics, the stimulating research environment and her consistently exceptional guidance.

A special thank to Prof. Dr. Matthias Bureik, whose mentorship not only ignited my scientific journey during my master's studies but also continued to be an unwavering source of support and inspiration throughout my doctoral pursuit.

I would like to thank Sijie Liu and Prof. Dr. Gerhard Wolber for the *in silico* data, and thank to Dr. Sangeeta Shrestha Sharma for providing the diploid yeast strains and related qPCR data, thank to them for the wonderful collaboration, which significantly enhanced the depth and breadth of this work.

I would like to thank Maxi Wenzel for the skillfully conducting the chemical synthesis of the substrates pivotal to the experiments outlined in this thesis.

I would like to thank Yanan and Lingyu for the accompany during the last few years. May the comradeship last forever!

I would like to thank Qi, those happy time we spent together discussing and sharing our favorite things really lifted me up during tough times, even though we are thousands miles apart.

I would like to thank all my friends, whether near or far, in Berlin or China, for your encouragement and putting up with my occasionally stressful ramblings on social media.

Last but not least, my deepest gratitude is reserved for my parents. Without their love, support and understanding, this achievement would not have been possible.



# Table of content

<b>1</b>	<b>INTRODUCTION</b> .....	<b>1</b>
<b>1.1</b>	<b>Human drug metabolizing enzymes (DMEs)</b> .....	<b>1</b>
1.1.1	DMEs in preclinical drug development .....	1
1.1.2	Human CYPs.....	2
1.1.3	Human UGTs .....	5
1.1.4	Protein-protein interactions between CYPs and UGTs .....	8
1.1.5	Conjugation of alternate UDP-sugars.....	10
<b>1.2</b>	<b>Methods involved in preclinical studies</b> .....	<b>11</b>
1.2.1	<i>In vitro</i> and <i>in vivo</i> studies on metabolism.....	11
1.2.2	Recombinant human CYPs and UGTs in <i>Schizosaccharomyces pombe</i> .....	13
1.2.3	Analytical techniques used in drug metabolism studies .....	15
<b>1.3</b>	<b>Propranolol and hydroxypropranolols</b> .....	<b>16</b>
1.3.1	The versatile role of propranolol .....	16
1.3.2	Phase I and phase II metabolism of propranolol and hydroxypropranolols....	16
<b>2</b>	<b>AIM OF THE PROJECT</b> .....	<b>19</b>
<b>3</b>	<b>MATERIALS AND METHODS</b> .....	<b>20</b>
<b>3.1</b>	<b>Materials</b> .....	<b>20</b>
<b>3.2</b>	<b>Methods</b> .....	<b>21</b>
3.2.1	Yeast strains, preparation, and long-time storage of enzyme bags .....	21
3.2.2	Biotransformation with enzyme bags .....	24
3.2.3	<i>In vitro</i> metabolism with HLMS .....	24
3.2.4	Urine sample collection .....	25
3.2.5	Synthesis of 4-, 5- and 7-methoxypropranolol.....	25
3.2.6	Derivatization with 1,2-dimethylimidazole-4-sulfonyl chloride (DMISC) .....	26
3.2.7	Analytical methods .....	27
3.2.7.1	GC-EI-MS analysis.....	27
3.2.7.2	LC-QQQ-MS/MS analysis .....	27
3.2.7.3	LC-QTOF-MS/MS analysis .....	29
<b>4</b>	<b>RESULTS AND DISCUSSION</b> .....	<b>31</b>

<b>4.1</b>	<b>Stereoselective glucuronidation of racemic propranolol</b> .....	<b>31</b>
4.1.1	Biotransformation of propranolol with 19 UGTs.....	31
4.1.2	Discussion .....	33
<b>4.2</b>	<b>Glucuronidation of hydroxypropranolols</b> .....	<b>34</b>
4.2.1	Identification 4-, 5- and 7-OHPG .....	34
4.2.2	Biotransformation of 4-, 5- and 7-OHP with 19 UGTs .....	36
4.2.3	Discussion .....	38
<b>4.3</b>	<b>Regioselectivity of hydroxypropranolols glucuronidation</b> .....	<b>39</b>
4.3.1	Pre-glucuronidation derivatization .....	39
4.3.1.1	Discussion .....	42
4.3.2	Post-glucuronidation derivatization.....	43
4.3.2.1	DMISC derivatives of propranolol and hydroxypropranolols .....	43
4.3.2.2	DMISC derivatives of hydroxypropranolol glucuronides.....	48
4.3.2.3	Discussion .....	50
<b>4.4</b>	<b>Glucosidation of propranolol and hydroxypropranolols</b> .....	<b>52</b>
4.4.1	<i>In vitro</i> metabolism with HLMs.....	52
4.4.2	Glucosidation of propranolol with four human UGTs .....	53
4.4.3	Discussion .....	55
<b>4.5</b>	<b>Mutual modulations of CYP2D6 and four UGTs on the metabolism of propranolol</b> .....	<b>56</b>
4.5.1	Optimization for biotransformation protocol .....	56
4.5.1.1	Liquid-liquid extraction with ethyl acetate .....	56
4.5.1.2	Long-time storage for enzyme bags .....	57
4.5.1.3	Optimization of the CYP reaction time for diploid yeast .....	58
4.5.2	Influence of UGT1A7,UGT1A8,UGT1A9 and UGT2A1 on CYP2D6 .....	60
4.5.3	Influence of CYP2D6 on four UGTs.....	62
4.5.4	Discussion .....	63
<b>5</b>	<b>SUMMARY AND OUTLOOK</b> .....	<b>67</b>
<b>6</b>	<b>ZUSAMMENFASSUNG</b> .....	<b>69</b>
<b>7</b>	<b>CV</b> .....	<b>72</b>
<b>8</b>	<b>REFERENCES</b> .....	<b>73</b>

<b>9</b>	<b>LIST OF FIGURES</b> .....	<b>89</b>
<b>9.1</b>	<b>List of figures in main text</b> .....	<b>89</b>
<b>9.2</b>	<b>List of supplementary figures</b> .....	<b>92</b>
<b>10</b>	<b>LIST OF TABLES</b> .....	<b>94</b>
<b>10.1</b>	<b>List of tables in main text</b> .....	<b>94</b>
<b>10.2</b>	<b>List of supplementary tables</b> .....	<b>94</b>
<b>11</b>	<b>APPENDIX</b> .....	<b>95</b>
<b>11.1</b>	<b>Supplementary figures</b> .....	<b>95</b>
<b>11.2</b>	<b>Supplementary tables</b> .....	<b>103</b>



# I ABBREVIATIONS

4-/5-/7-MeOP	4-/5-/7-Methoxypropranolol
4-/5-/7-MeOPG	4-/5-/7-Methoxypropranolol glucuronide
4-/5-/7-OHP	4-/5-/7-Hydroxypropranolol
4-/5-/7-OHPG	4-/5-/7-Hydroxypropranolol glucuronide
AAF	Adverse analytical finding
ADMET	Absorption, distribution, metabolism, excretion and toxicity
APCI	Atmospheric pressure chemical ionization
COMTs	Catechol O-methyltransferases
CYPs	Cytochrome P450
CPR	Cytochrome P450 oxidoreductase
DDIs	Drug-drug interactions
DIP	<i>N</i> -Desisopropylpropranolol
DMEs	Drug metabolising enzymes
DMISC	1,2-Dimethylimidazole-4-sulfonyl chloride
EI	Electron ionization
EMM	Edinburgh minimal medium
ESI	Electrospray ionization
FAD	Flavin adenine dinucleotide
FMN	Flavin mononucleotide
GC	Gas chromatography
GSTs	Glutathione S-transferases
HLMs	Human liver microsomes
LC	Liquid chromatography
MRM	Multiple reaction monitoring
MS	Mass spectrometry
MS/MS	Tandem mass spectrometry
MSTFA	<i>N</i> -Methyl- <i>N</i> -(trimethylsilyl)trifluoroacetamide

NADPH	Nicotinamide adenine dinucleotide phosphate
NATs	<i>N</i> -Acetyltransferases
NASIDs	Nonsteroidal anti-inflammatory drugs
NLA	Naphthoxylacetic acid
PG	Propranolol glucuronide
ppm	Parts per million
QQQ	Triple quadrupole
QTOF	Quadrupole time-of-flight
qPCR	Quantitative polymerase chain reaction
SER	Smooth endoplasmic reticulum
SFC	Supercritical fluid chromatography
S <sub>N</sub> 2	Type 2 nucleophilic substitution
SULTs	Sulfotransferases
TPMTs	Thiopurine <i>S</i> -methyltransferases
UDP	Uridine diphosphate
UDPGA	Uridine diphosphate glucuronic acid
UGDH	UDP-glucose 6-dehydrogenase
UGT	Uridine 5'-diphospho-glucuronosyltransferase
WADA	World anti-doping agency

# 1 Introduction

## 1.1 Human drug metabolizing enzymes (DMEs)

### 1.1.1 DMEs in preclinical drug development

ADMET properties are critical factors that must be taken into account during the early stages of drug development. These properties are absorption, distribution, metabolism, excretion and toxicity, all of which can impact a drug's efficacy and safety profile [1]. Therefore, it is crucial to thoroughly evaluate and optimize these properties in order to increase the possibility of success in the later stages of development and eventual market approval. Absorption is the process by which a drug enters the body and it includes several routes such as oral administration, inhalation, or injection. Distribution pertains to how the drug is distributed throughout the body, including regional blood flow rates and tissue penetration. Metabolism is the enzymatic modification of drugs by DMEs, which play a central role in determining the drug's efficacy and safety. Excretion refers to the elimination of drugs and their metabolites from the body through routes such as urine, feces, or breath. Finally, the potential for a drug to cause adverse effects on the body, known as toxicity, can be influenced by factors such as the dose, duration of exposure, and individual variability [2].

Drug metabolism is a crucial process in which the parent compound undergoes chemical modifications leading to the production of metabolites. These metabolites are generally more water-soluble and can be eliminated from the body via urine [3]. The drug metabolism process is normally divided into two stages, phase I and phase II. Phase I metabolism mainly involves oxidation, reduction, and hydrolysis reactions of the drugs or other xenobiotics, while phase II metabolism includes conjugative reactions such as glucuronidation, sulfation, and methylation [4]. Phase I metabolism is considered the preparatory stage for phase II metabolism as it introduces or unmask functional groups that can be utilized in phase II reactions. However, it is important to note that phase I and phase II metabolism should not be viewed as two necessarily sequential stages, as many drugs directly undergo phase II metabolism because they already possess functional groups [5].

DMEs are the core of the entire metabolic process. The most well-known and important enzymes of phase I metabolism are the cytochrome P450s (CYPs), which catalyze several reaction types, including oxidations, hydroxylations, and dealkylations [6]. In addition to CYPs, other phase I enzymes also play a role in the clearance of many drugs, such as alcohol dehydrogenases, monoamine oxidases, molybdenum hydroxylases, and flavin-containing monooxygenases [7]. The most common phase II

enzymes are uridine 5'-diphospho-glucuronosyltransferase (UGTs), sulfotransferases (SULTs), glutathione S-transferases (GSTs), thiopurine S-methyltransferases (TPMTs), *N*-acetyltransferases (NATs) and catechol *O*-methyltransferases (COMTs) [8]. UGTs, in particular, are responsible for catalyzing the transfer of sugar moieties from the cofactor to the functional group of parent compounds [9]. In humans, CYPs and UGTs are predominantly found in the liver and gut and are responsible for the clearance of over 90% of drugs, making the liver and gut the major metabolism organs [10].

### 1.1.2 Human CYPs

CYPs are a large superfamily of monooxygenases containing heme as a cofactor, they play a key role in the metabolism of drugs, xenobiotics, and endogenous compounds in humans and other organisms [6]. They were first found in the 1950s when researchers were attempting to identify the specific enzymes responsible for oxidizing lipophilic xenobiotics in mammalian cells [11, 12]. These membrane-bound heme-containing proteins are named for their characteristic absorption maximum at 450 nm when reduced and bound to carbon monoxide [13, 14].

As of present, more than 780 CYP families have been discovered, but only 18 of these have been found in humans [15]. Within these 18 families, 44 subfamilies have been identified (as by definition its members have a sequence homology of at least 55%) [16]. In total, 57 human P450s have been discovered, and although some have been extensively studied, there are still some P450s whose functions remain unknown [17].

Notably, only a quarter of all human CYPs are involved in phase I metabolism of xenobiotics, with many of them belonging to CYP1, 2, and 3 families [18]. Besides, it was observed that CYP21 is involved in the metabolism of certain xenobiotic compound, such as metandienone [19]. Many of the remaining CYPs are associated with the biosynthesis and metabolism of steroid hormones, bile acids, and other endogenous compounds [20]. The physiological functions and regulation of certain CYPs are poorly understood, leading to their classification as "orphan" CYPs. CYPs are widely distributed across various tissues, with the most abundant expression of CYPs related to xenobiotic metabolism observed in the liver (Figure 1). Certain hepatic CYPs are more abundantly expressed than others, which is illustrated for adult Caucasians in Figure 1 [21].

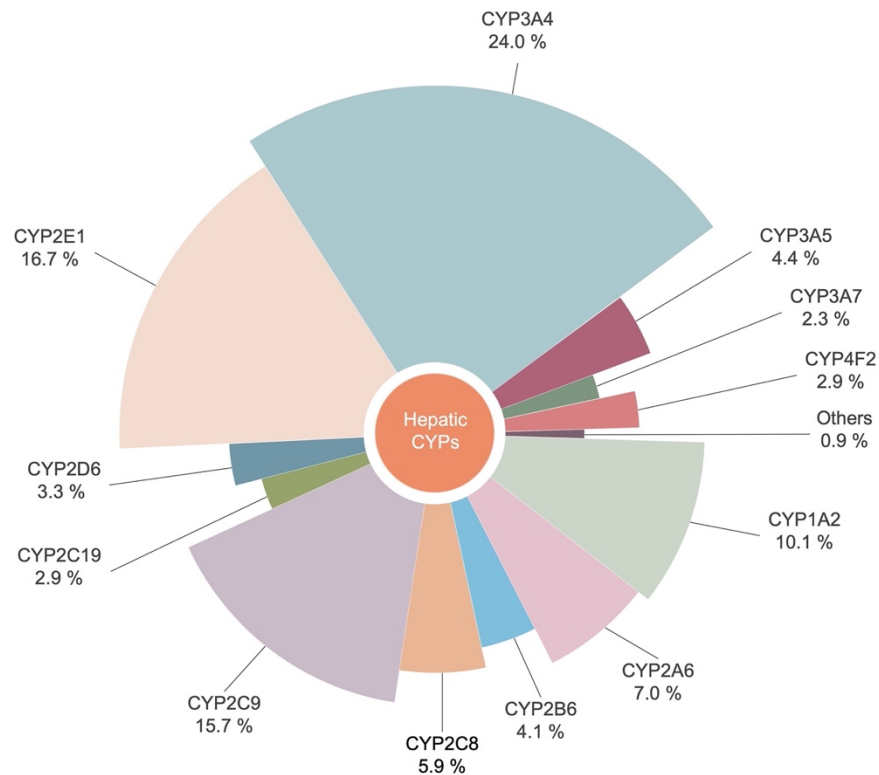


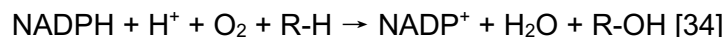
Figure 1. Pie chart of weighted mean abundances of CYPs in livers of adult caucasians, adapted from [21]. Others (0.9 %) include CYP3A43 (0.5 %), CYP2J2 (0.3 %) and CYP2C18 (0.1 %).

CYP3A4 is the most abundantly expressed hepatic isoform and is, therefore, considered the major biotransformation CYP isoform [21]. Its primary endogenous function is to metabolize steroids, making it essential in the homeostasis of bile acids and several steroids, including testosterone, progesterone, androstenedione, and cortisol [22]. Due to the flexible nature of its active site, this enzyme can also metabolize a wide range of lipophilic compounds with different structures [23, 24]. The CYP2 family is the most abundant group of hepatic expressed CYPs (Figure 1), with several extrahepatic enzymes and "orphan" P450s also found in this family whose functions are not yet well understood [25]. CYP2C9 is an extensively-studied isoform of CYP2 family, which also has a large number of substrates, including tolbutamide, dapsone, warfarin, and most nonsteroidal anti-inflammatory drugs (NSAIDs) [15].

CYP2D6 is notable among human CYPs as it is considered to be a non-inducible isoform [26-28] and is the only protein-coding gene of the CYP2D subfamily [16,17]. CYP2D6 is also the main example for the metabolic effects of genetic polymorphisms in CYPs, with 5 to 10% of caucasians having poor or even no CYP2D6 enzymatic activity [18]. Despite its relatively low expression in the liver, CYP2D6 is responsible for metabolizing almost 15% of all therapeutic clinical drugs, including antiarrhythmics, antidepressants, antipsychotics, analgesics, and beta-blockers [29, 30]. CYP2D6 is

also the main isoform responsible for the hydroxylation of propranolol [31], a beta-blocker which is the core research object of this thesis.

Although CYPs can metabolize so many substrates with different structures, the mechanism of their enzymatic function remains conserved. The heme group in CYP enzymes consists of a central iron ion that is coordinated by a porphyrin ring system and a distal histidine residue in the protein [32]. The iron ion within the heme group has the ability to bind and activate molecular oxygen, which is a crucial step in oxidation reactions [33]. The following equation represents the basic oxidative function of CYPs:



In this reaction, nicotinamide adenine dinucleotide phosphate (NADPH) is the cofactor, while R-H is any oxidizable substrate and R-OH is the oxidized metabolite.

The catalytic cycle of CYPs (Figure 2) involves several steps, including substrate and oxygen binding, reduction of the heme iron (from  $\text{Fe}^{3+}$  to  $\text{Fe}^{2+}$ ), splitting and transfer of oxygen molecules, rearrangement of products, and ultimately release of the product [35]. Human CYPs cannot bind to NADPH for reduction and thus rely on electron transfer proteins like cytochrome P450 reductase (CPR) to act as their reduction-oxidation partner [36]. CPR is a flavoprotein that contains the prosthetic groups FAD and FMN [37]. The two electrons are transferred from NADPH via FAD to FMN and finally to the CYP enzyme itself [34]. The second electron transfer step is thought to be the rate-limiting step, determining the speed of CYP catalytic reactions [34, 35]. Cytochrome *b5* may occasionally serve as an electron supplier to enhance the catalytic efficiency of CYPs [34, 38, 39].

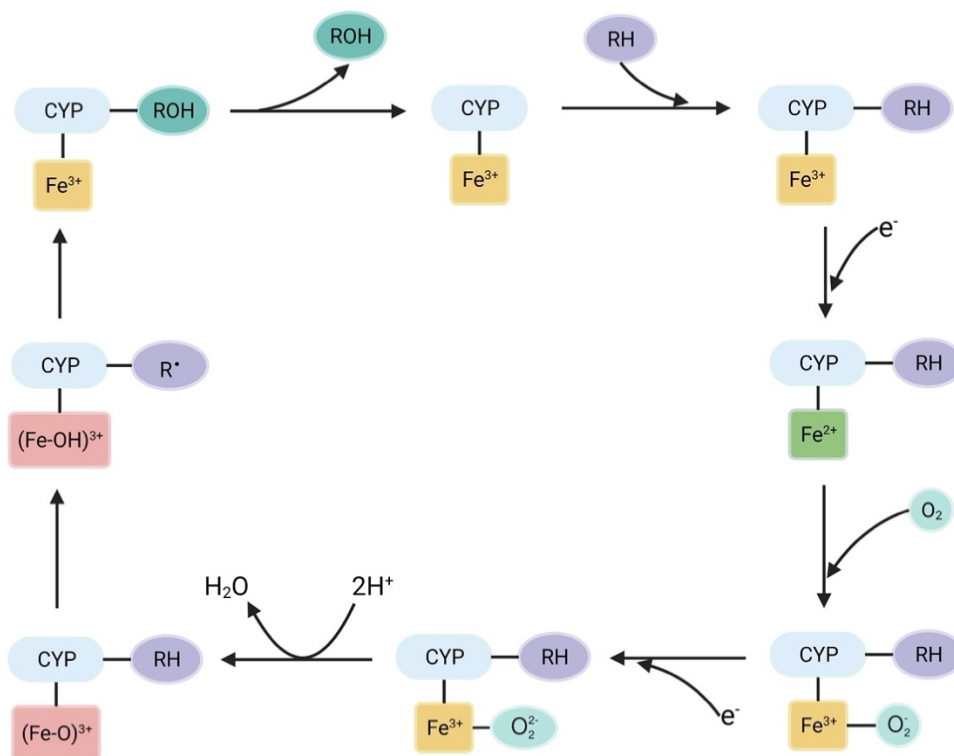


Figure 2. Simplified scheme of the catalytic cycle of CYPs, adapted from [35].

### 1.1.3 Human UGTs

UGTs are a superfamily of enzymes involved in phase II metabolism that catalyze the glucuronidation of various substrates. Like CYPs, UGTs exhibit a wide range of substrate selectivity and can metabolize many different endogenous compounds, environmental chemicals, and pharmaceutical drugs [40]. UGT enzymes, together with CYPs, play a significant role in the metabolism and elimination of drugs from the body. In fact, UGTs are responsible for deactivating nearly 55% of the 200 most prescribed drugs currently on the market [41-43], while UGTs and CYPs together metabolize and eliminate almost 90% of drugs [10]. Therefore, UGT enzymes have a special impact on the metabolism of drugs and their bioavailability. After being excreted into bile, conjugated drugs RH may be hydrolyzed by bacterial  $\beta$ -glucuronidases in the gut. The resulting deconjugated drugs can then be reabsorbed into the bloodstream, leading to a secondary rise in plasma drug levels. This process, known as enterohepatic recirculation, may lead to increased bioavailability but also gut toxicity in certain drugs [44].

Glucuronidation involves the transfer of a sugar moiety from uridine 5'-diphosphoglucuronic acid (UDPGA) to a functional moiety such as carbonyl, carboxy, sulfury, hydroxy, and amine groups [42]. UDPGA is formed from UDP-glucose by the

enzyme UDP-glucose 6-dehydrogenase (UGDH). UGTs catalyze this conjugation via type 2 nucleophilic substitution ( $S_N2$ ), resulting in the formation of  $\beta$ -D-glucuronides [45, 46] (Figure 3). The resulting  $\beta$ -D-glucuronide conjugates are generally more polar and more water-soluble than their aglycon counterparts, which facilitates their excretion from the body.

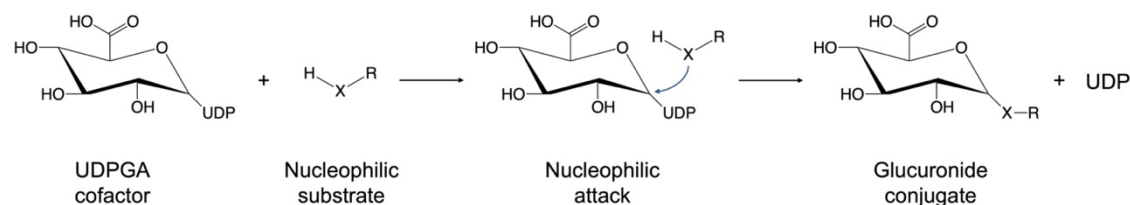


Figure 3. Scheme of glucuronidation reaction, adapted from [42]. UDPGA, uridine 5'-diphosphoglucuronic acid; X could be O, S, N or C for different functional groups.

There are 22 human UGT isoenzymes divided into four families (UGT1, UGT2, UGT3 and UGT8, Figure 4) [10]. The UGT2 family is further subdivided into two subfamilies, UGT2A and UGT2B [47]. UGT1A and UGT2B were found to be responsible for almost all the detoxification and metabolism of endogenous compounds and xenobiotic drugs. According to quantitative polymerase chain reaction (qPCR) analysis of UGT mRNA levels [42], members of UGT1A and UGT2B families were found highly expressed in human liver, which is the main organ for metabolism. However, in the intestine, UGT1A1 and UGT2B7 are expressed at similar levels to liver and it is noteworthy that a few UGT1A isoforms (UGT1A5, 1A7, 1A8, 1A10) are highly expressed in the intestine but are not detected in the liver, which may contribute to the first-pass effect and low oral bioavailability of some drugs [48, 49].

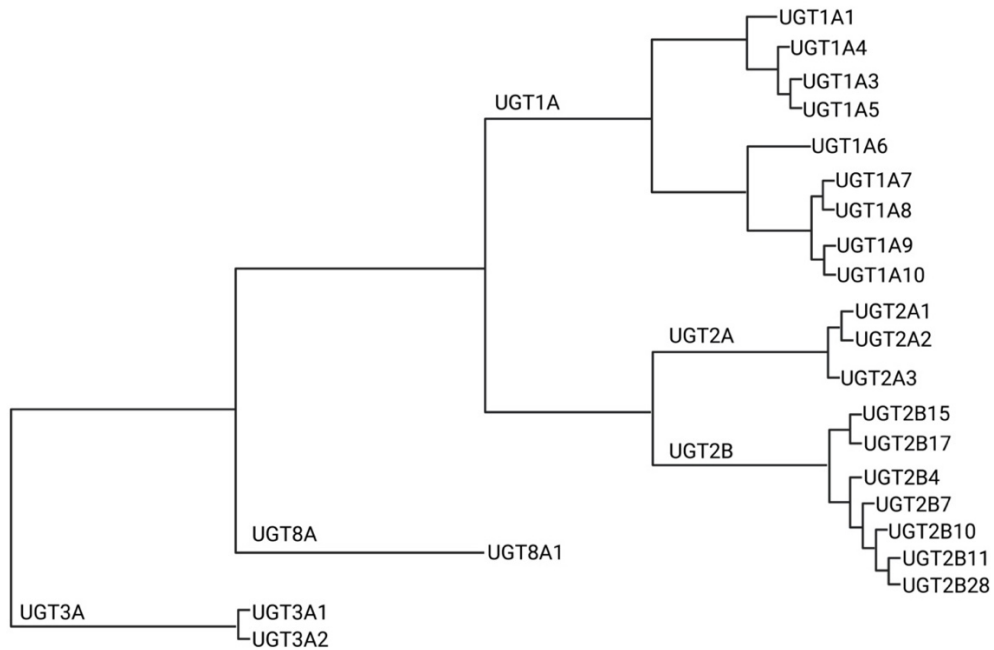


Figure 4. Phylogenetic tree of human UGT isoforms, adapted from [10].

Many UGT1As are highly expressed in the liver but some are exclusively encountered in extrahepatic tissues, namely UGT1A7, UGT1A8, and UGT1A10 [42]. The members of the UGT1A family are well recognized to conjugate many xenobiotics and are also involved in the metabolism of several endogenous compounds, such as bilirubin, bile acids, serotonin, and steroid hormones [50]. For example, UGT1A1 is considered to be the major isoform in the glucuronidation of bilirubin which facilitates its elimination through urine and bile [51]. Impaired bilirubin metabolism due to deficient UGT1A1 activity can lead to bilirubin accumulation in the blood and brain, causing jaundice, hyperbilirubinemia, Crigler-Najjar syndrome [52], Gilbert syndrome [53], and potentially fatal outcomes [54, 55].

The UGT2B family is also known to be a significant factor in determining how an individual responds to various xenobiotics and in the metabolism of commonly prescribed drugs. UGT2B7, being the most abundant isoform expressed in the liver (followed by UGT2B4, UGT2B15, and UGT2B17), is responsible for nearly 25% of the clearance of commonly used medications [56, 57]. In combination with other UGT2B isoforms, UGT2B7 is capable of metabolizing a diverse range of drugs, such as zidovudine, morphine, tamoxifen, lorazepam, and NSAIDs [41, 58]. In addition, UGT2B7, UGT2B15, UGT2B17 and UGT2B28 also play a critical role in the inactivation of sex steroids, and disruptions to these pathways have been implicated in various endocrine-related diseases [59].

UGT2A enzymes are expressed in the nasal epithelium and are involved in the metabolism of certain volatile organic compounds that contribute to the perception of odorants [60, 61]. UGT2A1 is preferentially and highly expressed in the olfactory epithelium, making the most active olfactory UGT for the metabolism of odorants [62].

UGT3A1 has been reported to use UDP-*N*-acetylglucosamine to conjugate various substrates, including bile acids, steroids, and bioflavones [63], while UGT3A2 prefers to use UDPGA, UGP-glucose and UDP-xylose as a cofactor for glucuronidation [64, 65]. These findings suggest that the UGT3 family is not involved in the elimination of exogenous chemicals, but rather in endogenous metabolism, such as maintaining the homeostasis of bilirubin. UGT8A1 is a UDP-galactose ceramide galactosyltransferase that uses UDP-galactose as the sugar donor and is also unlikely to contribute significantly to drug metabolism [66].

#### 1.1.4 Protein-protein interactions between CYPs and UGTs

CYPs and UGTs are localized in the membrane of smooth endoplasmic reticulum (SER) [67, 68]. The active site of CYP faces the cytosol with its *N*-terminus anchored in the SER membrane [67]. The redox partners (CPR and cytochrome *b5*) are believed to be positioned nearby, ensuring the supply of electrons for the oxidation reaction [37, 69]. In contrast, the active site of UGTs is situated inside the lumen of the SER membrane, and the C-terminus is linked to an anchor protein that crosses the membrane [46, 70]. Although CYPs and UGTs have been thought to work separately due to differences in their membrane topologies (Figure 5), a growing number of studies suggest that there is a functional interaction between them. Research in this field began around two decades ago when it was observed that rat CYP1A1 co-eluted with rat UGTs during affinity chromatography [71]. Further studies showed that the glucuronidation of 3-hydroxy-benzo(*a*)pyrene by a rat UGT was inhibited by a CYP1A inhibitor, which required intact microsomal membranes [72]. Immunoprecipitation experiments confirmed the interaction of human CYP3A4 with human UGT1A1, UGT1A6, and UGT2B7 [73]. In another example, co-expression of CYP3A4 and UGT2B7 in COS-1 cells resulted in a nearly tenfold increase in the  $K_m$  value for the glucuronidation of morphine compared to single-expressed UGT2B7 [74]. Further studies revealed that the J-helix of CYP3A4 contributes to its interaction with UGT2B7 [75]. CYP3A4 was also found to enhance the activity of UGT1A1 and UGT1A7 for the glucuronidation of the irinotecan metabolite SN-38 [76]. However, the activity of CYP3A4 was suppressed when UGT1A9 or UGT2B7 were co-expressed in a baculovirus-insect cell system [77, 78].

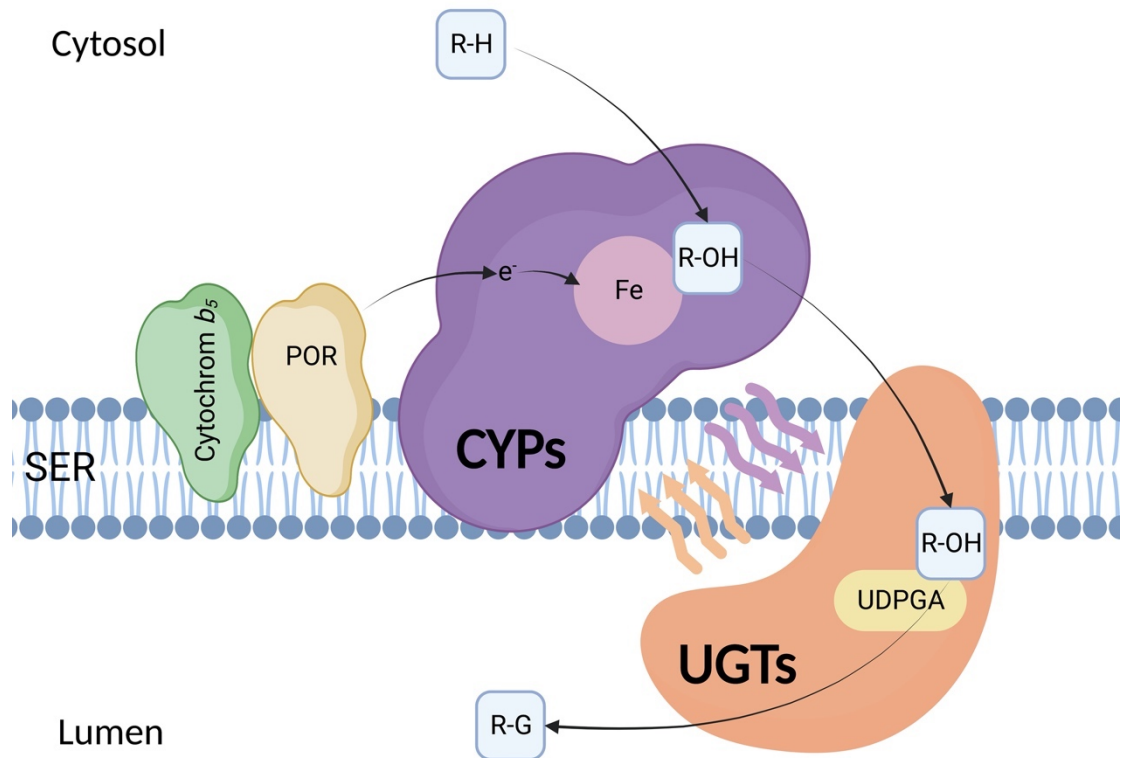


Figure 5. Proposed scheme showing the approximate position of UGTs in the smooth endoplasmic reticulum (SER) in relation to that of CYPs, adapted from [79].

Drug-drug interactions (DDIs) are a major concern in pharmaceutical development and clinical trials as well as in clinical practice. DDIs occur when perpetrator drugs affect the metabolism of victim drugs by inhibiting or inducing their key metabolic enzymes, leading to toxicity or treatment failure. However, it is now recognized that CYP-UGT protein-protein interactions, or DME-DME interactions, can also cause similar side effects through a different mechanism. For example, CYP3A is suppressed by UGT1As under physiological conditions [76, 80, 81], but dexamethasone, a known CYP inducer, can partially reverse UGT1A-mediated CYP3A suppression by inducing higher levels of CYP3A compared to UGTs [78]. Additionally, *Hypericum perforatum*, also known as St John's wort, can act as an alternative drug to phenobarbital in the treatment of Crigler-Najjar syndrome [82]. Unlike phenobarbital, which upregulates UGT1A1 expression, *H. perforatum* is a strong inducer of CYP3A4 but not UGT1A1, and CYP3A4 has been found to increase UGT1A1 activity through protein-protein interactions [78].

The evidence strongly suggests that protein-protein interactions between DMEs, particularly between CYPs and UGTs, play a crucial role in drug metabolism and clearance. The effects of these interactions can be as significant as those caused by classic DDIs. Therefore, it is crucial to thoroughly investigate and evaluate the impact

of DME-DME interactions in drug development and clinical trials and consider them alongside DDIs when assessing drug safety and efficacy.

### 1.1.5 Conjugation of alternate UDP-sugars

In section 1.1.3, the process of glucuronidation catalyzed by human UGTs with UDPGA as a cofactor in phase II metabolism has been introduced and described in detail. However, UGTs have been shown to catalyze not only the formation of glucuronides but also the glycosidation of many endobiotics and xenobiotics using alternative UDP-sugar donors such as UDP-glucose, UDP-galactose, UDP-xylose, and UDP-*N*-acetylglucosamine. For instance, human UGT1A1 has been found to catalyze glucosidation and xylosidation in bilirubin metabolism, using UDP-glucose and UDP-xylose as cofactors, respectively [83, 84]. UGT2B7 was found to be able to catalyze the glucosidation of hyodeoxycholic acid, forming its 6 $\alpha$ -*O*-glucoside [85, 86]

Moreover, glucosidation is also observed in some drugs and xenobiotics. Mycophenolic acid glucoside was found in plasma and also in *in vitro* assays with human liver, kidney, and intestine microsomes [87, 88]. Morphine 3- and 6-glucosides have been detected in the urine of cancer patients, suggesting a novel metabolic pathway for morphine in these patients [89]. Further research has shown that human UGT2B7 can form morphine-3-glucoside but not morphine-6-glucoside. Thereby, glucuronidation and glucosidation may act as two complementary metabolic pathways [90]. Moreover, UGT2B7 has been found to catalyze the production of Ibuprofen acyl glucosides [91]. Interestingly, some drugs are converted to *N*-glucosides instead of *O*-glucosides [92-94], with the *N*-glucoside even becoming the major metabolite in certain cases (e.g., phenobarbital *N*-glucoside) [95].

UGT3A1 catalyzes the *N*-acetylglucosaminidation of ursodeoxycholic acid using UDP-*N*-acetylglucosamine while showing no activity with UDPGA or other UDP-sugars [63]. UDP-*N*-acetylglucosamine has not been reported as a donor substrate for any other UGT isoform so far. In contrast, UGT3A2 has been shown to preferentially use UDP-glucose or UDP-xylose in conjugation reactions despite sharing 80% sequence identity with UGT3A1 [64]. UGT8A1, similarly to UGT3A1, uses UDP-galactose exclusively and has not shown activity with other UDP-sugars. UGT8A1 is involved in the biosynthesis of galactosylceramides, which play a crucial role in producing brain sphingolipids [96]. In addition, UGT8A1 was found to be efficient in galactosidating bile acids and bile acid analogs with drug-like properties [66].

The evidence suggests that glycosidation reactions using alternative UDP-sugar donors play a non-negligible role in metabolizing endogenous and exogenous

compounds and biosynthesis. The subtle variations in the UDP-sugar binding site of UGT enzymes allow for selective recognition of UDP-sugars. *In silico* study demonstrated that specific amino acids in the C-terminal domain of UGTs play an important role in the UDP-sugar selectivity [97]. Additionally, the conformation of the sugar ring, the presence of water molecules, and conformational changes are other factors that can influence this process [97]. Glucosides, galactosides, xylosides, and *N*-acetylglucosaminidation metabolites may be considered as potential targeted metabolites in drug development and pharmacokinetics if glucuronides are not detected.

## 1.2 Methods involved in preclinical studies

### 1.2.1 *In vitro* and *in vivo* studies on metabolism

The two primary reasons for drug development failure in recent years are lack of potency and safety concerns [98]. The withdrawal of drugs from the market due to safety issues can be more costly to pharmaceutical industries than ineffective candidates. Therefore, it is essential to investigate new drugs from various perspectives prior to human clinical trials, including potential metabolic pathways, pharmacokinetic properties, efficacy evaluation, and toxicity assessment.

The preclinical evaluation can be classified into two types, *in vitro* and *in vivo* studies, depending on the metabolic model involved. *In vitro* models include hepatic and non-hepatic microsomes, hepatocytes and liver slices, human liver cytosolic fractions, and recombinant human DMEs expressed in heterologous organisms. Human liver microsomes (HLMs) can be obtained from human liver tissue through a process of homogenization, centrifugation, and ultracentrifugation [99]. HLMs contain many CYPs with varying expression levels and part of the UGTs [21, 42], making them sufficient for metabolic studies of various drugs. However, as HLMs are small vesicles formed by the endoplasmic reticulum, cytosolic enzymes such as SULTs and GSTs are not contained in the microsomal fractions. Therefore, human liver cytosolic fractions (S9 fractions, obtained after the first centrifugation step at about 9000 *g* of subcellular fractions) [100], which contain both cytosol and microsomes, can be used to determine the catalytic reaction by SULTs and GSTs. In addition to HLMs, other human microsomes, such as from lung or intestine, are also used to investigate local metabolic properties [101].

Although HLMs are an efficient and easy-to-operate model, they have some drawbacks. For example, they cannot be used to study the effect of uptake and efflux transporters on drug metabolism, which have been shown to play a vital role in drug clearance [102]. To simulate *in vivo* metabolism more precisely, isolated hepatocytes and precision-cut

liver slices have been introduced for *in vitro* biotransformation. These models allow for exploration of the entire process of drug clearance, including various reactions and functions related to DMEs or transporters [103]. However, the relatively scarce availability, the need for inexpensive transportation and storage, and decreased enzymatic potency during culture period restrict their widespread utilization. Immortalized cell lines are considered to be an alternative because they have an unlimited lifespan and are easy to obtain and operate [104]. The expression of DMEs in these cell lines is often up-regulated to compensate for their otherwise low expression levels.

Once the basic metabolic properties of a new drug have been determined, such as the metabolic pathway, further studies can be conducted using recombinant expressing systems. The most common system involves expressing individual DMEs in bacterial, eukaryotic, or insect cells [105]. One of the key advantages of heterologous systems is that the expression of human DMEs is virtually unlimited [106]. This allows for easy access to a specific enzyme in large quantities without the disadvantages associated with human-derived methods, such as irregular availability, high functional variability between batches, and potential risk of infection.

In preclinical studies, *in vivo* testing of drug candidates is typically conducted in animal models, which can simulate drug metabolism in an intact living system and thus provide predictions for human response. The rodent system is the most commonly used animal model due to its cost-effectiveness, reproducibility, availability and its notable genetic resemblance to humans. A major limitation in using laboratory mice as models for human drug metabolism is the existence of numerous interspecies variations in the expression, activities, and inducibility of CYP enzymes [107]. To address this, genetically modified mouse models have been introduced as alternative or compensational options, such as knockout mice and humanized mice. Mouse Cyp1a2 shares several similarities with human CYP1A2 [108]. Therefore, Cyp1a2-knockout mice have been used to characterize the role of CYP1A2 in the metabolism of various therapeutic substances, including clozapine, caffeine, acetaminophen, and phenacetin [109]. CYP2D6-humanized mice have been successfully generated and used to characterize the metabolic ratio of debrisoquine/4-hydroxydebrisoquine, with data similar to that found in human extensive metabolizers [110]. Additionally, urokinase-type plasminogen activator/severe combined immunodeficiency (uPA/SCID) mice transplanted with human hepatocytes serve as practical chimeric mouse model for investigating antiviral drug and the treatment of viral hepatitis [111, 112].

Another significant limitation to consider is the ethical aspect associated with animal experiments. Ethical considerations in animal testing revolve around the welfare of humanity and the dignity of animal life. The principles of the 3Rs (Replacement, Reduction, and Refinement) were first outlined by British scientists William Russel and Rex Burch in 1959 [113] and have since been used as guidelines to promote the more ethical use of animals in scientific research and product testing. The aim of the 3Rs is to minimize or completely avoid animal experiments and to reduce both the number of animals used and any suffering they may experience during testing to the lowest possible level [114].

In the pharmaceutical industry, there is significant pressure to improve research and development productivity, primarily due to the substantial financial investments required and the lengthy timeframes involved. Approximately one out of every nine molecules fails to pass the stage of candidate screening, with many of these failures occurring at later stages [115]. These late-stage failures result in substantial costs, encompassing both actual financial outlays and the opportunities that are foregone. Consequently, they significantly increase the overall expenses associated with bringing a drug to market. Therefore, robust evaluation of a drug's efficacy and safety during the preclinical phase is critical to avoiding late failures. Although *in vitro* and animal models cannot fully replicate the pharmacodynamic and pharmacokinetic effects of a drug in humans, the data obtained from these models can still provide valuable insights and predictions about the clinical performance of a new drug. Such predictions can help minimize toxicity and side effects in clinical trials and identify potential issues that may arise during the development process. However, it is important to acknowledge the limitations and potential biases associated with these models and to strive continually to improve and refine their accuracy and reliability.

### **1.2.2 Recombinant human CYPs and UGTs in *Schizosaccharomyces pombe***

Yeast recombinant system is considered to be a suitable heterologous systems for expressing DMEs compared to bacterial and insect cells due to their endoplasmic reticulum membrane environment and cost-effective cultivation procedures [116]. As eukaryotic hosts, yeast cells possess a cellular structure that better supports protein folding and post-translational modification [117]. Moreover, yeast offers the advantage of being a unicellular organism with fewer nutritional needs compared to insect and mammalian cell lines [118]. The fission yeast *Schizosaccharomyces pombe* is a popular model system that has been used in studies of cell cycle, chromosome dynamics, and drug metabolism [116, 119]. Matthias Bureik's group established a recombinant yeast system using *S. pombe* as a host and created many strains that can

express a set of human phase I and phase II DMEs, including CYPs, UGTs, and SULTs [120-123]. This system has been used to test various xenobiotic compounds, such as drugs [124-126], and doping substances [19, 127, 128], using either whole-cell biotransformation or enzyme bags (permeabilized cells) [129, 130].

The whole-cell biotransformation method using recombinant *S. pombe* was initially developed to facilitate the production of target metabolites on a larger scale since a reference standard of metabolites is a crucial requirement in drug development. Compared to the classic chemical synthesis of metabolites, which can be complex and challenging, particularly for conjugated metabolites such as glucuronides, the whole-cell biotransformation method using recombinant *S. pombe* is considered straightforward and efficient. In addition to producing phase I metabolites, a series of UGTs strains that co-express human UGDH have also been developed, allowing for a self-sufficient glucuronide production by generating the essential cofactor UDPGA [120]. The whole-cell biotransformation method can also serve as a small-scale assay for testing the metabolism of different substrates. However, this approach is limited by the yeast cell wall, which can hinder the import of small molecules (especially charged ones) [131]. Therefore, the whole-cell biotransformation method requires longer incubation time and relatively high substrate concentration compared with microsomes.

The use of permeabilized fission yeast cells, also known as "enzyme bags," provides an *in situ* approach to address the limitations of whole-cell biotransformation. Specifically, the highly efficient enzyme bags made from fission yeast cells that express human UGDH have been shown to completely turn over a 3 mM substrate solution within three hours [132]. Prior to the biotransformation reaction, recombinant fission yeast cells are permeabilized with Triton X-100, resulting in porous cell walls which facilitate the entering of the substrates. Most of the intracellular enzymes remain in their original environment. This approach enables small molecules, like drugs, to diffuse freely inside the cells through the holes in the cell walls while larger molecules, such as enzymes, are remained within the cells. As such, this method does not require high substrate concentrations or long reaction times. The ideal substrate concentration and incubation time are reported as 1 mM and 3 hours, respectively, but these may be adapted depending on the enzymes and substrates under study [126, 133].

The enzyme bags method has proven to be useful for investigating various isoforms of DMEs, as demonstrated by previous studies [126, 130, 134, 135]. In recent studies, this method was further developed and applied to CYP-UGT co-expression yeast strains, demonstrating the versatility of this method for investigating enzymatic protein-protein interactions [136]. Additionally, the feasibility of long-term preservation of the

enzyme bags was demonstrated, further enhancing the applications of this method in drug discovery and development.

### 1.2.3 Analytical techniques used in drug metabolism studies

Liquid chromatography-mass spectrometry (LC-MS) is the most commonly used method in drug metabolism and pharmacokinetic research due to its high sensitivity and selectivity, wide range of suitable analytes, and relatively simple sample preparation procedure [137]. LC-MS is generally suited for analyzing polar conjugates, non-volatile or thermally unstable metabolites, and those compounds that are difficult to derivatize for gas chromatography-mass spectrometry (GC-MS) [138]. The introduction of electrospray ionization (ESI) and atmospheric pressure chemical ionization (APCI) sources has proven effective in ionizing a diverse range of molecules, including polar, high molecular mass drugs and metabolites. ESI is the method of choice in metabolites analysis, especially for conjugates such as glucuronides and sulfates, while APCI is better suited for weakly polar and lipophilic molecules [139].

GC-MS with an electron-ionization source is also widely used due to its established libraries. With appropriate derivatization, GC-MS can analyze a wide range of compounds, and is particularly useful in the metabolic study of steroids [140]. Supercritical fluid chromatography (SFC) has recently attracted attention due to its high separation efficiency and relatively short analysis time and is expected to gain popularity in bioanalysis in the future [141]. Moreover, chromatography coupled with tandem mass spectrometry is effective and widely used in identifying the structure of metabolites in metabolomics studies [142].

In addition to the characterization of drug metabolites, understanding the interaction mechanism between drug molecules and DMEs is crucial for screening potential drug candidates and reducing the cost of traditional drug development [143]. *In silico* studies, combined with *in vitro* experiments, can provide insights into the specificity of DME isoforms towards certain substrates, the stereoselectivity for racemic substrates, and the effect of mutations [122, 126, 144]. Furthermore, significant advances have been made in predicting the ADMET properties of drugs [145] and interactions between DMEs and transporters [146]. With the rapid advancement of computational techniques and increased computational power, it is anticipated that *in silico* studies will play an increasingly important role in drug discovery in the future.

## 1.3 Propranolol and hydroxypropranolols

### 1.3.1 The versatile role of propranolol

Propranolol, a non-selective beta-adrenergic receptor antagonist, was first discovered and developed in the early 1960s for its ability to competitively bind to beta-receptors and block the action of epinephrine and norepinephrine [147]. By inhibiting cardiac sympathetic activity, reducing cardiac output, and relaxing the peripheral vasculature, propranolol is effective in treating a range of cardiovascular diseases, including cardiac arrhythmias, sinus tachycardia, myocardial infarction, and hypertension [148, 149].

As a lipophilic drug, propranolol can cross the blood-brain barrier and block beta receptors in the central nervous system, leading to several psychiatric-related therapeutic effects [150, 151]. It has been used to treat anxiety disorders, panic management, and post-traumatic stress disorder due to its ability to inhibit the reconsolidation of fear memories [152-154]. Furthermore, in the past decade, propranolol has regained the attention of researchers due to its vital role in the treatment of Infantile Hemangioma, and rare diseases such as Hereditary Hemorrhagic Telangiectasia and Cerebral Cavernous Malformations [155-157].

Additionally, beta-blockers have been prohibited in certain sports by the International Olympic Committee (IOC) since 1985 because some athletes were found to misuse propranolol to improve performances in shooting or pentathlon [158]. Further research has shown that beta-blockers can reduce contraction force, cardiac frequency, and coronary flow, resulting in lower heart rates, muscle relaxation, and reduced tremors, which can enhance the performance of athletes in certain sports that require high accuracy but low muscle strength, such as shooting and archery [159-161]. However, it's important to highlight that monitoring for propranolol abuse may not be the primary focus in doping control. According to reports [162] from the World Anti-Doping Agency (WADA) spanning the last five years, from 2017 to 2021, the abuse of beta-blockers represented only a small fraction, accounting for approximately 0.5% (with an average ranging from 0.3% to 0.9%) of all adverse analytical findings (AAF).

### 1.3.2 Phase I and phase II metabolism of propranolol and hydroxypropranolols

Propranolol undergoes extensive metabolism in the human body, with only trace amounts of unchanged drug found in the urine [163]. Around 90% of the dose can be recovered in the urine as metabolites [164]. There are three main metabolic pathways for propranolol: *N*-Desisopropylation on the side-chain, ring hydroxylation, and

glucuronidation (Figure 6). *N*-Desisopropylpropranolol (DIP) is the primary *in vitro* metabolite of side-chain oxidation. This reaction is mainly catalyzed by CYP1A2, which also has some ability for ring hydroxylation [165]. DIP is a minor metabolite *in vivo*, as it is further oxidized to naphthoxylacetic acid (NLA) by mitochondrial and plasma monoamine oxidases [166, 167].

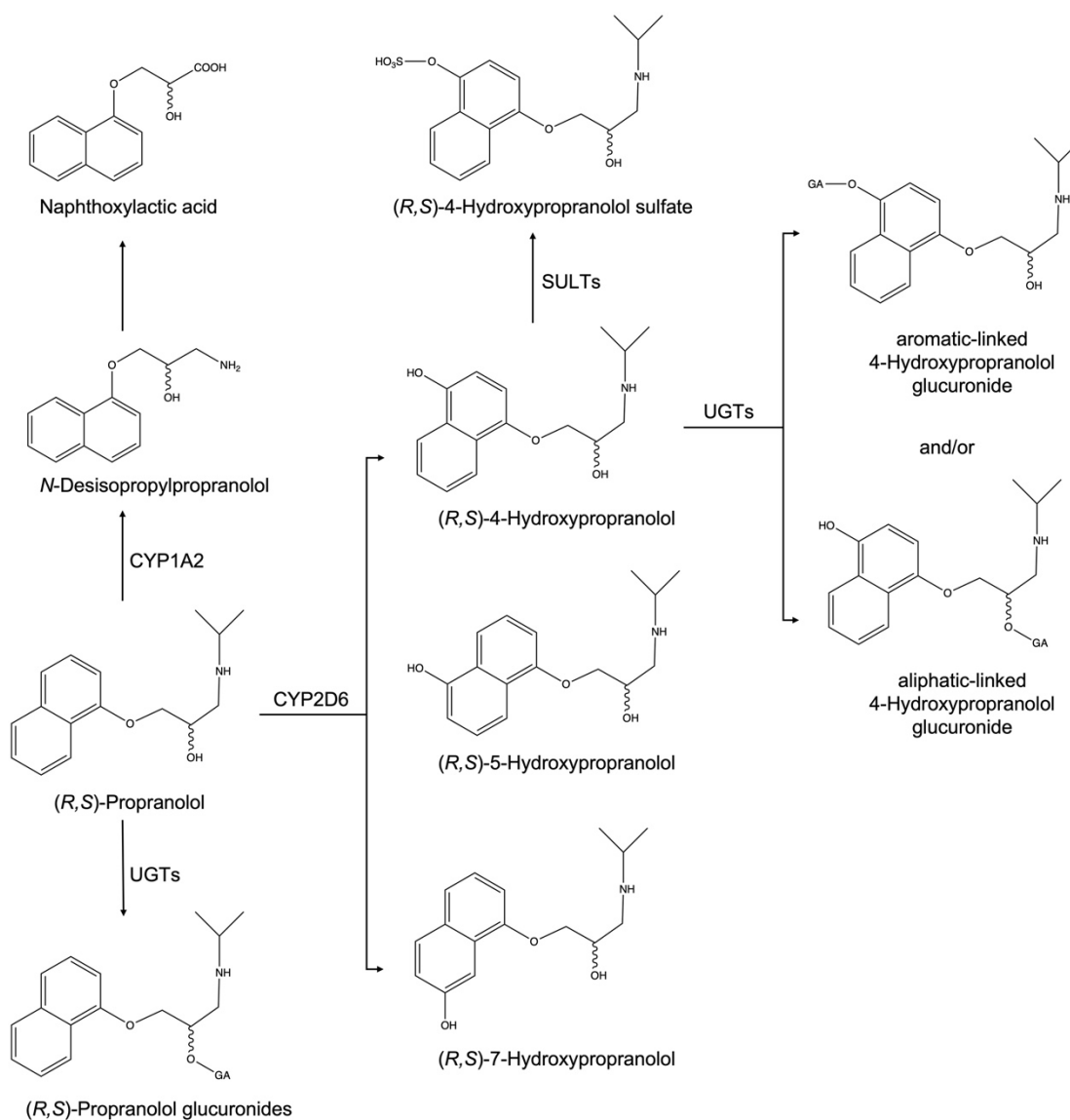


Figure 6. Proposed metabolic pathways of propranolol from *in vitro* studies, adapted from [126, 164, 168, 169]. GA, glucuronic acid.

CYP2D6 has been identified as the primary CYP isoform responsible for catalyzing the 4-, 5-, and 7-hydroxylation of propranolol, with only a small contribution to *N*-desisopropylation [170, 171]. Among the ring-hydroxylated metabolites, 4-hydroxypropranolol (4-OHP) is the most abundant, followed by 5-hydroxypropranolol (5-OHP). 7-Hydroxypropranolol (7-OHP) is a minor metabolite in humans but a major metabolite in rats [168, 172, 173]. Multiple studies have demonstrated that 4-OHP,

5-OHP, and DIP possess beta-blocking activity, with 4-OHP exhibiting equivalent potency to propranolol while the potency of others remains unknown [174-177].

In addition to oxidative metabolization, around 17% of the propranolol dose is cleared by direct glucuronidation [164]. Propranolol glucuronidation produces two glucuronic diastereomers due to the substrate chirality, with (*S*)-propranolol glucuronide being the predominant product in both plasma and urine after the administration of the racemate [178]. Given that (*S*)-propranolol is about 100 times more potent than the (*R*)-enantiomer in beta-blocking activity [179], it is essential to investigate the stereoselectivity of propranolol metabolism, as it may have therapeutic implications.

The phase I metabolites of propranolol can also undergo conjugative metabolism. Of these metabolites, 4-OHP has been extensively studied due to its equipotent activity and longer half-life compared to propranolol [176, 180, 181]. Along with sulfation, glucuronidation is considered an important pathway for eliminating 4-OHP [182-184]. Various derivatization strategies have been employed to investigate the glucuronidation position of 4-OHP, with the aromatic hydroxy group considered to be the primary reaction site. However, the aliphatic hydroxy group can also undergo glucuronidation under *in vitro* conditions [126, 169, 184]. Currently, there are no other studies on the conjugative metabolism of 5-OHP and 7-OHP, but their glucuronidation has been investigated and discussed in this thesis.

## 2 Aim of the project

Studies on the metabolites of propranolol mainly focus on the 4-hydroxypropranolol since it has been reported to be equipotent as propranolol on beta-blocking activity [176]. However, the metabolic pathway of 5- and 7-hydroxypropranolol has not been discussed yet. Therefore, the main objective of this project is to explore the metabolism of propranolol and its three monohydroxylated metabolites (4-, 5- and 7-hydroxypropranolol) using a recombinant fission yeast system expressing human UGTs.

The present thesis aims to investigate the enzymatic specificity, stereoselectivity and regioselectivity for the glucuronidation of propranolol and several hydroxypropranolols. The objectives include conducting comprehensive reaction phenotyping experiments on propranolol, along with 4-, 5-, and 7-hydroxypropranolol. These experiments will be carried out using a panel of 19 human UGTs, with the aim of identifying the specific human UGT isoforms responsible for catalyzing their glucuronidation reactions. In addition, this project seeks to determine whether the glucuronidation of the chiral drug propranolol exhibits stereoselectivity. In the case of hydroxypropranolols glucuronidation, investigations will be carried out to ascertain which hydroxy group serves as the reaction site using both pre- and post-glucuronidation methods.

Furthermore, this project also aims to examine the mutual modulation between individual UGTs and CYPs during propranolol metabolism using a diploid yeast system that coexpresses these enzymes. Moreover, glucosidation with UDP-glucose will be discussed, providing valuable insights into the study of conjugative metabolism catalyzed by UGTs with alternative sugar donors.

Additionally, this study is designed to establish a standard protocol for ADMET studies using permeabilized fission yeast cells, thus providing a powerful tool for future *in vitro* metabolic studies of other drugs.

### 3 Materials and Methods

#### 3.1 Materials

Table 1. Substrates and cofactors

4-Methoxy-1-naphthol	ThermoFisher GmbH (Kandel, Germany)
(S)-4-Hydroxypropranolol hydrobromide	Santa Cruz Biotechnology Inc.(California, USA)
(±)-4-Hydroxypropranolol hydrochloride	Sigma-Aldrich (St. Louis, USA)
(±)-5-Hydroxypropranolol	Cayman Chemical Company (Michigan, USA)
(±)-Propranolol hydrochloride	Sigma-Aldrich (St. Louis, USA)
(R)-Propranolol hydrochloride	Sigma-Aldrich (St. Louis, USA)
NADPH regeneration system	Promega Corporation (Madison, USA)
UDPGA	Sigma-Aldrich (St. Louis, USA)
UDP-glucose	EMD Millipore Corp. (Massachusetts, USA)

Table 2. Materials, reagents and solvents

Syringe/filter (CHROMAFIL®RC-45/15 MS, 0.45 µm)	Macherey-Nagel GmbH & Co. KG (Düren, Germany)
1,2-Dimethylimidazole-4-sulfonyl chloride (DMISC)	Sigma-Aldrich (St. Louis, USA)
Aceton (GC-MS grade)	Merck KGaA (Darmstadt, Germany)
Acetonitrile (LC-MS grade)	VWR International GmbH (Dresden, Germany)
Ammonium chloride	VWR International GmbH (Darmstadt, Germany)
Ammonium formate	VWR International GmbH (Darmstadt, Germany)
Ammonium hydrogen carbonate	VWR International GmbH (Darmstadt, Germany)
Calcium chloride dihydrate	Fisher Scientific (Loughborough, UK)
Disodium hydrogen phosphate	Carl Roth GmbH + Co. KG (Karlsruhe, Germany)
Epichlorohydrin	ThermoFisher GmbH (Kandel, Germany)

Ethyl acetate	VWR International GmbH (Dresden, Germany)
Formic acid (LC-MS grade)	Sigma Aldrich (Taufkirchen, Germany)
Glucose	Carl Roth GmbH + Co. KG (Karlsruhe, Germany)
Glycerol	Carl Roth GmbH + Co. KG (Karlsruhe, Germany)
Iron(III) chloride hexahydrate	Carl Roth GmbH + Co. KG (Karlsruhe, Germany)
Isopropylamine	TCI Europe N.V (Haven, Belgium)
Magnesium chloride	Carl Roth GmbH + Co. KG (Karlsruhe, Germany)
Methanol (LC-MS grade)	VWR International GmbH (Dresden, Germany)
Methylethylketone	T-E-Klebetchnik (Hannover, Germany)
<i>N</i> -Methyl- <i>N</i> -(trimethylsilyl)trifluoroacetamid (MSTFA)	Chemische Fabrik Karl Bucher GmbH (Waldstetten, Germany)
Phosphate buffered saline (PBS, pH 7.4)	VWR Chemicals. LLC (Ohio, USA)
Pooled human liver microsomes (protein concentration 5 mg/mL)	Corning Inc. (Massachusetts, USA)
Potassium carbonate	VWR International GmbH (Darmstadt, Germany)
Potassium chloride	Carl Roth GmbH + Co. KG (Karlsruhe, Germany)
Potassium hydrogen phthalate	Fisher Scientific (Loughborough, UK)
Sodium carbonate anhydrous	Ferak Berlin GmbH (Berlin, Germany)
Tris	Carl Roth GmbH + Co. KG (Karlsruhe, Germany)
Triton X-100	Carl Roth GmbH + Co. KG (Karlsruhe, Germany)
Water (LC-MS grade)	LaboStar 2-DI/-UV ultrapure water system; SG Wasseraufbereitung und Regenerierstation GmbH (Barsbüttel, Germany)

## 3.2 Methods

### 3.2.1 Yeast strains, preparation, and long-time storage of enzyme bags

All yeast strains used in this thesis and the references reporting their generation are listed in Table 3. The culture of haploid yeast that express UGTs was performed as described previously [122, 126, 135]. Fission yeast cells were first incubated on solid

Edinburgh Minimal Medium (EMM) supplemented with leucine for three days at 30 °C. The Edinburgh Minimal Medium (EMM) was prepared in-house based on the published protocol [185]. Then, the cells were incubated in 10 mL liquid EMM supplemented with leucine at 30 °C, under agitation at 230 rpm for 24 hours. For culturing diploid yeast that co-express CYP2D6 and UGTs, the procedure was adapted based on the growing condition of yeast cells. Diploid yeast strains SAN300, SAN306, SAN307, SAN308, and SAN310 were initially cultured on solid EMM supplemented with histidine for 5 days at 30 °C. Subsequently, the cells were transferred to 10 mL of liquid EMM containing histidine and incubated at 30 °C under agitation at 230 rpm for 24 hours. Afterwards, 10 mL of the pre-cultures (both haploid and diploid strains) were transferred into 100 mL of liquid EMM with histidine in a 200 mL flask and were incubated at 30 °C under agitation at 230 rpm for 48 hrs.

After the culturing, the yeast cell density was counted under the microscope. The calculated volume of liquid medium containing  $5 \times 10^7$  yeast cells was used for single enzyme bags reaction according to the previous study [122, 126, 135]. Following centrifugation at 3320 *g* for 5 minutes, the supernatant was discarded, and the cell pellets were obtained. To permeabilize the cell membrane, 1 mL of 0.3% Triton X-100 in Tris-KCL buffer was added to the tube, and the sample was incubated at 30 °C with agitation at 230 rpm for one hour. After permeabilization, the cell pellets were washed three times with 1 mL of  $\text{NH}_4\text{HCO}_3$  buffer (50 mM, pH 7.8) to remove the residual detergent.

Subsequently, the cell pellets were resuspended in 200  $\mu\text{L}$  of PBS containing 50% glycerol (*v/v*). Finally, the enzyme bag samples were flash frozen by liquid nitrogen and stored at  $-80$  °C. Prior to substrate incubation, the frozen enzyme bags were thawed on ice and washed twice with reaction buffer to remove the glycerol.

*Table 3. Fission yeast strains used in this study.*

Strain	Expressed protein	Genotype	Reference
DB1	UGT1A1	h- ura4-D18 leu1::pCAD1UGT1A1	[120]
DB21	UGT1A3	h- ura4-D18 leu1::pCAD1UGT1A3	[121]
DB2	UGT1A4	h- ura4-D18 leu1::pCAD1UGT1A4	[121]
DB22	UGT1A5	h- ura4-D18 leu1::pCAD1UGT1A5	[121]

*(Continued on next page)*

Strain	Expressed protein	Genotype	Reference
DB23	UGT1A6	h- ura4-D18 leu1::pCAD1UGT1A6	[120]
DB24	UGT1A7	h- ura4-D18 leu1::pCAD1UGT1A7	[120]
DB25	UGT1A8	h- ura4-D18 leu1::pCAD1UGT1A8	[120]
CAD200	UGT1A9	h- ura4-D18 leu1::pCAD1UGT1A9	[120]
DB26	UGT1A10	h- ura4-D18 leu1::pCAD1UGT1A10	[120]
DB3	UGT2A1	h- ura4-D18 leu1::pCAD1UGT2A1	[120]
DB27	UGT2A2	h- ura4-D18 leu1::pCAD1UGT2A2	[121]
DB28	UGT2A3	h- ura4-D18 leu1::pCAD1UGT2A3	[121]
DB29	UGT2B4	h- ura4-D18 leu1::pCAD1UGT2B4	[121]
DB7	UGT2B7	h- ura4-D18 leu1::pCAD1UGT2B7	[91]
DB30	UGT2B10	h- ura4-D18 leu1::pCAD1UGT2B10	[121]
DB31	UGT2B11	h- ura4-D18 leu1::pCAD1UGT2B7	[121]
DB32	UGT2B15	h- ura4-D18 leu1::pCAD1UGT2B15	[120]
DB33	UGT2B17	h- ura4-D18 leu1::pCAD1UGT2B17	[120]
DB34	UGT2B28	h- ura4-D18 leu1::pCAD1UGT2B28	[121]
SAN300	hCPR, CYP2D6	h+/h- ade6-M210/ade6-M216 ura4-D18/ura4-D18 his3.Δ1/his3.Δ1 leu1::pCAD1-CPR/leu1::pCAD1/pREP1-CYP2D6	[136]
SAN306	hCPR, CYP2D6, UGT1A7	h+/h- ade6-M210/ade6-M216 ura4-D18/ura4-D18 his3.Δ1/his3.Δ1 leu1::pCAD1-CPR/leu1::pCAD1-UGT1A7/pREP1-CYP2D6	[136]
SAN307	hCPR, CYP2D6, UGT1A8	h+/h- ade6-M210/ade6-M216 ura4-D18/ura4-D18 his3.Δ1/his3.Δ1 leu1::pCAD1-CPR/leu1::pCAD1-UGT1A8/pREP1-CYP2D6	[136]
SAN308	hCPR, CYP2D6, UGT1A9	h+/h- ade6-M210/ade6-M216 ura4-D18/ura4-D18 his3.Δ1/his3.Δ1 leu1::pCAD1-CPR/leu1::pCAD1-UGT1A9/pREP1-CYP2D6	[136]
SAN310	hCPR, CYP2D6, UGT2A1	h+/h- ade6-M210/ade6-M216 ura4-D18/ura4-D18 his3.Δ1/his3.Δ1 leu1::pCAD1-CPR/leu1::pCAD1-UGT2A1/pREP1-CYP2D6	[136]

### 3.2.2 Biotransformation with enzyme bags

The enzyme bags were prepared before the biotransformation as explained in section 3.2.1. For the glucuronidation or glucucosidation of propranolol and hydroxypropranolols, enzyme bags prepared from haploid fission yeast that express UGTs were resuspended in 200  $\mu\text{L}$  of  $\text{NH}_4\text{CO}_3$  buffer (50 mM, pH 7.8) containing 1 mM cofactor (UDPGA or UDP-glucose) and 1 mM substrate and incubated for 15 hours at 37  $^\circ\text{C}$ , 300 rpm in the incubator. Afterwards, the mixtures were centrifuged at 14100  $g$  for 5 min. The supernatants were taken for analysis by LC-MS/MS.

For the metabolism study with the diploid yeast system, frozen enzyme bags were used. The frozen enzyme bags were thawed on ice and washed twice with  $\text{NH}_4\text{HCO}_3$  buffer to remove glycerol. Afterwards, samples were resuspended in 200  $\mu\text{L}$  of  $\text{NH}_4\text{HCO}_3$  buffer (50 mM, pH 7.8) containing 1 mM UDPGA, 1x NADPH regeneration system, and 1 mM propranolol and incubated for the indicated amounts of time at 37  $^\circ\text{C}$ , agitating at 300 rpm (section 4.5.1). After incubation, 5  $\mu\text{L}$  of 4-methoxypropranolol (4-MeOP) (200  $\mu\text{g}/\text{mL}$ ) were added to each diploid strain reaction sample as internal standard. Afterwards, the mixtures were extracted thrice with an equal volume of ethyl acetate, and then the organic phases were combined and dried under  $\text{N}_2$ . The extracts were redissolved in methanol and analyzed by LC-MS/MS for 4-OHP formation. The aqueous residues were centrifuged at 14100  $g$  for 5 min to obtain supernatants and then analyzed by LC-MS/MS as well for glucuronide detection. For comparison, the reaction mixtures from CAD200 enzyme bag samples were centrifuged for 5 min at 14100  $g$ , and the supernatants were used directly for LC-MS/MS analysis of propranolol glucuronides.

### 3.2.3 *In vitro* metabolism with HLMs

*In vitro* incubations with HLMs were performed as two groups for two purposes: firstly, to generate reference samples with an incubation time of 4 hours for identifying glucuronides or glucosides in urine or enzyme bag samples. Secondly, to produce sufficient amounts of hydroxypropranolol glucuronides (OHPGs) with a longer incubation time of 24 hours for derivatization reaction.

For generating reference samples that only containing (*R*)-form glucuronides, (*R*)-propranolol was used as the substrate for synthesizing the respective diastereomeric OHPGs via HLMs-catalyzed enzymatic reactions since enantiopure 5- and 7-OHP were not available. The reaction required NADPH regeneration system and UDPGA as cofactors to enable phase I and phase II metabolism. A total of 5  $\mu\text{L}$  of pooled HLMs (5 mg/mL) were added to a 50 mM  $\text{NH}_4\text{HCO}_3$  buffer containing 3 mM  $\text{MgCl}_2$ , 1 mM (*R*)-propranolol, 1 mM UDPGA, and 1x NADPH regeneration system,

which is composed of a 1× concentration of solution A containing NADP<sup>+</sup> and glucose-6-phosphate, and a 1× concentration of solution B containing glucose-6-phosphate dehydrogenase. The final reaction volume was 200 μL. The reaction mixture was incubated at 37 °C with agitation at 1000 rpm for 4 hours, and then centrifuged at 14100 *g*. The supernatant was collected for analysis.

For generating reference samples that containing both (*R*)- and (*S*)-form of glucuronides or glucosides, the NADPH regeneration system was not required because phase I reaction was not needed. The substrate was replaced with either racemic propranolol or racemic hydroxypropranolols at the same concentration (1 mM). The other components of the reaction mixture remained unchanged, and UDP-glucose was used instead of UDPGA for glucosidation.

To generate sufficient amounts of OHPGs, 5 μL of pooled human liver microsomes (5 mg/mL) were added to the 50 mM NH<sub>4</sub>HCO<sub>3</sub> buffer containing 3 mM MgCl<sub>2</sub>, 1 mM 4-, 5- or 7-OHP, and 1 mM UDPGA. The reaction mixture was incubated at 37 °C with agitation at 1000 rpm for 24 hours. After incubation, 400 μL of acetonitrile were added to the system, and the samples were centrifuged at 14100 *g* for 5 minutes to separate the supernatant. Aliquots of 300 μL of the supernatant were utilized for the derivatization reaction, while the remaining portion of the supernatant was preserved as underivatized samples for comparison with the derivatized samples.

### 3.2.4 Urine sample collection

Urine samples were collected for seven days after administering a single dose of 40 mg of racemic propranolol. During the first 24 hours, continuous urine collection was performed, while only morning urine samples were collected for the subsequent days. All urine samples were stored at -20 °C until further analysis. Before analysis, 200 μL of each urine sample were diluted with 800 μL of methanol. The diluted samples were then centrifuged at 3320 *g* for 10 minutes. The resulting supernatants were collected for subsequent analysis. All urine samples were analyzed by LC-MS/MS and the abundant of analytes are listed in Supplementary Table 1. Among the collected urine specimens, the sample obtained at 17.6 hours after the oral administration of propranolol was specifically chosen for comparison with the incubations with HLMS and enzyme bags. This is because 4-, 5- and 7-OHPGs were found in this urine sample and their amounts were higher than in the other urine samples.

### 3.2.5 Synthesis of 4-, 5- and 7-methoxypropranolol

The synthesis method of 4-, 5- and 7-MeOP was adapted from the previous method that was applied for the synthesis of 4-, 5- and 7-OHP [168, 186]. 4-Methoxy-1-

naphthol (1 g) and potassium carbonate (2.5 g) were suspended in 12.5 mL methylethylketone and 15 mL epichlorohydrin. The mixture was refluxed for 6 hours in an oil bath. Then the reaction mixture was filtrated to remove the potassium carbonate and the solvent was evaporated. To the residue, 10 mL of isopropylamine and 1 mL of water were added, and the reaction mixture was refluxed again for 5 hours. After evaporation of the solvent, 50 mL hexane were added for recrystallization. The final product was cooled down to 4 °C overnight. The crystals were filtrated, dried, and redissolved in methanol to get the stock solution of 4-MeOP. The product was derivatized with *N*-methyl-*N*-(trimethylsilyl)trifluoroacetamid (MSTFA) and analyzed by GC-MS to confirm the structure and purity (section 4.3.1). The procedure for synthesizing 5- and 7-MeOP was the same but with 5-methoxy-1-naphthol or 7-methoxy-1-naphthol as starting compounds, respectively.

### 3.2.6 Derivatization with 1,2-dimethylimidazole-4-sulfonyl chloride (DMISC)

All substrates, including (±)-propranolol, (*R*)-propranolol, (*S*)-4-OHP, (±)-5-OHP, (±)-7-OHP, (±)-4-MeOP, (±)-5-MeOP, and (±)-7-MeOP, were prepared as 10 mM stock solutions with methanol (LC-MS grade). For DMISC derivatization, all substrate stock solutions were further diluted to 10 µM with methanol.

The DMISC derivatization solution was prepared at a concentration of 20 mg/mL with acetone in accordance with previous studies [169, 187-189]. The solution was subjected to ultrasonic treatment for 15 minutes to improve the dissolution of DMISC. Subsequently, the solution was centrifuged at 3320 *g* for 10 minutes, and the resulting supernatant was utilized for derivatization.

The derivatization method used in this study was described in previous publications [169, 187]. Before the derivatization process, 300 µL of either a 10 µM substrate solution or the supernatant from HLM incubations were evaporated to dryness under N<sub>2</sub> flow in a heating block at 65 °C. Subsequently, 100 µL of sodium carbonate buffer (0.1 M, pH 10.5) were added to the dried residues, and the tubes were vortexed for 1 minute to dissolve the residue. Next, 100 µL of DMISC solution were added. After incubation in a 60 °C water bath for 10 minutes the samples were cooled to room temperature and filtered through 0.45 µm filters for subsequent LC-MS/MS analysis.

### 3.2.7 Analytical methods

#### 3.2.7.1 GC-EI-MS analysis

Analysis was performed on an Agilent 7890A gas chromatographic system (Agilent Technologies GmbH, Waldbronn, Germany) coupled to an Agilent 5975 C inert mass selective detector, equipped with an Agilent HP1 column (17 m, 0.2 mm, 0.11  $\mu$ m) with helium as the carrier gas. The following parameters were used for the analysis of methoxypropranolols: oven program, 150 °C, + 10 °C/min to 250 °C (rate 1), + 40 °C/min to 310 °C (rate 2), hold for 2 minutes; injection volume, 2  $\mu$ L; split, 16:1; injection temperature, 300 °C; electron ionization (EI): 70 eV, full scan mode from m/z 40 to 1000. Before GC-MS analysis, the dried residues were derivatized with MSTFA to a final concentration of 100 ppm for 20 minutes at 75 °C.

#### 3.2.7.2 LC-QQQ-MS/MS analysis

Analysis was performed on an Agilent Technologies 1290 infinity II high-performance liquid chromatograph equipped with an Agilent 6495 triple quadrupole mass spectrometer (Agilent Technologies, Waldbronn, Germany). Propranolol and propranolol glucuronides were separated on an Agilent Poroshell phenyl hexyl column (100 mm  $\times$  3.0 mm, 1.9  $\mu$ m). The flow rate was 0.4 mL/min, and the column temperature was 25 °C. For the simultaneous detection of the substrate and glucuronides, the initial mobile phase composition was 98% water with 0.1% formic acid and 10 mM ammonium formate (A) and 2% acetonitrile with 0.1% formic acid, 10% water and 10 mM ammonium formate (B). The amount of A was decreased to 85% within 7 minutes, to 60% within 7 to 14 minutes, and 5% within 14 to 15 minutes. Then, A maintained at 5% until 17 minutes, which is the end of the run. The separation of 4-, 5- and 7-OHP was performed using the same column and solvents but in a different elution gradient: starting from 95% A, the amount of A was then decreased to 60% within 25 minutes and to 5% from 25 to 26 minutes. Finally, A was maintained at 5% until the end of the run (28 minutes).

The separation of 4-, 5- and 7-hydroxypropranolol glucuronide diastereomers and propranolol glucosides was achieved on an Agilent ZOBRA Eclipse Plus C18 column (100 mm  $\times$  2.1 mm, 1.8  $\mu$ m) using a flow rate of 0.4 mL/min and a column temperature of 30 °C. The mobile phase consisted of 95% water with 20 mM ammonium formate (A) and 5% methanol with 20 mM ammonium formate (B) as starting conditions. Over a period of 25 minutes, the percentage of A was linearly reduced to 60%. From 25 to 26 minutes, the percentage of A was further decreased to 5%, and this concentration was maintained until the end of the 28-minute run.

In order to separate 4-, 5- and 7-MeOP and their respective glucuronides, similar conditions were applied. Aberrantly, for the gradient mobile phase A was decreased from the starting conditions to 60% within 25 minutes, further reduced to 40% from 25 to 30 minutes, and then to 5% from 30 to 31 minutes. Following this, A was maintained at 5% until the end of the run, which was 33 minutes in total.

The details of the transitions of analytes are listed in Table 4. The presented peak areas were provided by transitions of the highest intensity.

Table 4. Transitions and retention time for all analytes in MRM

Analytes	Retention time (min)	Precursor ions ( <i>m/z</i> )	Product ions ( <i>m/z</i> )	CE (eV)	ESI
Propranolol	16.4	260	183	20	+
			116	20	
			56	36	
4-Hydroxypropranolol	13.2		116	12	
5-Hydroxypropranolol	11.8	276	72	16	+
7-Hydroxypropranolol	22.1		58	44	
4-Methoxypropranolol	27.6		187	12	
5-Methoxypropranolol	25.1	290	116	16	+
7-Methoxypropranolol	27.6		72	44	
( <i>R</i> )-Propranolol glucuronide	12.7		258	12	
( <i>S</i> )-Propranolol glucuronide	13.1	436	183	16	+
			116	28	
( <i>R</i> )-Propranolol glucoside	24.2		258	12	
( <i>S</i> )-Propranolol glucoside	23.5	422	183	16	+
			116	28	
( <i>R</i> )-4-Hydroxypropranolol glucuronide	8.7		276	12	
( <i>S</i> )-4-Hydroxypropranolol glucuronide	8.5	452	199	20	+
( <i>R</i> )-5-Hydroxypropranolol glucuronide	6.4		173	24	

Analytes	Retention time (min)	Precursor ions ( <i>m/z</i> )	Product ions ( <i>m/z</i> )	CE (eV)	ESI
( <i>S</i> )-5-Hydroxypropranolol glucuronide	6.7		116	28	
( <i>R</i> )-7-Hydroxypropranolol glucuronide	17.3		98	40	
( <i>S</i> )-7-Hydroxypropranolol glucuronide	16.6		72	44	
4-Methoxypropranolol glucuronide I	13.3		290	25	
4-Methoxypropranolol glucuronide II	13.6		213	30	
5-Methoxypropranolol glucuronide I	24.4		187	30	
		466			+
5-Methoxypropranolol glucuronide II	26.1		116	28	
7-Methoxypropranolol glucuronide I	25.7		72	44	
7-Methoxypropranolol glucuronide II	27.0				
			276	12	
			199	20	
4-/5-/7-Hydroxypropranolol glucosides	*	438	173	24	
			116	28	+
			98	40	
			72	44	

CE, collision energy; ESI, electrospray ionization; Drying gas temperature, 160 °C; Drying gas flow, 11 L/min; Nebulizer, 30 psi; Sheath gas heater, 375 °C; Sheath gas flow, 12 L/min; Capillary voltage, 3000 V; Nozzle voltage, 1500 V.

\* "-", 4-/5-/7-Hydroxypropranolol glucosides were not observed during the analysis and therefore there's no retention time displayed.

### 3.2.7.3 LC-QTOF-MS/MS analysis

The separation and structural confirmation of DMISC derivatives and underivatized glucuronides and glucosides was performed using an Agilent Technologies 1290 Infinity II high-performance liquid chromatograph coupled to an Agilent 6550 QTOF

mass spectrometer (Agilent Technologies, Santa Clara, CA). The column employed was an Agilent ZOBRA Eclipse Plus C18 column (100 mm × 2.1 mm, 1.8 μm).

The separation for DMISC derivatives of propranolol and hydroxypropranolols was achieved using the same elution method for separating propranolol and hydroxypropranolols (see in section 3.2.7.2) but with a flow rate of 0.35 mL/min.

The separation of DMISC derivatives of 4-, 5- and 7-OHPG was achieved using a gradient with a flow rate of 0.2 mL/min and a column temperature of 35 °C. The initial composition of the mobile phase consisted of 80% water containing 20 mM ammonium formate (A) and 20% methanol with 20 mM ammonium formate (B). Subsequently, the proportion of component B was gradually increased to 32% over a period of 14 minutes, followed by a further increase to 43% between 14 to 25 minutes. After this, B was raised to 90% and maintained until the end of the 30-minute run.

For the structural confirmation of glucuronides, glucosides and DMISC derivatives, targeted MS/MS was performed. MS parameters were set using electrospray ionization in positive ion mode (ESI+) with spectra acquired over a mass range of  $m/z$  100 – 1000; capillary voltage 3500 V; dry gas temperature 200 °C; dry gas flow 12 L/min; the specific collision energies used in each particular analysis are given in the individual figure legends.

## 4 Results and Discussion

### 4.1 Stereoselective glucuronidation of racemic propranolol

#### 4.1.1 Biotransformation of propranolol with 19 UGTs

In the current study, the activity of all 19 human members of the UGT1 and UGT2 families towards propranolol was tested. An overview of the results on the activity of respective UGTs with racemic propranolol is given in Supplementary Table 2. The presented peak areas were provided by transitions of the highest intensity. Among the 19 UGTs, UGT1A7, UGT1A9, UGT1A10, and UGT2A1 were found to glucuronidate racemic propranolol with different activity. Figure 7 displayed the chromatograms of propranolol glucuronides obtained from UGT1A7, UGT1A9, UGT1A10, and UGT2A1 enzyme bag samples, respectively. As a result of the conjugation with enantiopure  $\beta$ -D-glucuronic acid, two diastereomeric glucuronides were detected.

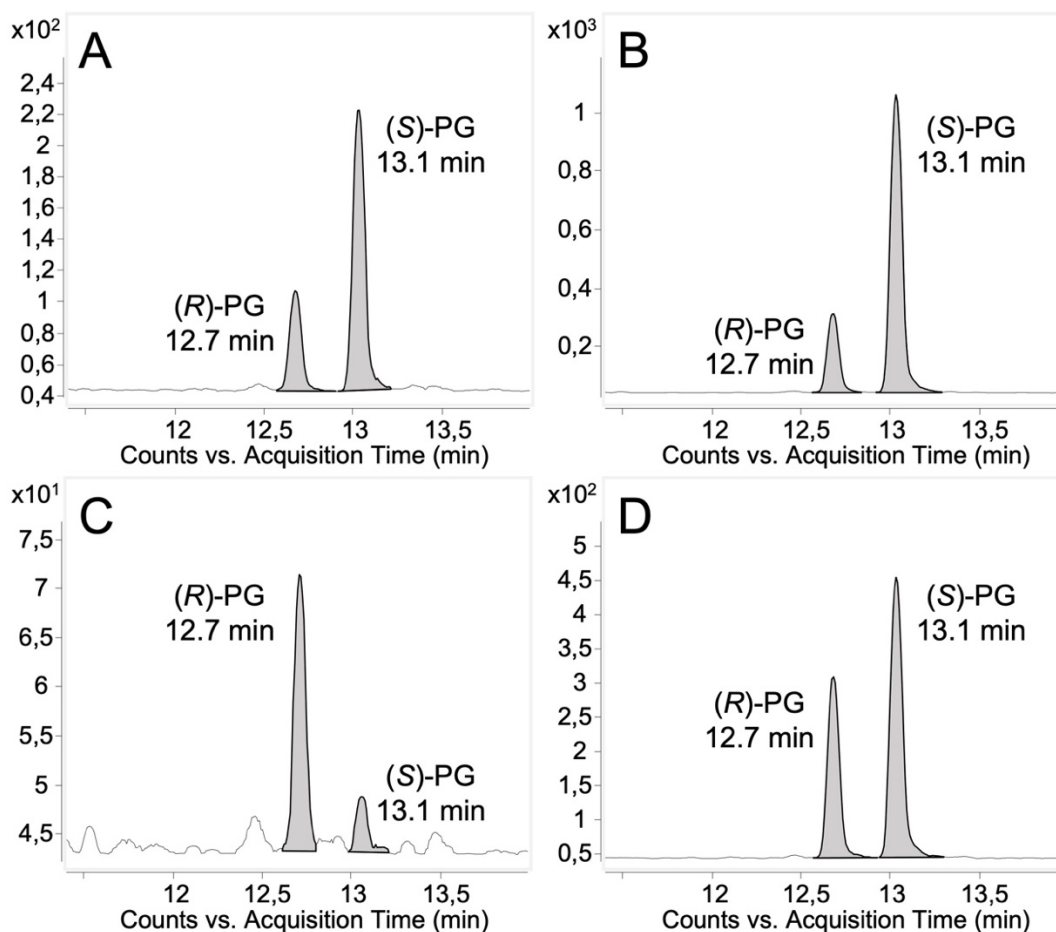


Figure 7. Chromatograms (LC-QQQ-MS/MS) of (R)-propranolol glucuronide and (S)-propranolol glucuronide obtained from UGT-dependent enzyme bag samples. Ion transition  $m/z$  436 $\rightarrow$ 116 is monitored. (R)-PG, (R)-propranolol glucuronide, retention time 12.7 min. (S)-PG, (S)-propranolol glucuronide, retention time 13.1 min. (A) UGT1A7. (B) UGT1A9. (C) UGT1A10. (D) UGT2A1. This figure is adapted from my published paper [126].

Additionally, (*R*)-propranolol was utilized as a substrate to assign the diastereomers. Figure 8 displayed the chromatograms of (*R*)-propranolol glucuronide obtained from UGT1A7, UGT1A9, UGT1A10, and UGT2A1 enzyme bag samples using (*R*)-propranolol as substrate, respectively. The chromatograms in Figure 8 depicted that (*R*)-propranolol produced only one glucuronide product (retention time 12.7 min), thereby assigning the other diastereomer (retention time 13.1 min) to (*S*)-propranolol glucuronide.

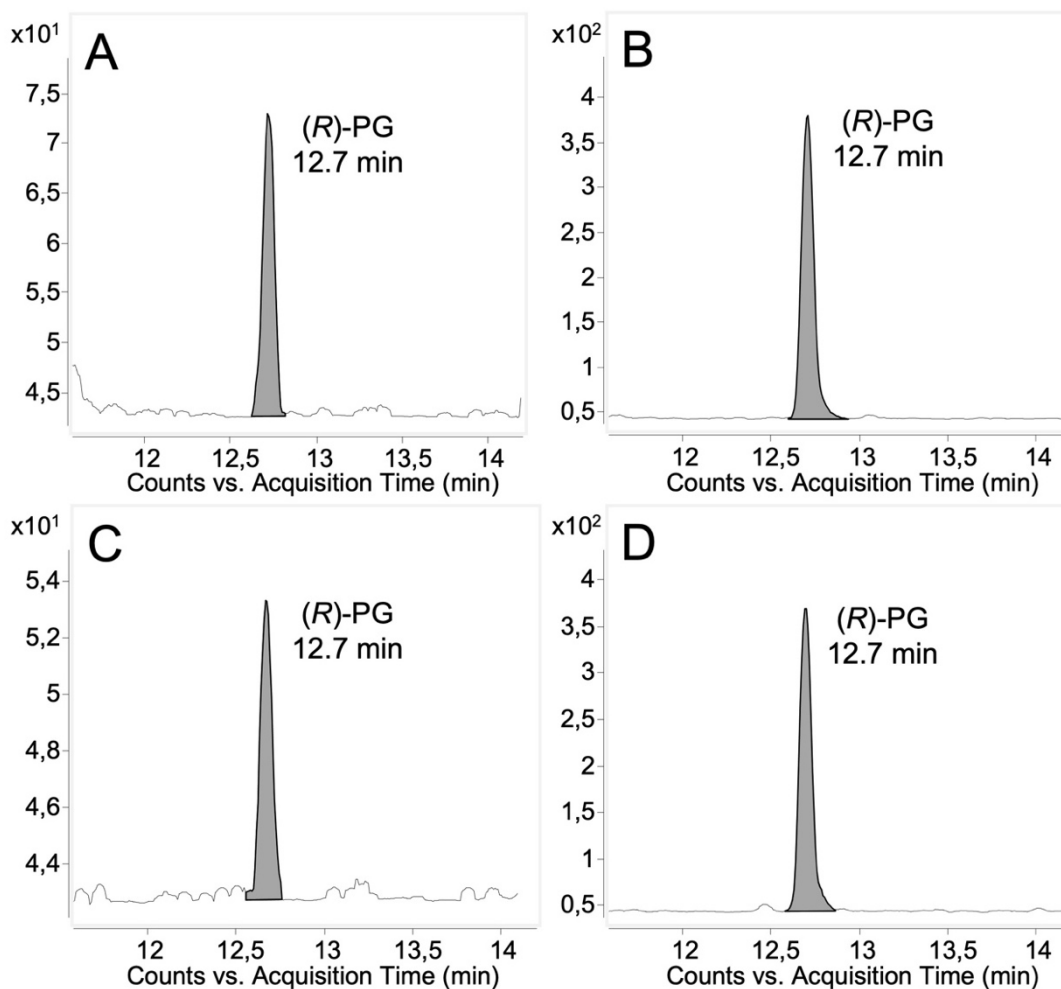


Figure 8. Chromatograms (LC-QQQ-MS/MS) of (*R*)-propranolol glucuronide obtained from UGT-dependent enzyme bag samples using (*R*)-propranolol as the substrate. Ion transition  $m/z$  436  $\rightarrow$  116 is monitored. (*R*)-PG, (*R*)-propranolol glucuronide, retention time 12.7 min. (A) UGT1A7. (B) UGT1A9. (C) UGT1A10. (D) UGT2A1. This figure is adapted from my published paper [126].

The biocatalytic yields of (*R*)-propranolol glucuronide were found to be 27.9%, 19.3% and 32.8% of the overall production of both (*R*)- and (*S*)-propranolol glucuronide for UGT1A7, UGT1A9, and UGT2A1, respectively. These results suggest a preference for (*S*)-propranolol as the substrate for these three enzymes. Conversely, the biocatalytic yield of (*R*)-propranolol glucuronide was 78.6% of the total production of both (*R*)- and

(S)-propranolol glucuronide for UGT1A10, indicating a preference for (*R*)-enantiomer by UGT1A10. Notably, the yield of (*R*)-propranolol glucuronide by UGT1A9 is still higher than that produced by UGT1A10 even though (*R*)-propranolol is the predominant substrate for UGT1A10 compared to (*S*)-propranolol. This may be attributed to the differences in catalytic activities exhibited by different UGT isoforms when it comes to the glucuronidation of propranolol.

To further characterize propranolol glucuronide, MS/MS analysis was performed using a quadrupole time of flight (QTOF) instrument, enabling high-resolution accurate mass spectrometry. The product ion spectrum is shown in Figure 9. The loss of 176.0305 Da indicates the loss of the glucuronic acid moiety. The fragment ion  $m/z$  183 was considered to be generated by a combined elimination of water ( $-H_2O$ , 18 Da) and isopropylamine group ( $-C_3H_9N$ , 59 Da) from protonated propranolol ( $m/z$  260). The fragment ion  $m/z$  116 resulted from the loss of hydroxy naphthyl ring ( $-C_{10}H_8O$ , 144 Da) and additional elimination of water generated the ion  $m/z$  98. The structures of these fragments have been demonstrated by previous study [169, 190] and were used to deduce the fragmentation of DMISC derivatives in section 4.3.2.

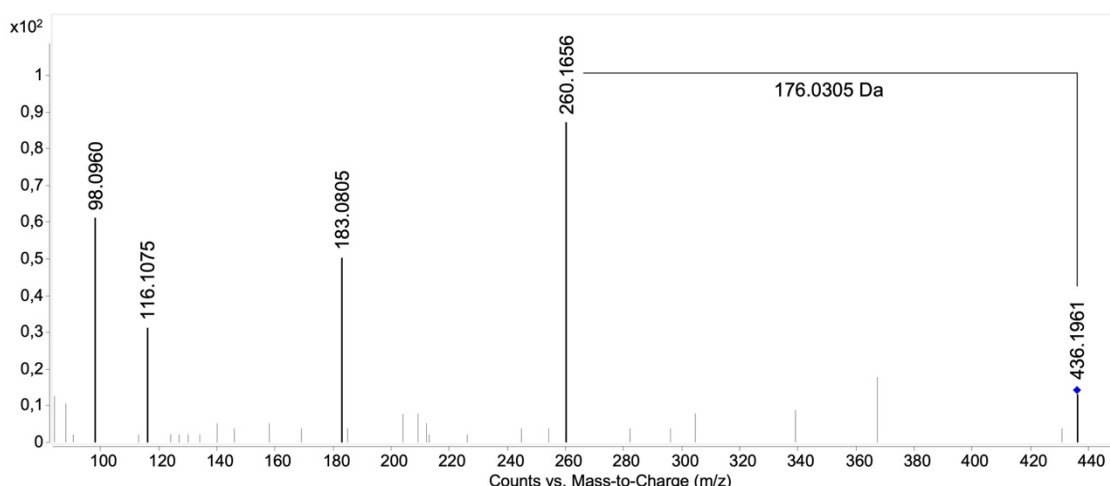


Figure 9. Product ion spectra (LC-QTOF-MS/MS) of propranolol glucuronide obtained by UGT-dependent biotransformation. Propranolol glucuronide,  $C_{22}H_{29}NO_8$ ,  $[M+H]^+$  theor. = 436.1971,  $[M+H]^+$  exp. = 436.1961,  $\Delta m/z = -2.29$  ppm; collision energy, 30 eV. This figure is adapted from my published paper [126].

#### 4.1.2 Discussion

The glucuronidation of propranolol has been previously reported in various studies. Early research suggested that propranolol is metabolized through multiple pathways, including ring oxidation, side-chain oxidation, and glucuronidation [164, 166, 173, 174]. Due to the chirality of the substrate, glucuronidation may lead to the production of two glucuronide diastereomers. Given that (*S*)-propranolol is about 100 times more potent

than the (*R*)-enantiomer in beta blocking activity [175], it is essential to investigate the stereoselectivity of propranolol glucuronidation, as it may have therapeutic implications.

After the administration of racemic propranolol by human, it was found that (*S*)-propranolol glucuronide exceeded the other diastereomer in both plasma and urine by more than four times, suggesting that (*S*)-propranolol is the predominant substrate of glucuronidation in humans [178, 191]. In the current study, a complete reaction phenotyping reaction of propranolol by 19 human UGTs was performed to investigate which UGT isoforms are active. It was observed that four UGTs, namely UGT1A7, UGT1A9, UGT1A10, and UGT2A1, were found to be responsible for the glucuronidation, each exhibiting varying levels of activity. Additionally, a stereoselectivity preference was noted, with (*S*)-propranolol being favored as a substrate by UGT1A7, UGT1A9, and UGT2A1, while UGT1A10 has a preference for (*R*)-propranolol as its substrate.

The stereoselective glucuronidation of propranolol has been investigated previously through enzyme kinetic analyses. It was observed that the  $K_m$  values for (*S*)-propranolol and (*R*)-propranolol differed less than the corresponding  $V_{max}$  values in the case of UGT1A9 and UGT1A10, indicating that the rate of glucuronic acid transfer to the already bound aglycone substrate may be the major determinant [192]. In my published paper [126], an alternative approach utilizing *in silico* studies is used to provide further insights into the stereoselectivity from a different perspective. Briefly, the interaction between the hydroxy group (site of metabolism) of (*R*)-propranolol and Arg88 in UGT1A7, UGT1A9, UGT2A1 appeared to be a key contributor. This interaction resulted in the UDPGA to move away from the hydroxy group, thus hindering the reaction. Conversely, for (*S*)-propranolol, due to its distinct binding orientation with the enzyme, this interference on the hydroxy group did not occur. These results served as a practical example for investigating enzyme-drug interaction mechanisms at the molecular level through *in silico* studies. These findings will contribute to future studies of enzyme stereoselectivity from a geometric standpoint.

## 4.2 Glucuronidation of hydroxypropranolols

### 4.2.1 Identification 4-, 5- and 7-OHPG

For preparing reference samples that containing hydroxypropranolol glucuronides, 4-, 5- and 7-OHP were incubated with HLMs and UDPGA for 4 hours, respectively (Figure 10b, 10e and 10h). These *in vitro* samples were analyzed by LC-MS/MS and compared with urine samples (Figure 10a, 10d and 10g) for the identification of hydroxypropranolol glucuronides in human urine. Furthermore, HLMs were incubated

with (*R*)-propranolol in the presence of both NADPH and UGPGA as cofactors. This experiment allowed for the generation of the (*R*)-forms of 4-, 5-, and 7-OHP, which were subsequently glucuronidated to generate the corresponding (*R*)-OHPG metabolites (Figure 10c, 10f and 10i). This HLMs incubation was used for assigning the individual (*R*)-OHPG isomers in urine samples. By identifying the (*R*)-diastereomer, the remaining diastereomer was assigned to the (*S*)-form.

Figure 10 illustrates the presence of two diastereomeric glucuronides in both urine and HLMs samples for 4-OHP and 7-OHP incubation. By comparison with (*R*)-propranolol incubation (Figure 10c) (*R*)-4-OHPG was assigned to the peak eluting at 8.7 min, thus (*S*)-4-OHPG eluted at 8.5 min (Figure 10a and b). Similarly, (*S*)-7-OHPG and (*R*)-7-OHPG were assigned to the peaks eluting at 16.6 min and 17.3 min, respectively (Figure 10g, 10h and 10i). In the case of 5-OHP, the HLMs incubation resulted in two glucuronides (Figure 10e), while only the (*R*)-diastereomer was detected in the urine sample (Figure 10d). (*S*)-5-OHPG and (*R*)-5-OHPG were eluted at 6.4 min and 6.6 min, respectively.

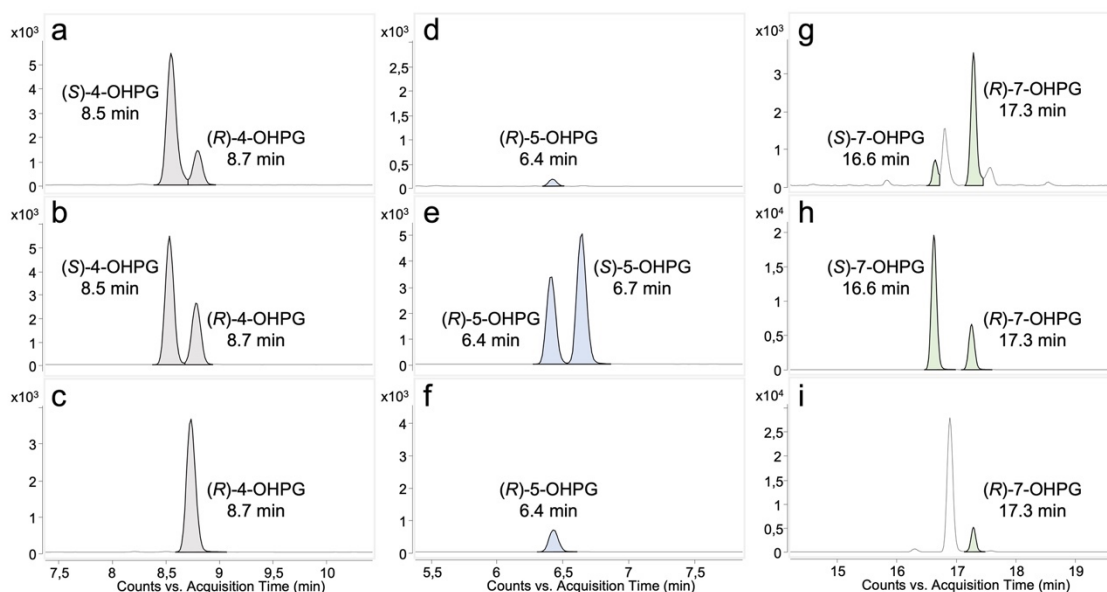


Figure 10. Chromatograms of 4-, 5- and 7-hydroxypropranolol diastereomeric glucuronides in urine sample and HLMs incubations. The displayed ion transitions are  $m/z$  452  $\rightarrow$  116 (4-OHPG), 452  $\rightarrow$  98 (5-OHPG) and 452  $\rightarrow$  276 (7-OHPG). OHPG, hydroxypropranolol glucuronide. (a), (d) and (g) refer to the analysis of urine sample (collected 17.6 h post administration). (b), (e) and (h) are from incubation of HLMs with ( $\pm$ )-4-hydroxypropranolol, ( $\pm$ )-5-hydroxypropranolol and ( $\pm$ )-7-hydroxypropranolol, respectively. (c), (f) and (i) were from HLMs incubated with (*R*)-propranolol, UDPGA and NADPH.

Targeted MS/MS analysis was performed on each diastereomer. Figure 11 showed the product ion spectra of (*R*)-5-OHPG, the loss of 176.0324 Da further confirmed the structure of hydroxypropranolol glucuronides. The fragment ion  $m/z$  234 resulted from protonated 5-OHP losing isopropyl group ( $-C_3H_6$ , 42 Da) after the cleavage of sugar.

The fragment ion  $m/z$  199 was considered to be generated by a combined elimination of water ( $-H_2O$ , 18 Da) and isopropylamine group ( $-C_3H_9N$ , 59 Da) from protonated 5-OHP. The fragment ion  $m/z$  173 resulted from the loss of the alcoholic side-chain ( $-C_5H_{13}ON$ , 103 Da) of protonated 5-OHP. The fragment ion  $m/z$  116 was considered to be generated by elimination of dihydroxy naphthyl ring ( $-C_{10}H_8O_2$ , 160 Da). The structures of these fragments have been demonstrated by previous study [169, 193] and were used to deduce the fragmentation of DMISC derivatives in section 4.3.2.

The product ion spectra of 4- and 7-OHPG were highly similar to Figure 11 and are shown in Supplementary Figure 1.

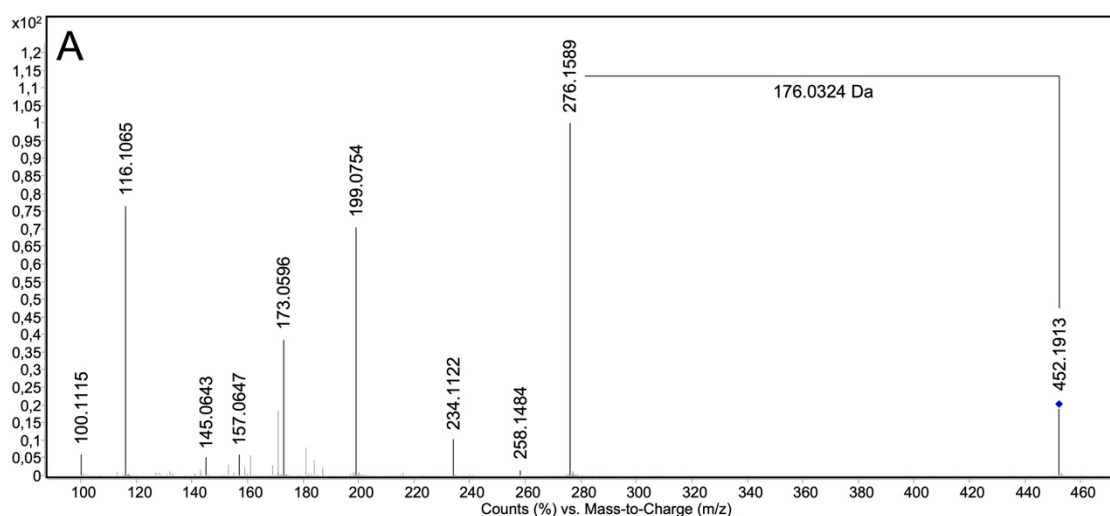


Figure 11. Product ion spectra (LC-QTOF-MS/MS) of (*R*)-5-hydroxypropranolol glucuronide obtained from HLMs incubations. (*R*)-5-hydroxypropranolol glucuronide,  $C_{22}H_{29}NO_9$ ,  $[M+H]^+$  theor. = 452.1915,  $[M+H]^+$  exp. = 452.1913,  $\Delta m/z$  = -0.44 ppm; collision energy 20 eV.

#### 4.2.2 Biotransformation of 4-, 5- and 7-OHP with 19 UGTs

It is reasonable to perform a reaction phenotyping on 4-, 5- and 7-OHP with 19 human UGTs from UGT1 and 2 families in order to find out which UGTs are responsible for their glucuronidation since their glucuronides were detected in both urine and HLM incubations (section 4.2.1). To accomplish it, the same experimental protocol used previously to investigate propranolol glucuronidation in section 4.1 was applied here.

Four UGTs, UGT1A7, UGT1A8, UGT1A9, and UGT2A1, were found to produce 4-OHPG (Figure 12, a1 to a4). Glucuronidation of 5-OHP was observed in eight UGTs, namely UGT1A1, 1A3, 1A7, 1A8, 1A9, 1A10, 2A1, and 2A2, with varying degrees of activity. These eight UGTs, along with UGT1A6, were also involved in the glucuronidation of 7-OHP. Although five extra UGTs were found to be involved in the glucuronidation of 5- and 7-OHP, UGT1A7, UGT1A8, UGT1A9, and UGT2A1 were found as most active isoforms for the glucuronidation of 5- and 7-hydroxypropranolol

(Figure 12). The activity of 19 UGTs towards racemic 4-, 5- and 7-OHP is summarized in Supplementary Table 3. The activity was determined by the chromatographical peak areas of produced OHPGs, respectively.

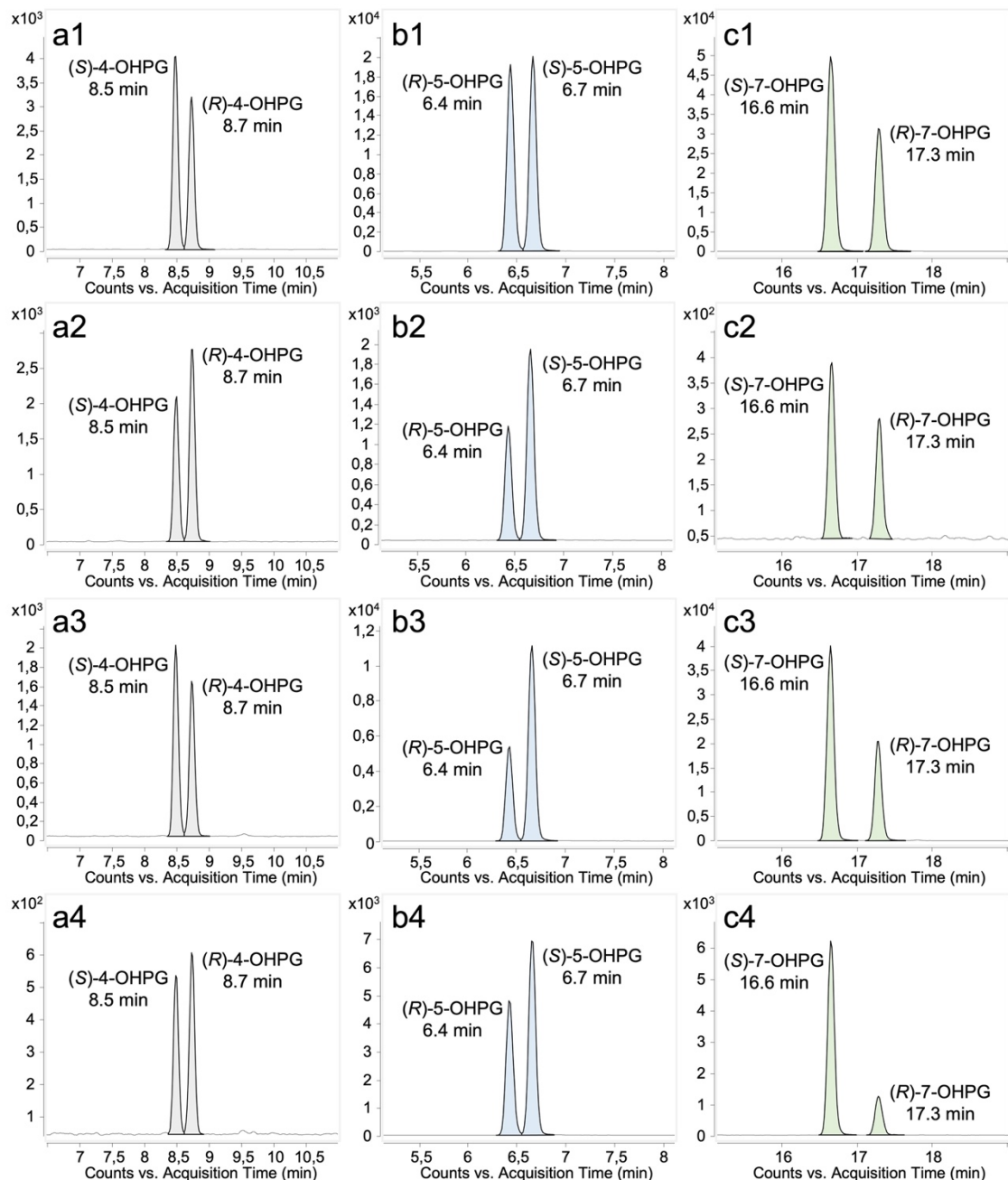


Figure 12. Chromatograms (LC-QQQ-MS/MS) of diastereomeric glucuronides of 4-, 5- and 7-hydroxypropranolol obtained from UGT-dependent enzyme bag samples. Ion transitions  $m/z$  452 $\rightarrow$ 116 (4-OHPG),  $m/z$  452 $\rightarrow$ 98 (5-OHPG) and  $m/z$  452 $\rightarrow$ 276 (7-OHPG) were monitored. (a1) (b1) (c1) were from UGT1A7 enzyme bags samples. (a2) (b2) (c2) were from UGT1A8 enzyme bags samples. (a3) (b3) (c3) were from UGT1A9 enzyme bags samples. (a4) (b4) (c4) were from UGT2A1 enzyme bags samples.

The determination of (R)- and (S)-diastereomers of 4-, 5-, and 7-OHPG was achieved by comparing the retention times presented in Figure 10, as shown for Figure 12. The glucuronidation of racemic 5-, and 7-OHP demonstrated stereoselectivity in the four

dominant UGTs: UGT1A7, UGT1A8, UGT1A9, and UGT2A1. Stereoselective preference for the glucuronidation of (*S*)-5-, and (*S*)-7-OHP was observed in the incubations with the four UGT enzyme bags, except for UGT1A7, which did not show obvious stereoselectivity towards racemic 5-OHP when compared to the other three UGTs (Figure 12, b1 to b4 and c1 to c4).

### 4.2.3 Discussion

Since the 1980s, mono-hydroxylated metabolites of propranolol, specifically 4-OHP, 5-OHP, and 7-OHP, have been detected in both human and rat urine [164, 173]. Among these, 4-OHP has long been recognized as the primary phase I metabolite of propranolol in humans and laboratory animals [164, 180, 194]. Together with sulfation, glucuronidation is an important elimination pathway of 4-OHP [182]. However, investigations into the phase II metabolism of the other two monohydroxylated metabolites, 5-OHP and 7-OHP, have been relatively limited. In this study, we conducted an investigation into the glucuronidation of 5-OHP and 7-OHP and compared the results with the glucuronidation of 4-OHP [126].

The glucuronidation of all three monohydroxylated phase I metabolites of propranolol was found to be carried out in the human body, as evidenced by the combined analysis of hydroxypropranolol glucuronidation in both *in vivo* (human urine) and *in vitro* (HLMs) samples (Figure 10). The results of reaction phenotyping of 4-, 5- and 7-OHP by 19 UGTs (Supplementary Table 3) indicated the involvement of nine UGTs in the glucuronidation of hydroxypropranolols. Importantly, the most active isoforms for the glucuronidation of 5- and 7-OHP were found to be the same as those identified for 4-OHP: UGT1A7, UGT1A8, UGT1A9, and UGT2A1. Furthermore, four additional UGTs, namely UGT1A1, UGT1A3, UGT1A10, and UGT2A2, were found to be active in the glucuronidation of 5-OHP. Moreover, UGT1A6 also exhibited certain glucuronidation activity towards 7-OHP, in addition to the aforementioned eight UGTs for 5-OHP.

It is worth noting that in both urine and HLMs samples (Figure 10a and 10b), (*S*)-4-OHPG is observed as the predominant metabolite. However, the results for 5- and 7-OHPG present a contradictory picture. Specifically, in the case of 5-OHPG, Figure 10d illustrates that only (*R*)-5-OHPG is detected in the urine sample, with no observation of (*S*)-5-OHPG, or the produced quantity being below the limit of detection. In contrast, in HLMs sample, (*S*)-5-OHPG is the dominant metabolite compared to (*R*)-5-OHPG. A similar contradictory outcome was also observed for 7-OHPG, with (*R*)-7-OHPG being the primary metabolite in urine sample (Figure 10g), while the reverse is true in HLMs sample (Figure 10h).

Previous research has consistently indicated that (*R*)-propranolol is the preferred substrate for hydroxylation at the 5- and 7-positions [168, 173, 194]. Given these findings, it is reasonable to infer that the observed preference for (*R*)-5-OHP (Figure 10d) and (*R*)-7-OHP (Figure 10g) may be a consequence of the stereoselective 5- and 7-hydroxylation of (*R*)-propranolol, rather than the stereoselective glucuronidation of (*R*)-5- and (*R*)-7-OHP. Furthermore, it's important to note that 4-hydroxylation of propranolol has been found to exhibit either minimal or no stereoselectivity in both urine samples and CYP2D6 incubations [168, 173]. Therefore, the stereoselectivity observed in the glucuronidation of 4-OHP remains consistent in both urine and HLMs samples (Figure 10a and 10b). These results emphasize the importance of phase I metabolism in explaining the variations between *in vitro* and *in vivo* data when studying the phase II metabolism of chiral drugs. Recognizing this factor is crucial when establishing correlations between *in vitro* and *in vivo* data for drug metabolism and pharmacokinetics studies.

Interestingly, an additional peak with a retention time of approximately 16.9 min was observed in both urine and HLM-(*R*)-propranolol incubation (Figure 10g and 10i). MS/MS analysis of this peak (Supplementary Figure 2) revealed that its fragmentation pattern was identical to that shown in Figure 11, suggesting that it may also be a glucuronic metabolite of hydroxypropranolol. One possible explanation could be that an additional glucuronide, different from the glucuronides depicted in Figure 10, may have been formed from 4-, 5-, or 7-OHP. However, such glucuronides were not detected at the same retention time in HLM-OHPs incubations or enzyme bags samples with OHPs as substrates. Therefore, it is unlikely that the peak at 16.9 min is related to the glucuronidation of 4-, 5-, or 7-OHP.

The other possibility is the potential formation of another hydroxypropranolol during the hydroxylation of propranolol, apart from 4-, 5-, and 7-OHP. Previous studies have detected 2-OHP in both rat and human samples, albeit in minor quantities [173]. Further investigations will be needed to determine whether the peak at 16.9 minutes corresponds to 2-OHP glucuronide or not.

### 4.3 Regioselectivity of hydroxypropranolols glucuronidation

#### 4.3.1 Pre-glucuronidation derivatization

Methoxypropranolols were tested as substrates to assess the regioselectivity of hydroxypropranolol glucuronidation. The rationale behind this method is that the aromatic hydroxy group is occupied by a methyl group, so if the glucuronides are aromatic-linked metabolites, no glucuronides would be produced. Thus, analysis of the

glucuronidation of methoxypropranolols allows the relevant reaction site of hydroxypropranolols for the same enzyme to be inferred.

4-MeOP was synthesized chemically using a method adapted from previous studies [168, 186]. The synthesis was stopped before the final demethylation step, and thus, 4-MeOP was obtained. The product was derivatized with MSTFA and analyzed by GC-MS for structure confirmation. The TMS-derivative of 4-MeOP was eluted at 8.27 min (Figure 13A). The MS showed the molecular ion  $M^{+\bullet}$  ( $m/z$  361.3) and the characteristic fragment ions  $m/z$  174.1 and  $m/z$  72.1 (Figure 13B). 5- and 7-MeOP synthesis follows the same procedure explained in section 3.2.5 but with 5- or 7-methoxy-1-naphthol as starting compounds.

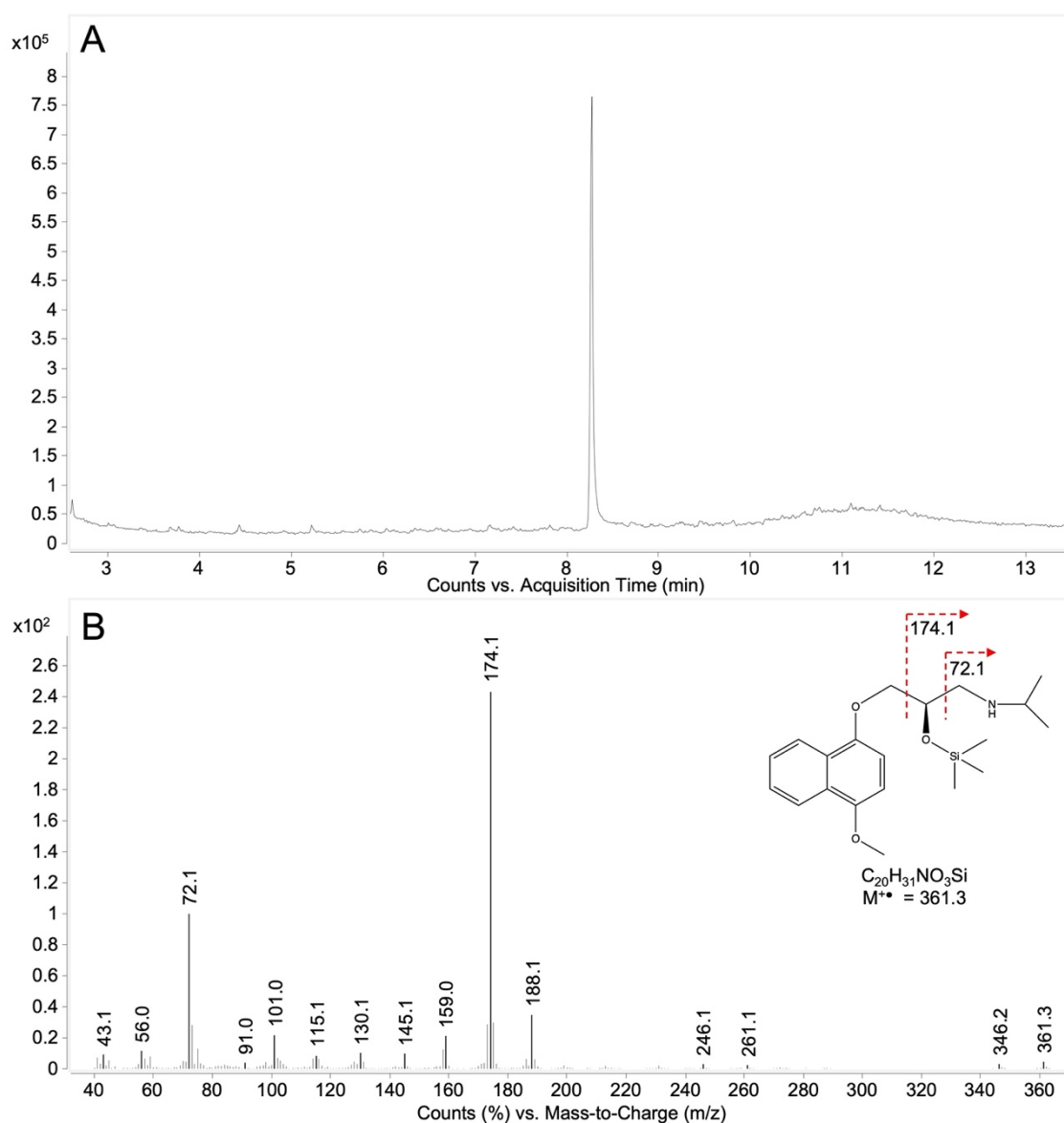


Figure 13. GC/MS analysis of O-TMS-derivative of 4-methoxypropranolol. (A) Total ion chromatogram, retention time 8.27 min; (B) MS spectra,  $M^{+\bullet} = m/z$  361.3

Due to their ability to glucuronidate 4-OHP, UGT1A7, UGT1A8, UGT1A9, and UGT2A1 were tested with 4-MeOP as substrate. UGT1A9 and 2A1 were found to glucuronidate 4-MeOP, producing two glucuronides, while UGT1A7 and UGT1A8 were inactive. Similarly, 5- and 7-MeOP were catalyzed by the 9 UGTs previously identified as active in the 5- and 7-OHP glucuronidation. LC-QQQ-MS/MS chromatograms of 4-, 5- and 7-MeOPG are shown in Figure 14. Because of the lack of enantiopure methoxypropranolols, the configuration of the two methoxypropranolol glucuronide diastereomers could not be assigned. Thus, they were labeled as glucuronide I and II. 4-MeOPG I was eluted at 13.3 min, and 4-MeOPG II was eluted at 13.6 min. 5-MeOPG I and II were eluted at 24.4 min and 26.1 min, while 7-MeOPG I and II were eluted at 25.7 min and 27.0 min, respectively. It may be hypothesized from the comparison of the elution orders of the propranolol enantiomers (Figure 7) that the earlier eluting methoxypropranolol glucuronide I corresponds to the (*R*)-enantiomer, while II may correspond to the (*S*)-form. However, further investigations are needed for confirmation.

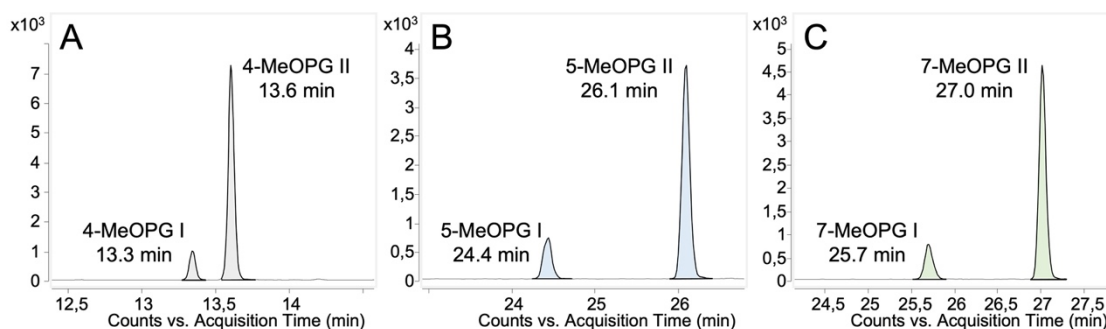


Figure 14. Chromatograms (LC-QQQ-MS/MS) of 4-, 5- and 7-methoxypropranolol glucuronic diastereomers obtained from UGT1A9 enzyme bag samples. The displayed ion transitions are  $m/z$  466 $\rightarrow$ 72 (A, 4-MeOPG),  $m/z$  466 $\rightarrow$ 290 (B, 5-MeOPG), and  $m/z$  466 $\rightarrow$ 116 (C, 7-MeOPG). 4-/5-/7-MeOPG, 4-/5-/7-methoxypropranolol glucuronide.

For 4-MeOP, only UGT1A9 and UGT2A1 showed their ability to glucuronidation. Among the tested 9 UGTs, 6 UGTs, (UGT1A1, UGT1A3, UGT1A7, UGT1A9, UGT1A10, and UGT2A1) have demonstrated their activity on the glucuronidation of 5- and 7-MeOP. The activity of each UGT in glucuronidation towards racemic 4-, 5- and 7-MeOP is summarized in Supplementary Table 4.

Additional MS/MS analyses were performed to characterize 4-, 5- and 7-MeOPG with high-resolution accurate mass spectrometry. The loss of 176.0312 Da indicated the loss of the glucuronic acid moiety (Figure 15). The product ion spectra of 4- and 7-MeOPGs were highly similar to 5-MeOPG (Figure 15) and are shown in (Supplementary Figure 3).

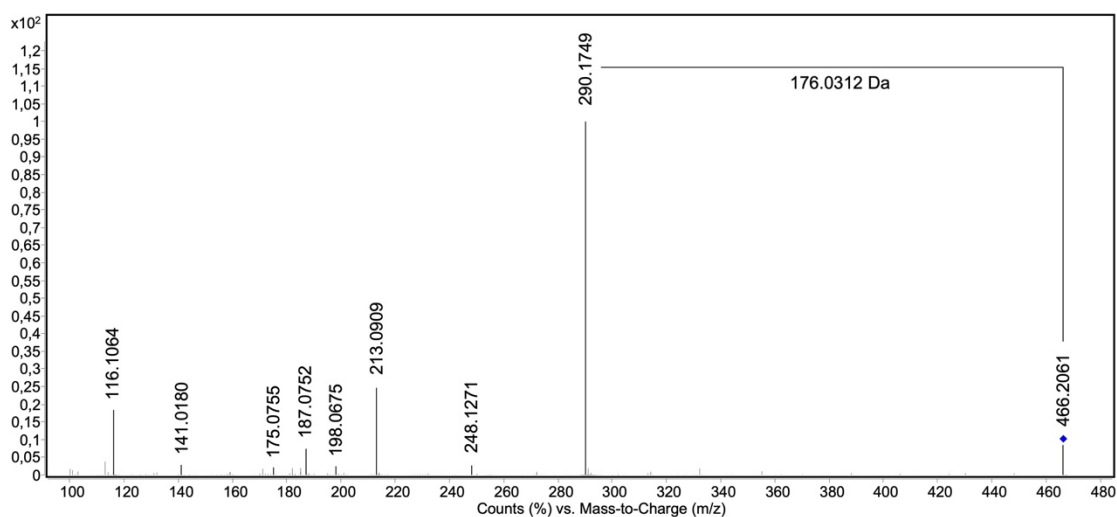


Figure 15. Product ion spectra (LC-QTOF-MS/MS) of 5-methoxypropranolol glucuronide obtained from UGT1A9 enzyme bag incubations. 5-methoxypropranolol glucuronide,  $C_{23}H_{31}NO_9$ ,  $[M+H]^+$  theor. = 466.2072,  $[M+H]^+$  exp. = 466.2061,  $\Delta m/z = -2.36$  ppm; collision energy 20 eV.

#### 4.3.1.1 Discussion

It is clear that the structural identification and assignment of the conjugative site of glucuronides is an important aspect in the study of pharmacology and toxicology. The example of morphine-6-glucuronide and morphine-3-glucuronide shows that different glucuronic regio-isomers may have vastly different properties [195]. In the case of propranolol, the CYP-catalyzed phase I reaction adds an aromatic hydroxy group, which raises a question about the regioselectivity of glucuronidation on hydroxypropranolols. Previous results about propranolol glucuronidation (section 4.1) have demonstrated that the aliphatic hydroxy group on the side chain can be glucuronidated. Therefore, it seems unlikely that glucuronidation of hydroxypropranolols only occurs at the aromatic hydroxy group. Tandem mass spectrometry analysis is a practical method for confirming the structure, as it offers less restrictions in terms of sample purity and concentration compared to NMR. However, direct fragmentation of glucuronides leads to the loss of the glucuronic acid, hampering the determination of the glucuronidation site. To address this issue, two methods were employed in the current study.

In section 4.3.1, a pre-glucuronidation derivatization was performed to investigate the glucuronidation position. 4-, 5- and 7-MeOP were incubated with the UGTs that were previously identified to be active in the glucuronidation of 4-, 5- and 7-OHP. The rationale behind this method is that the phenolic group is occupied by a methyl group, so if the glucuronides were aromatic-linked metabolites, no glucuronides would be produced. However, UGT1A1, 1A3, 1A7, 1A9, and 2A1 still exhibited varying abilities to glucuronidate the side-chain hydroxy group, as listed in Supplementary Table 4. Those

results indicated that glucuronidation can occur on the aliphatic hydroxy group under certain circumstances when the aromatic hydroxy group is blocked.

In my previous published paper [126], docking experiments between UGTs and 4-OHP were performed. The results suggested a different conformation of 4-OHP compared with propranolol. In this model, an additional cation- $\pi$  interaction between the aromatic ring of 4-OHP and Arg88 exists. Thus, the overall orientation of 4-OHP at the substrate-binding site significantly differs from that of propranolol.

Further docking experiments of UGTs with 4-MeOP indicated that there is no additional interaction between the methoxy group and the enzyme, suggesting that the conformation of UGTs with propranolol and 4-MeOP are equivalent. Therefore, it is concluded that the additional interactions with the aromatic hydroxy group play an important role in the binding conformation with UGTs. When the aromatic hydroxy group is occupied, UGTs may also glucuronidate the aliphatic hydroxy group instead. In that case, their binding conformation with the enzyme is the same as propranolol.

In the case of 4-MeOP glucuronidation, UGT1A9 and UGT2A1 show higher flexibility than other UGTs, as suggested by previous homology modeling and MD simulation results [126]. The movement of the enzymes will shift the relative position of substrate and cofactor, thus satisfying the distance requirement for both aromatic and aliphatic glucuronidation. It is reasonable to hypothesize that the situation of 5- and 7-MeOP glucuronidation are consistent with 4-MeOP. Further docking experiments may be considered to validate and gain more insights into the regioselectivity of these glucuronidation reactions, if necessary. These findings demonstrate that changes in important functional groups can influence the conformation of enzymes and substrates, resulting in changes in the site of metabolism.

### 4.3.2 Post-glucuronidation derivatization

#### 4.3.2.1 DMISC derivatives of propranolol and hydroxypropranolols

The full-scan analysis of HLM incubations after derivatization with DMISC shows the molecular ion  $[M+H]^+$  of the DMISC derivatives of propranolol and 5-OHP, as illustrated in Figure 16. Previous studies indicated that DMISC is phenolic selective but can also react with secondary amines when added with excess amount [169, 187, 188]. Indeed, propranolol yielded one DMIS derivative (Figure 16A). Due to a lack of a phenolic hydroxy group, this was tentatively assigned to the *N*-derivatized propranolol. In the case of hydroxypropranolol, two derivatives were observed, i.e. *O*-DMIS and *N,O*-bis-DMIS derivatives (Figure 16B and 16C). Targeted MS/MS analysis was performed on the precursor corresponding to protonated propranolol-DMIS ( $m/z$  418), 5-OHP-*O*-DMIS ( $m/z$  434), as shown in Figure 17A and 17B. All fragments of

(*R*)-propranolol-DMIS and 5-OHP-DMIS are summarized in Table 5 and Table 6, respectively. The fragmentation of underivatized propranolol and 5-OHP demonstrated in section 4.1.1 and section 4.2.1 are used for the interpretation of Figure 17.

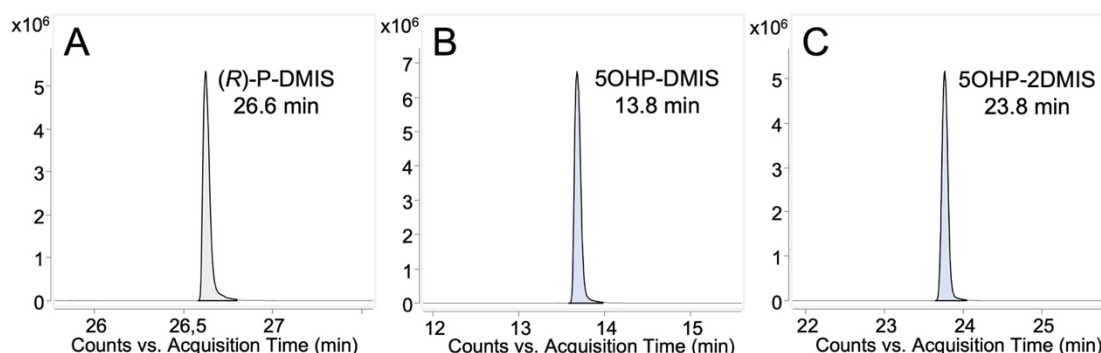


Figure 16. Extracted ion chromatograms obtained from MS full-scan analysis (LC-QTOF-MS) of DMIS derivatives of propranolol and 5-hydroxypropranolol. (A) (*R*)-P-DMIS,  $[M+H]^+$   $m/z$  418, single-DMIS-derivatized (*R*)-propranolol. (B) 5OHP-DMIS,  $[M+H]^+$   $m/z$  434, single DMIS-derivatized 5-hydroxypropranolol. (C) 5OHP-2DMIS,  $[M+H]^+$   $m/z$  592, double DMIS-derivatized 5-hydroxypropranolol. OHP, hydroxypropranolol.

Table 5. Postulated fragments, elementary composition, their theoretical mass, observed mass, and the resulting mass differences for (*R*)-propranolol DMIS, corresponding to Figure 17A.

Postulated fragment	Elementary composition	Theoretical mass ( $m/z$ )	Experimental mass ( $m/z$ )	Mass error (ppm)
$[M+H]^+$	$[C_{21}H_{28}N_3O_4S]^+$	418.1795	418.1797	0.48
$[M+H-C_3H_6]^+$	$[C_{18}H_{22}N_3O_4S]^+$	376.1326	376.1332	1.60
$[M+H-C_3H_6-H_2O]^+$	$[C_{18}H_{20}N_3O_3S]^+$	358.1220	358.1212	-2.23
$[M+H-C_{10}H_8O]^+$	$[C_{11}H_{20}N_3O_3S]^+$	274.1220	274.1214	-2.19
$[M+H-C_{10}H_8O-C_3H_6]^+$	$[C_8H_{14}N_3O_3S]^+$	232.0750	232.0752	0.86
$[M+H-C_{10}H_8O-C_3H_6-H_2O]^+$	$[C_8H_{12}N_3O_2S]^+$	214.0645	214.0642	-1.40
$[DMIS-NCH_2+H]^+$	$[C_6H_{10}N_3O_2S]^+$	188.0488	188.0487	-0.53
$[DMIS-NH_2+H]^+$	$[C_5H_{10}N_3O_2S]^+$	176.0488	176.0488	0.00

The postulated structure of those fragments were listed in Supplementary Table 5.

As shown in Table 5, ions  $m/z$  376.1332 and  $m/z$  358.1212 are generated from the precursor ion  $m/z$  418.1797 after loss of the isopropyl group ( $-C_3H_6$ , 42 Da) and water ( $-H_2O$ , 18 Da). The ion  $m/z$  274.1214 may be explained by the loss of the hydroxy naphthyl ring ( $-C_{10}H_8O$ , 144 Da) from precursor ion  $m/z$  418.1797. The additional loss

of the isopropyl group and water results in  $m/z$  232.0752 and  $m/z$  214.0642. In the propranolol-DMIS derivative, the basic dimethylimidazole ring probably got protonated as demonstrated in previous study [169], generating charged fragments  $m/z$  188.0487 and  $m/z$  176.0488 that still contain DMIS moiety.

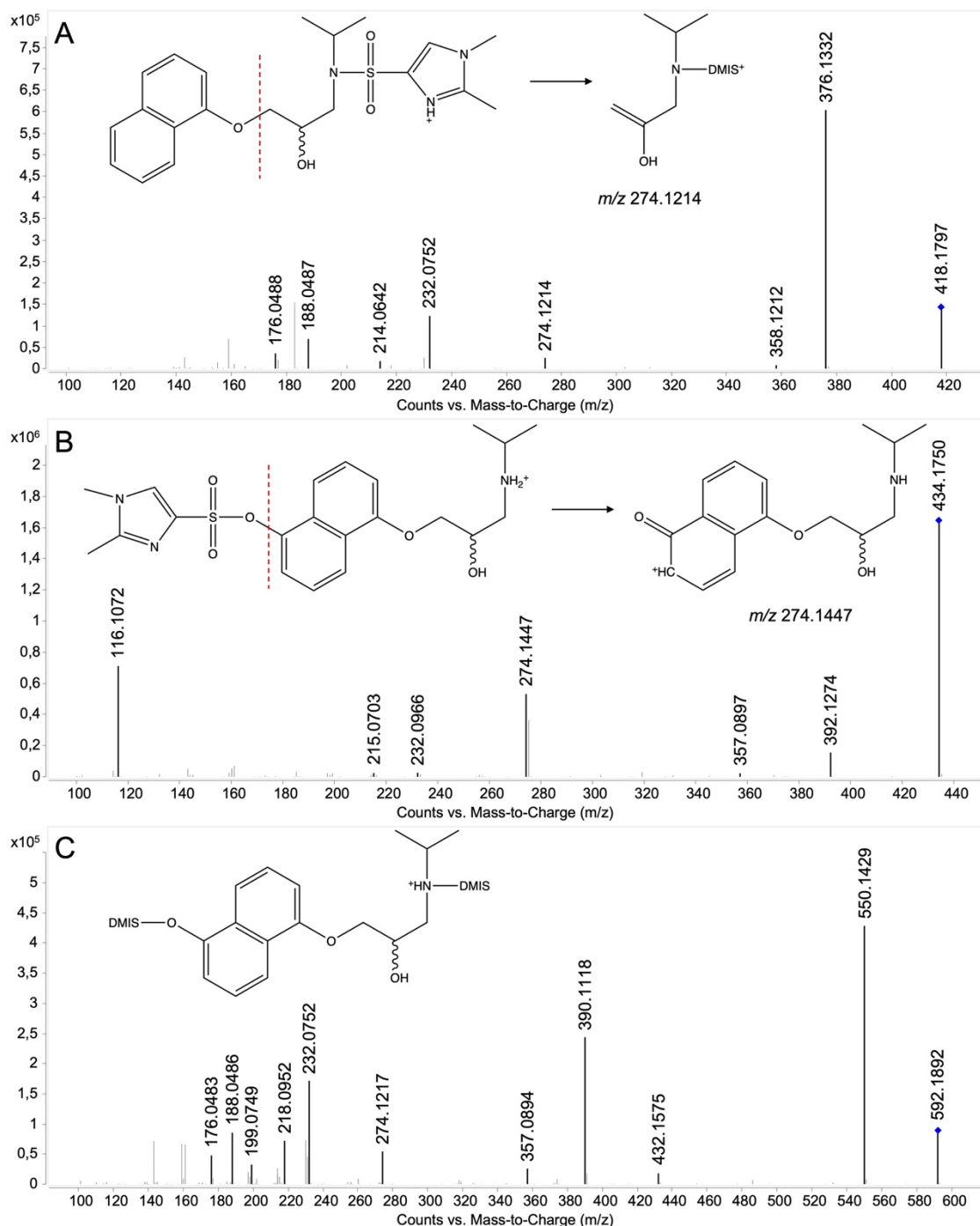


Figure 17. Product ion spectra of (*R*)-propranolol and 5-hydroxypropranolol DMISC derivatives. (A) (*R*)-propranolol-DMIS,  $C_{21}H_{27}N_3O_4S$ , corresponding to the peak in Figure 16A, collision energy 20 eV. (B) 5-hydroxypropranolol-DMIS,  $C_{21}H_{27}N_3O_5S$ , corresponding to the peak in Figure 16B, collision energy 20 eV. (C) 5-hydroxypropranolol-2DMIS,  $C_{26}H_{33}N_5O_7S_2$ , corresponding to the peak in Figure 16C, collision energy 30 eV. DMIS, dimethylimidazole-4-sulfonyl.

In contrast, the fragmentation pattern of 5-OHP-DMIS is distinctly different (Figure 17B). As shown in Table 6, the ion  $m/z$  392.1274 derived from the protonated precursor ion  $m/z$  434.1750 by losing the isopropyl group. Fragment  $m/z$  357.0897 indicates a loss of 77 Da from  $[M+H]^+$  ( $m/z$  434.1750), which is suggested to result from the combined elimination of water ( $-H_2O$ , 18 Da) and isopropylamine ( $-C_3H_9N$ , 59 Da). As demonstrated in the study about DMISC derivatives of 4-OHP by Salomonsson *et al.*[169], the DMIS moiety is suggested to be lost as a neutral sulfone, resulting in the fragment  $m/z$  274.1447 with the charge on the naphthyl ring (Figure 17B). The subsequent loss of isopropyl ( $-C_3H_6$ , 42 Da) or isopropylamine group generates  $m/z$  232.0966 or  $m/z$  215.0703. Fragment  $m/z$  116.1072 indicates the intact aminoalcoholic chain without DMIS attached. Notably, in the high-resolution mass spectrum, the ions  $m/z$  274.1447 and  $m/z$  232.0966 have different digits after the decimal point, compared with the ions  $m/z$  274.1214 and  $m/z$  232.0752 obtained from propranolol-DMIS ( $m/z$  418.1797, Figure 17A) indicating that their structures were different and therefore can be used for identification given a resolution over 10,000.

Table 6. Postulated fragments, elementary composition, their theoretical mass, observed mass, and the resulting mass differences for single-DMIS-derivatized 5-hydroxypropranolol, corresponding to Figure 17B.

Postulated fragment	Elementary composition	Theoretical mass ( $m/z$ )	Experimental mass ( $m/z$ )	Mass error (ppm)
$[M+H]^+$	$[C_{21}H_{28}N_3O_5S]^+$	434.1744	434.1750	1.38
$[M+H-C_3H_6]^+$	$[C_{18}H_{22}N_3O_5S]^+$	392.1275	392.1274	-0.26
$[M+H-C_3H_9N-H_2O]^+$	$[C_{18}H_{17}N_2O_4S]^+$	357.0904	357.0897	-1.96
$[M+H-DMIS]^+$	$[C_{16}H_{20}NO_3]^+$	274.1438	274.1447	3.28
$[M+H-DMIS-C_3H_6]^+$	$[C_{13}H_{14}NO_3]^+$	232.0968	232.0966	-0.86
$[M+H-DMIS-C_3H_9N]^+$	$[C_{13}H_{11}O_3]^+$	215.0703	215.0703	0.00
$[M+H-DMIS-C_{10}H_8O]^+$	$[C_6H_{14}NO]^+$	116.1070	116.1072	0.00

The postulated structure of those fragments were listed in Supplementary Table 6.

The MS full-scan analysis of the DMISC derivative of 5-OHP revealed that DMIS may attach to both the phenolic and the secondary amine groups when derivatization reagent is added in excess (Figure 16C). To further investigate this, a targeted MS/MS analysis of the corresponding 2-fold derivatized 5-OHP (precursor  $m/z$  592) was performed. The resulting spectra (Figure 17C) show combined fragmentation pathways

from P-DMIS and 5-OHP-DMIS. Table 7 shows all fragments of double-DMIS-derivatized 5-OHP. Two DMIS moieties were inferred to be attached based on the detection of ion  $m/z$  550.1429, which was generated by the loss of an isopropyl group ( $-C_3H_6$ , 42 Da) from the precursor ion  $m/z$  592.1892. The loss of aromatic-linked DMIS moiety from precursor ion results in the ion  $m/z$  432.1575. The loss of aromatic-linked DMIS moiety from ion  $m/z$  550.1429 results in the ion  $m/z$  390.1118. Comparison with Figure 17A indicates that the ions  $m/z$  218.0952, 188.0486, and 176.0483 are fragments where DMIS was attached to the amine group. Similarly, the ion  $m/z$  357.0894 is a fragment where DMIS is attached to the phenolic group. The ion  $m/z$  199.0749 is considered as that protonated precursor ion  $m/z$  592.1892 losing both DMIS moieties, isopropylamine ( $-C_3H_9N$ , 59 Da) and water ( $-H_2O$ , 18 Da). The ions  $m/z$  274.1217 and  $m/z$  232.0752 are supposedly fragments where DMIS was amine-linked because the digits after the decimal point were closer to the fragment ions produced by protonated propranolol-DMIS (Figure 17A).

Table 7. Postulated fragments, elementary composition, their theoretical mass, observed mass, and the resulting mass differences for double-DMIS-derivatized 5-hydroxypropranolol, corresponding to Figure 17C.

Postulated fragment	Elementary composition	Theoretical mass ( $m/z$ )	Experimental mass ( $m/z$ )	Mass error (ppm)
$[M+H]^+$	$[C_{26}H_{34}N_5O_7S_2]^+$	592.1894	592.1892	-0.33
$[M+H-C_3H_6]^+$	$[C_{23}H_{28}N_5O_7S_2]^+$	550.1425	550.1429	0.73
$[M+H-DMIS]^+$	$[C_{21}H_{26}N_3O_5S]^+$	432.1588	432.1575	-3.00
$[M+H-C_3H_6-DMIS]^+$	$[C_{18}H_{20}N_3O_5S]^+$	390.1118	390.1118	0.00
$[M+H-DMIS-C_3H_9N-H_2O]^+$	$[C_{18}H_{17}N_2O_4S]^+$	357.0904	357.0894	-2.80
$[M+H-DMIS-C_{10}H_8O]^+$	$[C_{11}H_{20}N_3O_3S]^+$	274.1220	274.1217	-1.09
$[M+H-DMIS-C_{10}H_8O-C_3H_6]^+$	$[C_8H_{14}N_3O_3S]^+$	232.0750	232.0752	0.86
$[NH_2-(CH_3)_2-DMIS]^+$	$[C_8H_{16}N_3O_2S]^+$	218.0958	218.0952	-2.75
$[M+H-2DMIS-C_3H_9N-H_2O]^+$	$[C_{13}H_{11}O_2]^+$	199.0754	199.0749	-2.51
$[DMIS-NCH_2+H]^+$	$[C_6H_{10}N_3O_2S]^+$	188.0488	188.0486	-1.06
$[DMIS-NH_2]^+$	$[C_5H_{10}N_3O_2S]^+$	176.0488	176.0483	-2.84

The postulated structure of those fragments were listed in Supplementary Table 7.

Full-scan and MS/MS analyses were performed on the DMISC derivatives (one-fold and two-fold derivatives) of 4-OHP (Supplementary Figure 4 and Supplementary Figure 5) and 7-OHP (Supplementary Figure 6 and Supplementary Figure 7) as well. The resulting fragmentation patterns were found to be highly similar to those of 5-OHP-DMIS and 5-OHP-2DMIS. Furthermore, additional full-scan analyses were conducted in search of aliphatic-linked DMISC derivatives of propranolol and hydroxypropranolols, but no such derivatives were detected. These results are in line with earlier reports that such derivatization does not occur on the aliphatic hydroxy group located on the side chain.

#### 4.3.2.2 DMISC derivatives of hydroxypropranolol glucuronides

The full-scan LC-MS analysis of hydroxypropranolol glucuronide-DMIS derivatives shows chromatographic peaks at  $m/z$  610 for 5- and 7-OHPG-DMISC derivatives (Figure 18). Four DMIS derivatives of 5-OHPG were observed and indicated as 5-OHPG-DMIS I, II, III, and IV with retention times of 13.7 min, 14.0 min, 16.3 min, and 17.6 min. In Figure 18B, two DMISC derivatives of 7-OHPG were found and indicated as 7-OHPG-DMIS I and II with retention times of 22.4 min and 22.8 min.

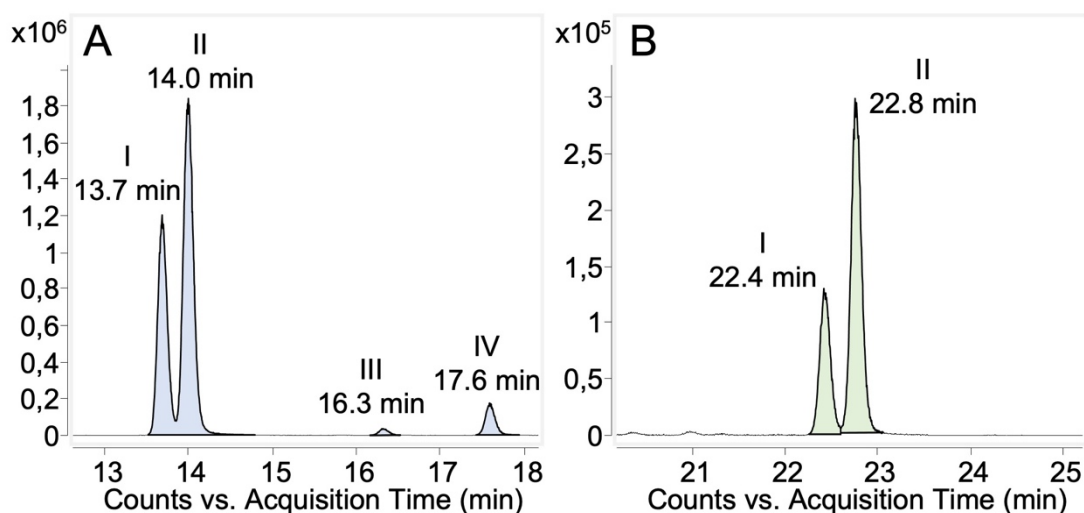


Figure 18. Extracted ion chromatograms from MS full-scan (LC-QTOF-MS) of HLMs-generated 5- and 7-hydroxypropranolol derivatized with DMISC. (A)  $[M+H]^+$   $m/z$  610, 5-hydroxypropranolol glucuronide DMISC derivatives; (B)  $[M+H]^+$   $m/z$  610, 7-hydroxypropranolol glucuronide DMISC derivatives.

A targeted MS/MS analysis was conducted on 5-OHPG-DMIS I, II, III, and IV. Two pairs of similar product ion spectra of 5-OHPG-DMIS (I and II as well as III and IV) were obtained. Therefore, only the 5-OHPG-DMIS I and III spectra are displayed in Figure 19A and Figure 19B. In Figure 19A, the product ion  $m/z$  568.1611 indicated the

loss of the isopropyl moiety from the protonated precursor  $m/z$  610.2077. The additional loss of the sugar moiety (from  $m/z$  610.2077) resulted in  $m/z$  434.1779. The ion  $m/z$  392.1314 is derived from the additional loss of an isopropyl group from  $m/z$  434.1779. The ions  $m/z$  214.0670, 188.0504, and 176.0500 are produced from the fragments where the DMIS moiety is attached to the amine group. Additionally, the ions  $m/z$  274.1250 and 232.0776 are considered fragments where DMIS was amine-linked because their accurate mass are closer to the fragment ions generated from protonated propranolol-DMIS (Figure 17A). Therefore, it was concluded that 5-OHPG-DMIS I and II are phenolic-linked glucuronides since DMIS was attached to the amine group.

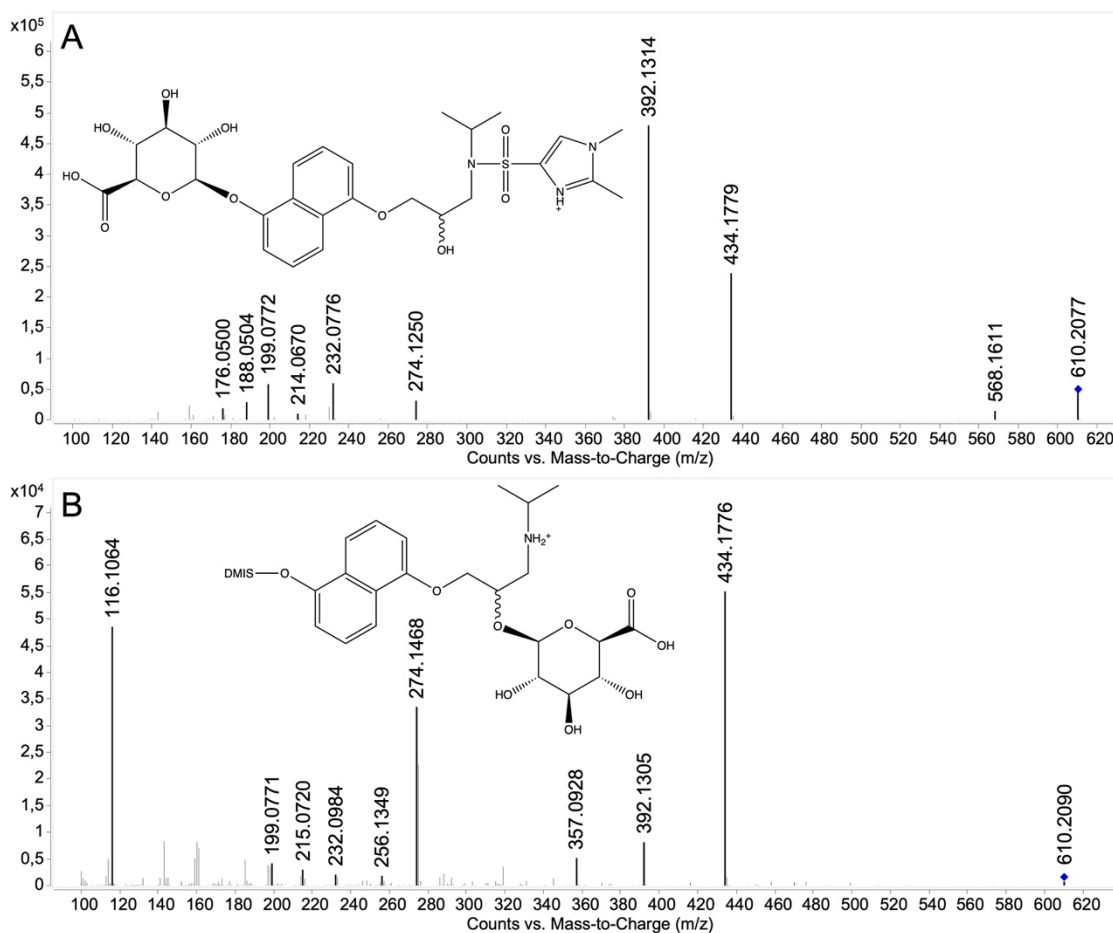


Figure 19. Product ion spectra of 5-hydroxypropranolol glucuronides DMIS derivatives obtained from HLMs samples after derivatization. (A) 5-hydroxypropranolol glucuronide-DMIS I,  $C_{27}H_{35}N_3O_{11}S$ ,  $[M+H]^+$  theor. = 610.2065,  $[M+H]^+$  exp. = 610.2077,  $\Delta m/z$  = 1.97 ppm, collision energy 30 eV, (B) 5-hydroxypropranolol glucuronide-DMIS III,  $C_{27}H_{35}N_3O_{11}S$ ,  $[M+H]^+$  theor. = 610.2065,  $[M+H]^+$  exp. = 610.2090,  $\Delta m/z$  = 4.10 ppm, collision energy, 30 eV.

Conversely, as shown in Figure 19B, the ions  $m/z$  357.0928 and 215.0720 are derived from the fragments where DMIS was attached to the phenolic group. The ion  $m/z$  392.1305 also results from the subsequent loss of the isopropyl group from  $m/z$  434.1779. Besides, the ions  $m/z$  274.1468 and 232.0984 are identified as fragments

where DMIS is phenolic-linked, considering their accurate mass are closer to that of the fragment ions generated from protonated 5-OHP-DMIS with DMIS moiety attached to the phenol group (Figure 17B). Therefore, 5-OHPG-DMIS III and IV are considered aliphatic-linked glucuronides since the DMIS was attached to the phenolic group.

#### 4.3.2.3 Discussion

Although the pre-glucuronidation method demonstrated that aliphatic hydroxy groups of hydroxypropranolols can be glucuronidated (section 4.3.1), direct methods for determination of the regio-isomeric hydroxypropranolol glucuronides is required. Therefore, a post-glucuronidation derivatization strategy was applied. During the 1980s, researchers investigated the regioselectivity of 4-hydroxypropranolol glucuronidation using GC-MS after derivatization with diazomethane [184]. The resulting 4-OHPG obtained from both *in vivo* and *in vitro* assays were found to be linked to the aromatic hydroxy group. However, it is important to note that diazomethane is a highly reactive and potentially hazardous compound, requiring proper precautions and protective equipment during handling [196]. As an alternative, 1,2-dimethylimidazole-4-sulfonyl chloride (DMISC) has been utilized as a new derivatization reagent for phenolic compounds and has been successfully employed in the derivatization of various compounds, including propofol, hydroxypyrene, naphthol, estrone, and others [188, 189]. Furthermore, DMISC has effectively confirmed the glucuronidation position of 4-OHPG [169]. In that study, Salomonsson *et al.* discovered that both aromatic-linked and aliphatic-linked 4-OHPG were formed under *in vitro* conditions.

Thus, DMISC was employed to differentiate 5- and 7-OHPG regio-isomers in this study. Following incubation of 5-, and 7-OHP with HLMs and UDPGA for 24 hours, the solutions were subjected to derivatization using DMISC. For comparison, propranolol and hydroxypropranolols were also incubated with DMISC, and all derivative samples were analyzed by full-scan and targeted MS/MS by LC-QTOF-MS. Moreover, 4-OHP was incubated with HLMs and the generated 4-OHPG was derivatized with DMISC as well. The derivatives were also analyzed for additional confirmation of this protocol developed by Salomonsson *et al.* [169].

Four DMISC derivatives of 5-OHPG were observed in the 24-hour-incubated HLMs sample after the derivatization. However, in the urine sample and 4-hour-incubated HLMs sample (Figure 10d and 10e), two 5-OHPGs were observed, which raising an intriguing question. To gain further insights, additional LC-QQQ-MS/MS analysis was conducted on the 24-hour-incubated HLMs sample prior to derivatization with DMISC. In this analysis, the two 5-OHPGs that previously identified in Figure 10d and 10e were intentionally excluded by cutting off from the MS analysis based on the retention time

(go to the waste), in order to eliminate the influence of their high signals. Interestingly, this led to the observation of two additional glucuronides, eluted at 15.0 min and 16.4 min (Supplementary Figure 8 and Supplementary Figure 9). However, it is worth noting that these glucuronides exhibited much lower abundance than the two 5-OHPGs previously identified in Figure 10d and 10e. This finding suggests that these newly identified glucuronides may be minor metabolites.

Therefore, it is hypothesized that the two less abundant 5-OHPG-DMIS derivatives, 5-OHPG-DMIS III and IV (Fig. 18A), could have originated from these two additional glucuronides, as they were similarly less abundant. Consequently, the two additional 5-OHPGs observed in HLMs-24 hour incubations are believed to be the aliphatic-linked hydroxypropranolol glucuronides, which making the previously identified 5-OHPGs in urine, 4-hour-incubated HLMs sample, and enzyme bags samples aromatic-linked hydroxypropranolol glucuronides.

The same LC-QQQ-MS/MS analysis was conducted on urine samples 4-hour-incubated HLMs sample and enzyme bags samples. Such extra glucuronides, eluted at 15.0 min and 16.4 min, were detected in enzyme bags samples, but not in urine sample and 4-hour-incubated HLMs sample. The possible explanation is that the HLMs samples used for derivatization were incubated with a higher concentration of 5-OHP and a prolonged incubation time of 24 hours. Similarly, the enzyme bags samples were incubated with a long period of 15 hours. Under such reaction conditions, it is possible that more glucuronides may be generated. However, *in vivo* metabolic studies have suggested that 5-OHP accounts for only 7% to 11% of the total monohydroxylated propranolol [164, 173], which is a relatively low concentration to produce additional aliphatic-linked glucuronides. Therefore, no extra 5-OHPG were found in urine. It is hypothesized that the 5-OHPG observed in urine (Figure 10d) may be related to the amine-linked DMISC derivative (Figure 18 A) and is considered to be aromatic-linked hydroxypropranolol glucuronide. Due to the complexity of urine samples, derivatization with DMISC gave more complicated results to interpret. Further derivatization experiments with isolated 5-OHPGs from urine samples will be needed for the confirmation of inference above.

Product ion spectra of 7-OHPG-DMIS I and II (Supplementary Figure 10) showed the same fragmentation pattern as 5-OHPG-DMIS I (Figure 19A). Therefore, the two derivatives of 7-OHPG were assigned to amine-linked DMISC derivatives. Thus, the diastereomeric glucuronides of 7-OHP were considered to be aromatic-linked glucuronides since the glucuronic acid occupied the phenolic hydroxy group and thereby has not been derivatized.

As a positive control and double confirmation of the feasibility of post-glucuronidation derivatization method which is adapted from the previous study [169], same derivatization reaction were conducted on (S)-4-OHPG (derived from HLMs incubations) and the samples were analyzed by full-scan MS and target MS/MS. The chromatograms and product ion spectra of (S)-4-OHPG-DMIS I and II are shown in Supplementary Figure 11 and Supplementary Figure 12. The product ion spectra indicated that (S)-4-OHPG-DMIS I and II are aromatic-linked glucuronide and aliphatic-linked glucuronide after comparing their fragmentation pattern with those of 5-OHPG-DMIS (Figure 19). Those results are in line with the previous study [169] that both aromatic and aliphatic-linked glucuronides of 4-OHP are able to be generated under *in vitro* conditions.

In summary, the findings from both pre- and post-derivatization studies indicate that the aliphatic hydroxy group of hydroxypropranolol can undergo glucuronidation in principle. However, under the *in vivo* environment, it appears to be less favorable compared to aromatic-linked glucuronidation. On the other hand, *in vitro* studies with high concentrations of hydroxypropranolols and extended incubation time demonstrated the possibility of aliphatic-linked glucuronidation. Overall, it can be concluded that under physiological conditions, aromatic-linked glucuronidation is the preferred glucuronic pathway for the elimination of hydroxypropranolols.

## 4.4 Glucosidation of propranolol and hydroxypropranolols

### 4.4.1 *In vitro* metabolism with HLMs

The investigation on glucosidation of propranolol and hydroxypropranolols was performed using HLMs as starting point. Racemic propranolol or 4-/5-/7-OHP were subjected to incubation with HLMs and UDP-glucose. Two diastereomeric propranolol glucosides were eluted at 23.5 min and 24.2 min (Figure 20). The diastereomers were identified as (S)- and (R)- by comparison with enantiopure (R)-propranolol incubation (Figure 20B). However, no hydroxy propranolol glucosides were detected, so further glucosidation by enzyme bags of respective UGTs was not carried out.

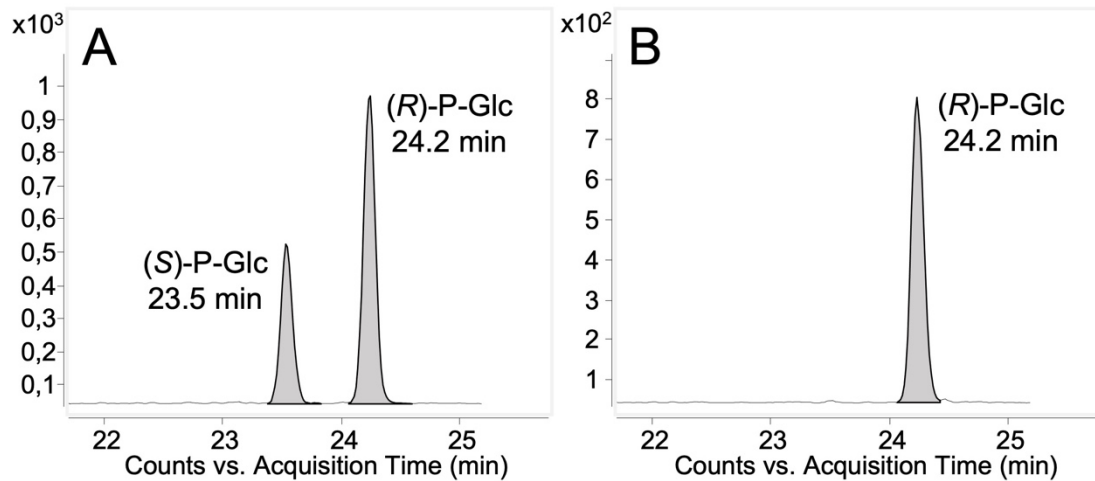


Figure 20. Chromatograms (LC-QQQ-MS/MS) of (S)- and (R)-propranolol glucoside from HLMs incubations. (A) HLMs incubation with racemic propranolol; (B) HLMs incubated with (R)-propranolol. The displayed ion transition is  $m/z$  422 $\rightarrow$ 260.

#### 4.4.2 Glucosidation of propranolol with four human UGTs

The activity of UGT1A7, UGT1A9, UGT1A10, and UGT2A1 on propranolol glucosidation was tested using the enzyme bag method, as these four UGTs have demonstrated their ability for glucuronidation in previously presented work (section 4.1). All four UGTs were found to be active in glucosidation of racemic propranolol, producing two diastereomers (Figure 21).

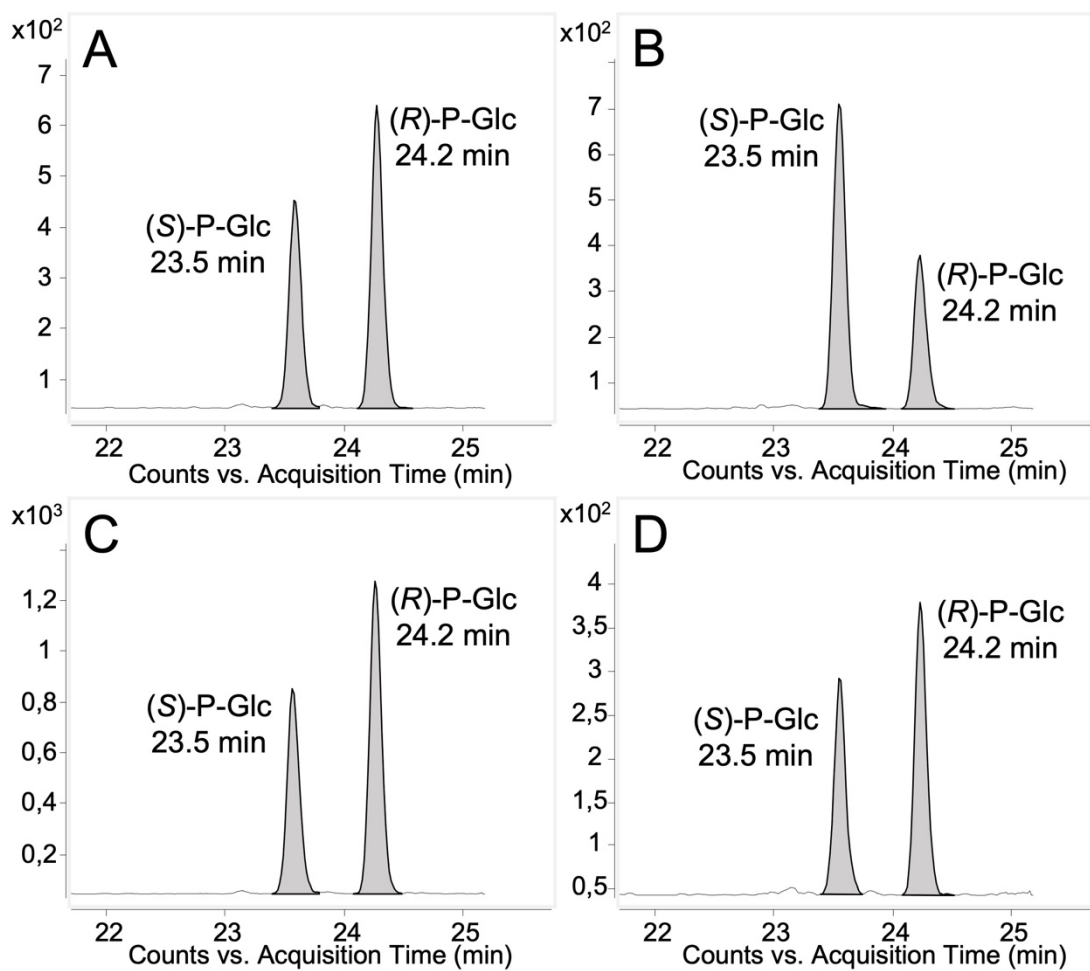


Figure 21. Chromatograms (LC-QQQ-MS/MS) of (S)- and (R)-propranolol glucoside from enzyme bag samples. (A) obtained from UGT1A7 enzyme bag samples. (B) obtained from UGT1A9 enzyme bag samples. (C) obtained from UGT1A10 enzyme bag samples. (D) obtained from UGT2A1 enzyme bag samples. The displayed ion transition is  $m/z$  422 $\rightarrow$ 260.

Further MS/MS analysis was carried out to characterize propranolol glucosides using high-resolution accurate mass spectrometry. The product ion spectra is shown in Figure 22, and the loss of 162.0493 Da indicates the loss of the glucose moiety. The fragment ions  $m/z$  116 and  $m/z$  183 can also be found in the product ion spectra of propranolol glucuronide (Figure 9). The ions  $m/z$  183 was generated by a combined elimination of water ( $-H_2O$ , 18 Da) and isopropylamine ( $-C_3H_9N$ , 59 Da) from protonated propranolol after losing the sugar moiety. The ions  $m/z$  116 was results from the loss of hydroxy naphthyl ring ( $-C_{10}H_8O$ , 144 Da) from protonated propranolol. The two additional ions  $m/z$  157 and  $m/z$  218 that indicated in Figure 22 were considered to be generated by losing the alcoholic side-chain ( $-C_5H_{13}ON$ , 103 Da) and by losing isopropyl group ( $-C_3H_6$ , 42 Da) from protonated propranolol.

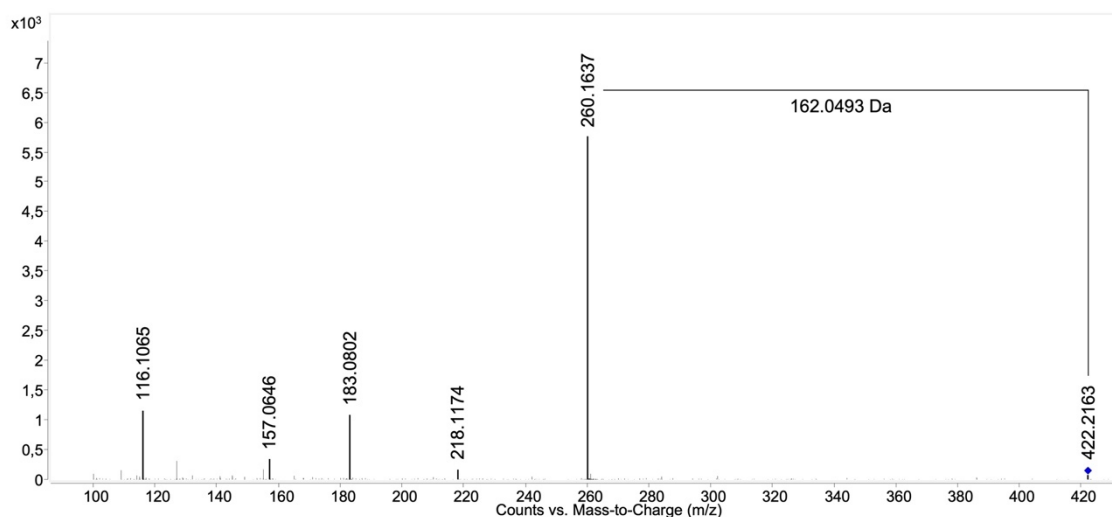


Figure 22. Product ion spectra (LC-QTOF-MS) of (R)-propranolol glucoside obtained from HLMs incubations. (R)-propranolol glucoside,  $C_{22}H_{31}NO_7$ ,  $[M+H]^+$  theor. = 422.2173,  $[M+H]^+$  exp. = 422.2163,  $\Delta m/z = -2.37$  ppm; collision energy, 30 eV.

#### 4.4.3 Discussion

Besides glucuronidation, UGTs are known to catalyze glucosidation reactions of various endobiotics and xenobiotics using UDP-glucose as the sugar donor. For instance, bilirubin can undergo glucosidation catalyzed by human UGT1A1 in addition to glucuronidation [83]. UGT2B7 has been found to catalyze the glucosidation of hydoxycholeic acid, ibuprofen, and morphine [85, 86, 89, 91]. These studies indicate that glucosidation can serve as an alternative metabolic pathway under certain circumstances.

Given this background, it is of great interest to investigate whether the UGTs involved in the glucuronidation of propranolol can also utilize UDP-glucose for conjugative reactions. In the current study, four UGTs (UGT1A7, UGT1A9, UGT1A10 and UGT2A1), which have demonstrated their ability for glucuronidation in previously presented work, were tested with propranolol and UDP-glucose. The results suggested that all four UGTs were capable of catalyzing the glucosidation of propranolol. Additional analysis were performed on urine samples as well, but no glucosides were observed.

UDP-glucose 6-dehydrogenase (UGDH), the enzyme responsible for converting UDP-glucose to UDP-glucuronic acid, is expressed in various human tissues but exhibits prominent expression in the liver and gastrointestinal tract [197]. On the other hand, UGT1A7, UGT1A9, and UGT2A1 are predominantly expressed in the proximal digestive tract, kidney, and endocrine tissues, according to data from the Human Protein Atlas database [198]. Based on this information, it can be inferred that in tissues where the availability of UDP-glucuronic acid is limited but a particular UGT is

abundantly expressed, these UGTs may utilize UDP-glucose and catalyze glucosidation as an alternative metabolic pathway.

The process of glucuronidation introduces a negative charge and diminishes lipid solubility, resulting in reduced passive permeability for the formed glucuronides. As a consequence, these metabolites are commonly transported out of cells (such as hepatocytes) by the action of anion transporters [102]. On the contrary, glucosides don't have negative charges unless their aglycon does, so they may not be exported by anion transporters and thereby they have a higher chance of not being detected as they might stay inside the cells much longer. This may explain to some extent why propranolol glucosides were not (yet) found in human urine during the current study. Furthermore, it would be valuable to explore the potential presence of propranolol glucosides in bile, feces or other tissues in future investigations, which may provide additional insights into the fate of propranolol in the body.

## **4.5 Mutual modulations of CYP2D6 and four UGTs on the metabolism of propranolol**

### **4.5.1 Optimization for biotransformation protocol**

The previously published protocol for CYP-UGT activity assays with diploid fission yeasts was established using pro-luciferin probe substrates [20]. For monitoring propranolol metabolism, this protocol needed to be optimized as this is a much more lipophilic substrate with a logD (7.4) value of 1.2 [199].

#### **4.5.1.1 Liquid-liquid extraction with ethyl acetate**

In the previously published enzyme bag method [122, 126, 130, 135], recombinant fission yeast cells are permeabilized by detergent, forming holes on the cell membrane and thus facilitating small molecules (such as substrate and cofactors) and hydrophilic products to enter and exit the cells [132]. However, lipophilic substrates (and their metabolites) are likely to be embedded in the cellular membranes of the enzyme bags. In such cases, a liquid-liquid extraction of the metabolites from the aqueous reaction buffer is required. In previous study, ethyl acetate was used to extract CYP metabolites of testosterone [135].

In this study, the extraction efficiency of ethyl acetate at different pH levels of the buffer system was tested as this parameter was expected to be a key factor influencing the extraction efficiency. The three compounds (propranolol, 4-OHP, and 4-MeOP) were extracted using a 50 mM ammonium hydrogen carbonate buffer (adjusted to pH 5, 6, 7, 8, 9, 10, or 11) and ethyl acetate as the organic solvent and analyzed. Extraction

efficiencies were evaluated as peak areas in the resulting chromatograms. As shown in Figure 23A, the extraction of all three compounds is not effective (lower than 65 %) when the pH value is below 6. As the pH value increases, the extracted amount of all three compounds was found to be stable and the extraction efficiency was above 95 %. The extraction efficiency was calculated as follows:

$$\text{Extraction efficiency} = \frac{\text{Peak Area}_{\text{extracts}}}{\text{Peak Area}_{\text{residues}} + \text{Peak Area}_{\text{extracts}}} \times 100\%$$

Peak Area<sub>extracts</sub> is the peak area of a compound after extraction by ethyl acetate; Peak Area<sub>residues</sub> is the peak area of a compound left in the aqueous residue after extraction.

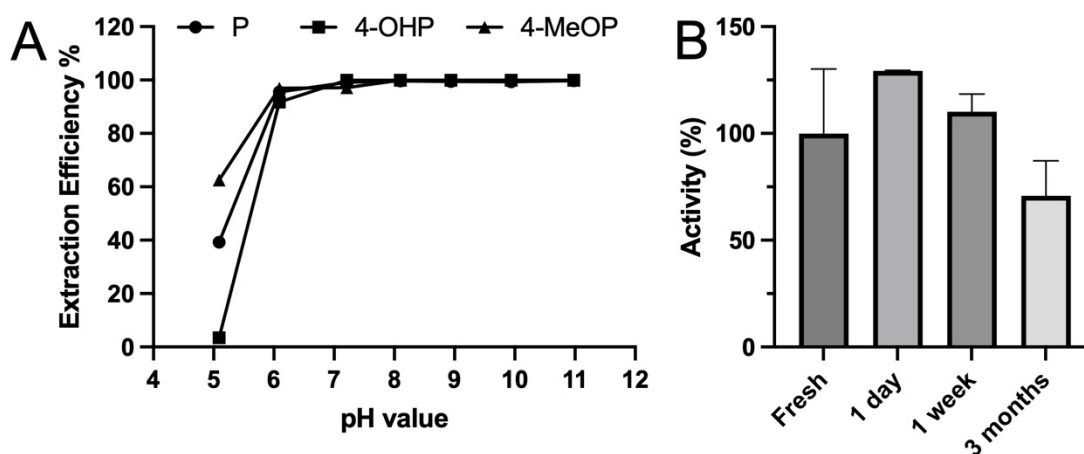


Figure 23. (A) Extraction efficiency of propranolol (P), 4-hydroxypropranolol (4-OHP), and 4-methoxypropranolol (4-MeOP) at different pH values as indicated; (B) Comparison of the activity of freshly made SAN308 enzyme bags and those stored in a deep freezer (-80 °C) for the times indicated. All reactions were done in triplicates. This figure is adapted from my published paper [79].

Therefore, the reaction buffer used in this study (50 mM ammonium hydrogen carbonate, pH 7.8) is well-compatible with the extraction procedure. Thus, ethyl acetate was used for the extraction of hydroxypropranolols for all biotransformation samples and 4-MeOP was used as the internal standard. In contrast, the aqueous residue was analyzed for glucuronides since they are highly hydrophilic and not easily extracted by ethyl acetate based on previous study [135].

#### 4.5.1.2 Long-time storage for enzyme bags

As in any biological reaction system, batch-to-batch variability is an issue. One solution to this problem is using cells from a single batch throughout a project. However, this requires a method for the preservation of the biocatalysts. In the previous study, the possibility of long-time storage for enzyme bag samples was discussed [134]. Still, the question of activity alteration during long-term storage was not addressed [134]. Therefore, the enzymatic activity during long-term storage was monitored. For this purpose, the production of 4-OHP from propranolol in SAN308 enzyme bag samples

(which co-expresses CYP2D6 and UGT1A9) was monitored to evaluate the degradation of the activity after deep freezer storage (-80 °C) for 1 day, 1 week, or 3 months, respectively, and compared with the freshly made ones. All enzyme bags were produced from the same culture and stored in -80 °C for all biotransformation assays. The activity of the freshly made enzyme bags was defined as 100 %.

No statistically significant differences in the activities between the freshly made samples and those stored for different time intervals were observed (Figure 23B). Thus, stored enzyme bags can be used for at least three months after preparation. This information allowed us to perform all biotransformation from a single batch of enzyme bags prepared from each strain used in this study.

#### **4.5.1.3 Optimization of the CYP reaction time for diploid yeast**

Both hydroxylation and glucuronidation reactions were investigated in the biotransformation with CYP-UGT co-expression yeast strains. In the previous studies with enzyme bags, optimal reaction times varied for CYPs, UGTs, and SULTs [122, 126, 135]. Therefore, several different reaction times were tested in this study to find the most suitable one for the potential enzymatic chain reaction. The most suitable reaction time for CYP2D6 was evaluated by monitoring the production of the relative abundances of the metabolite after five different reaction times (2 hours, 4 hours, 8 hours, 16 hours, 24 hours) using strain SAN308.

As shown in Figure 24B, two major hydroxy propranolol products were found in all CYP2D6-UGT co-expression samples. These were identified as 4-OHP and 5-OHP by LC-MS/MS comparison with reference standards. For the production of 4- and 5-OHP, the highest yield was reached at a reaction time of 4 hours (Figure 24A). Afterwards, the amount of 4- and 5-OHP decreased to nearly zero as the reaction time increased to 24 hours. To cope with potential differences in extraction yields, the production of 4- and 5-OHP was determined by calculating the ratio of the peak area of 4- and 5-OHP to 4-MeOP. Unexpectedly, no propranolol glucuronides or hydroxy propranolol glucuronides were detected at any reaction time.

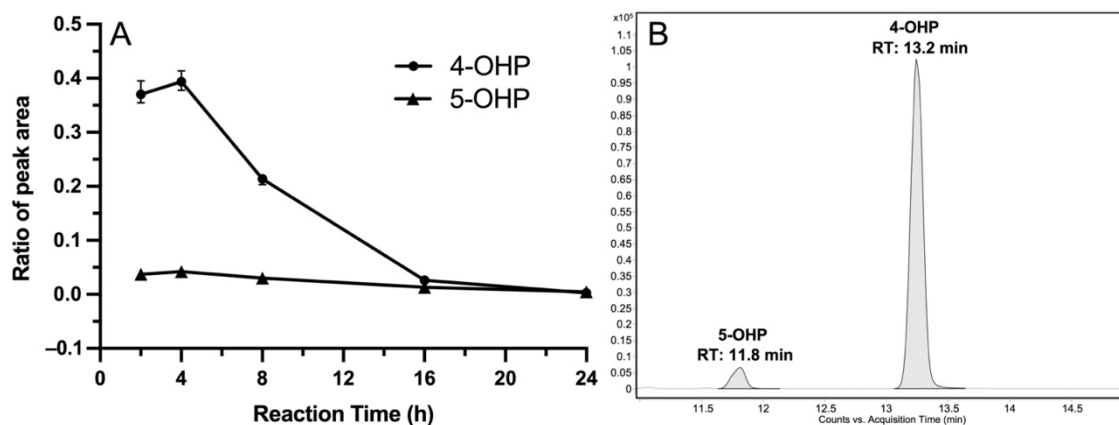


Figure 24. (A) Yield of hydroxypropranolol isomers and glucuronic acid conjugates at different reaction times (2h, 4h, 8h, 16h and 24h). Ratio of peak area is the ratio of peak area of 4- or 5-OHP divided by the peak area of 4-MeOP; OHP-G, hydroxypropranolol glucuronides. (B) Chromatogram (LC-QQQ-MS/MS) of hydroxypropranolol isomers obtained from SAN308-dependent biotransformation of propranolol. Ion transition  $m/z$  276 $\rightarrow$ 58 was monitored for 4-hydroxypropranolol (4-OHP) and 5-hydroxypropranolol (5-OHP). All reactions were done in triplicates. This figure is adapted from my published paper [79].

Formation of *N*-desisopropylated metabolites was also observed at lower levels, but no increased production was found as the incubation time increased, which means the generation of *N*-desisopropylated metabolites may not be the reason for the decrease of 4-OHP. Further experiments were carried out by incubating 4-OHP in  $\text{NH}_4\text{HCO}_3$  buffer for the same time intervals as in SAN308 reactions. The results revealed a decline in the peak area of 4-OHP (Figure 25), similar to that shown in Figure 24A. This finding suggested that the degradation of 4-OHP does not reach saturation within 4 hours and follows a first-order kinetic behavior. This outcome is in line with previous investigations that reported the instability of 4-OHP in aqueous solution and have recommended that urine samples containing this compound be analyzed promptly after collection [176, 200, 201]. Therefore, the reaction time of 4 hours was chosen for the biotransformation of the CYP2D6-UGT co-expression yeast as the degradation of 4-OHP had not caused a significant effect, and no glucuronides were found at any reaction time.

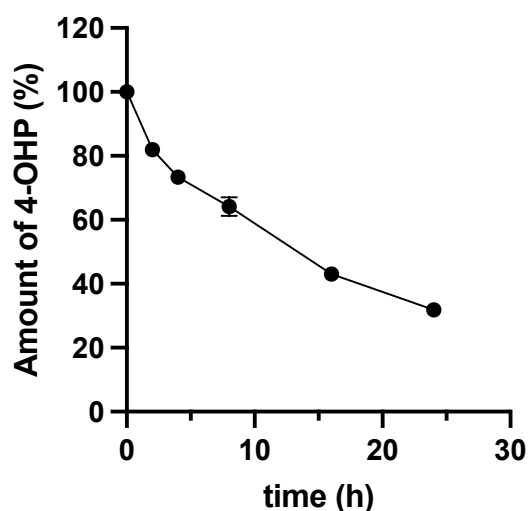


Figure 25. Degradation assay of 4-hydroxypropranolol in  $\text{NH}_4\text{HCO}_3$  buffer. The amounts of 4-hydroxypropranolol left at six time points (0 h, 2 h, 4 h, 8 h, 16 h and 24 h) were analyzed and normalized to values at  $T_0 = 0$  h. All reactions were done in triplicates. This figure is adapted from my published paper [79].

#### 4.5.2 Influence of UGT1A7,UGT1A8,UGT1A9 and UGT2A1 on CYP2D6

Under these optimized conditions, the influence of UGTs on CYP2D6 activity was investigated by monitoring the production of 4- and 5-OHP in four diploid yeast strains which co-express CYP2D6 and one of four UGTs (UGT1A7, UGT1A8, UGT1A9, or UGT2A1). The diploid yeast strain SAN300 which only expresses CYP2D6 and human CPR was used as a control. Both cofactors (an NADPH regeneration system and UDPGA) were added to the reaction system to enable the hydroxylation and the glucuronidation reactions. The concentrations of 4- and 5-OHP were calculated using a standard calibration curve, and all the results were normalized by quantitative polymerase chain reaction (qPCR) data of CYP2D6 expression in five diploid strains in the previous study [136]. In comparison with control CYP2D6 samples, production of 4-OHP by UGT1A7, UGT1A8, and UGT1A9 co-expression was significantly enhanced by a factor of 3.3, 2.1, or 2.8, respectively (Figure 26A). For the production of 5-OHP, the yields increased by 8.4, 4.8, and 5.8 times in UGT1A7, UGT1A8, or UGT1A9 co-expression samples as compared with control CYP2D6 samples (Figure 26B). By contrast, in biotransformation with strain SAN310 (which co-expresses CYP2D6 and UGT2A1), the production of either 4-OHP or 5-OHP showed no significant alteration compared with CYP2D6 control samples.

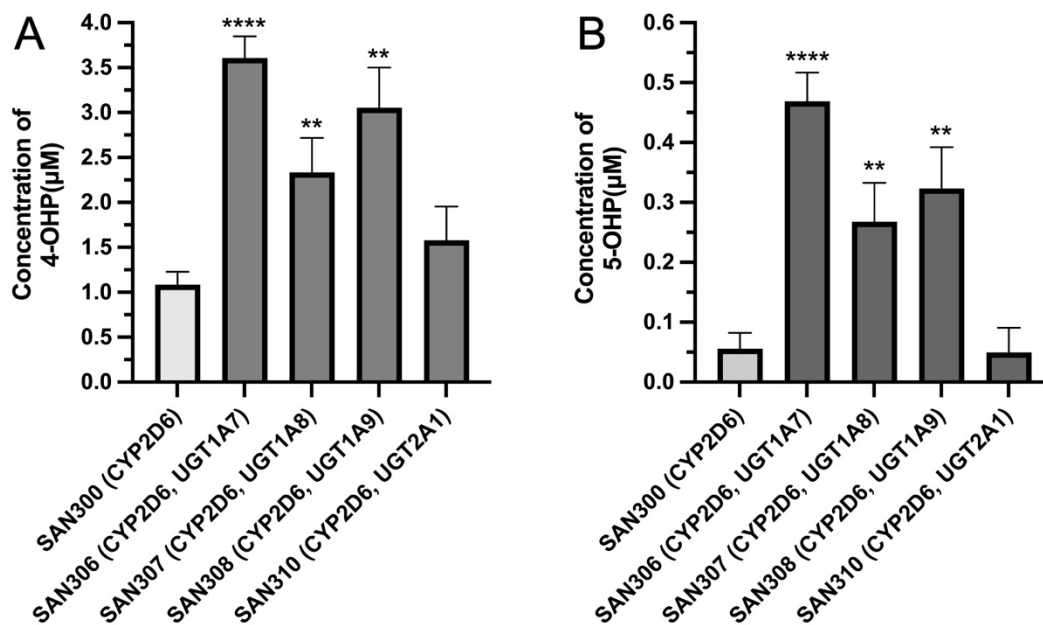


Figure 26. Comparison of the production of 4-hydroxypropranolol (A) and 5-hydroxypropranolol (B) in CYP2D6-UGTs co-expression yeast samples with the control CYP2D6 strain. All reactions were done in triplicates. All the enzyme bags used were stored within 3 months. \*  $p < 0.05$ , \*\*  $p < 0.01$ , \*\*\*  $p < 0.005$ , \*\*\*\*  $p < 0.0001$ . This figure is adapted from my published paper [79].

As a further control experiment, mixtures of enzyme bags prepared from SAN300 (expressing CYP2D6 only) and from one out of four strains (DB24, DB25, CAD200, or DB3) that expresses single UGTs were also tested in biotransformation experiments. The idea behind this approach is that as the CYP and the UGTs are present in different enzyme bags, there is no possibility for their protein-protein interaction. Thus, they should not influence each other's activities. In other words, it should not matter which UGT expressing strain was used in these experiments. As hypothesized, the amounts of both products (4-OHP and 5-OHP) were found not to be significantly different from each other in all of these reactions (Figure 27). These data suggested that the activity differences observed in the CYP-UGT co-expressing strains (Figure 26) are indeed due to interactions between these enzymes.

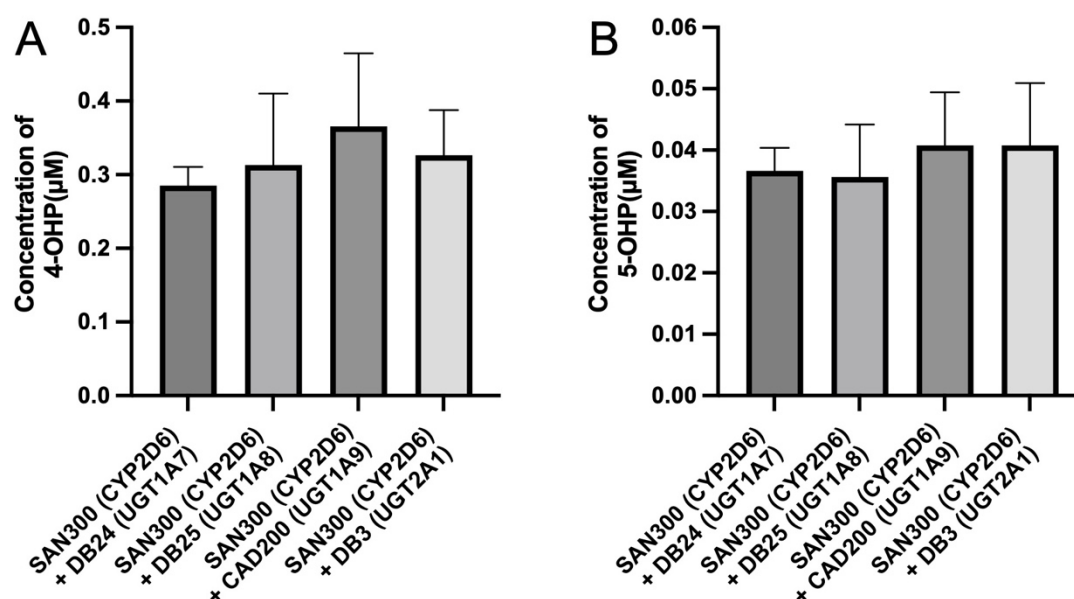


Figure 27. Comparison of the production of 4-hydroxypropranolol (A) and 5-hydroxypropranolol (B) in mixed samples of control CYP2D6 samples (SAN300) and four UGT single-expression yeast strains (DB24, DB25, CAD200, and DB3). All reactions were done in triplicates. All the enzyme bags used were stored within 3 months. This figure is adapted from my published paper [79].

Moreover, two propranolol glucuronic diastereomers were found in three mixed samples, which are CYP2D6 mixed with UGT1A7, UGT1A9, or UGT2A1, but not in the CYP2D6 and UGT1A8 mixed group. This result is in accordance with the previous results (section 4.1) that propranolol is glucuronidated by UGT1A7, UGT1A9, and UGT2A1 but not by UGT1A8 [126]. The activities of haploid UGT strains in mixtures are similar to the results in section 4.1, with UGT1A9 and UGT2A1 having higher activity compared to UGT1A7. This data demonstrates that the UGTs employed in this study were active under the reaction conditions used as long as they were not co-expressed with CYP2D6. No hydroxypropranolol glucuronides were detected in any of the reactions, which is expected as CYP2D6 and UGTs are not physically proximate in this assay, making subsequent glucuronidation after hydroxylation unlikely.

#### 4.5.3 Influence of CYP2D6 on four UGTs

The aqueous residues obtained after ethyl acetate extraction of CYP2D6-UGT expressing diploid yeast samples were analyzed for glucuronides. Additionally, 4-OHP was used as substrate and incubated with CYP2D6-UGT co-expression samples and the samples were analyzed as well. Unexpectedly, no UGT activity towards propranolol or 4-OHP was found in any of the CYP2D6-UGT co-expression samples. In contrast, the activity of all four UGTs towards propranolol or 4-OHP were demonstrated in the

previous part of the thesis upon recombinant expression in fission yeast (section 4.1 and 4.2.2). However, in the present study, the reaction conditions were slightly different. As a control for the experimental setup, the biotransformation of racemic propranolol by UGT1A9 over time was exemplarily monitored using the haploid yeast strain CAD200 applying the reaction protocol developed for the diploid yeast strain SAN308 described above. For quantitation, the peak area of (S)-propranolol glucuronide was used. It was found that product yield reached a maximum at 8 hours and remained stable until 24 hours (Figure 28A). The observed activities were in a similar range as reported in previous work, with larger peak areas found for (S)- than (R)-propranolol glucuronide (Figure 28B).

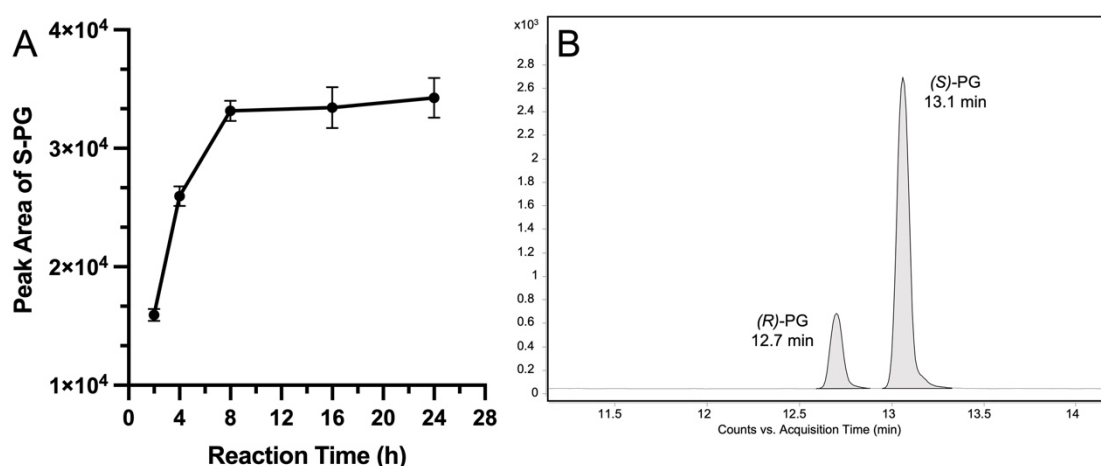


Figure 28. Yield of (S)-propranolol glucuronide at different reaction times (A) and chromatogram (LC-QQQ-MS/MS) of propranolol glucuronides (B) produced by UGT1A9 enzyme bags samples. Ion transition 436 $\rightarrow$ 116 was monitored for (R)-propranolol glucuronide (R-PG) and (S)-propranolol glucuronide (S-PG). This figure is adapted from my published paper [79].

These data give further evidence that the new protocol developed in this study is well-suited for the UGT-dependent biotransformation of propranolol. Thus, the observed lack of finding propranolol glucuronides in the diploid strain experiments described above is not due to the reaction conditions but due to strongly reduced activities of the UGTs when co-expressed with CYP2D6. If the CYP2D6-UGT co-expressing enzyme bags had produced any propranolol or hydroxypropranolol glucuronides, they would have been detectable; alternatively, their concentrations were lower than the detection limit if they were formed at all.

#### 4.5.4 Discussion

Most mammalian CYPs are located on the cytoplasmic side of the endoplasmic reticulum, while UGTs are embedded on the other side of the same membrane. Due to their co-localization in tissues and the proximity within the endoplasmic reticulum,

protein-protein interactions between these two types of enzymes are possible under *in vivo* conditions [202]. Although protein-protein interactions between CYPs and UGTs have been studied for decades, their consequences for the activity of the enzymes involved are not well understood yet. Upon CYP-UGT co-expression in a variety of host systems, activity changes had been observed in experiments that involved human CYP1A2, CYP2C9, or CYP3A4, as well as UGT1A1, UGT1A6, UGT1A7, UGT1A9, or UGT2B7, respectively [74, 76-78]. Next to the CYP3A family, CYP2D6 is arguably one of the most important human drug-metabolizing enzymes. Moreover, the CYP2D6 gene is highly polymorphic, and varying CYP2D6 activities are associated with both adverse drug reactions and reduced drug efficacy [203].

Although commonly used in various studies, liver microsomes from humans and rats may not be the ideal enzyme resource for investigating the functional interaction between CYPs and UGTs. The presence of multiple CYPs and UGTs in the liver leads to a large number of potential protein-protein interactions, making data interpretation complex. Moreover, many substrates of both enzyme families are not specific to a single enzyme, further complicating the analysis. To overcome these challenges, recombinant microbial systems that overexpress CYPs and UGTs offer a viable alternative for studying their functional interactions. The fission yeast *S. pombe* has been successfully used for expressing human CYPs and UGTs [120, 121, 204]. Previous studies have demonstrated the proper recognition of human subcellular localization sequences of CYPs in fission yeast systems [205]. Furthermore, in a study where CYP1A1 and UGT1A6 were co-expressed in yeast, protease treatment of the microsomes showed the correct topological orientation of the UGT in the membranes [206]. This indicates that the topology of CYP and UGT enzymes expressed in yeasts should closely resemble that of the ER membrane in humans.

Recently, diploid fission yeast strains have been developed, where each of the 19 human members of UGT families 1 and 2 are co-expressed with either CYP2C9, CYP2D6, or CYP4Z1 [136]. Using pro-luciferin probe substrates, 72 interactions between CYPs and UGTs were observed in these new strains [136]. Specifically, for CYP2D6, co-expression with eleven UGTs (including UGT1A7) resulted in a statistically significant decrease in activity, while six UGTs (including UGT1A8, UGT1A9, and UGT2A1) caused an increase, and the remaining two had no effect.

The present study has expanded these studies using the drug propranolol, which is metabolized by both CYP2D6 and several UGTs. CYP2D6 has been found to be responsible for the hydroxylation of propranolol, thereby producing the phase I metabolites 4-, 5-, and 7-OHP [164, 173, 207]. In the section 4.1 and 4.2.2, I

demonstrated that propranolol can be glucuronidated by UGT1A7, UGT1A9, UGT1A10, and UGT2A1, while its CYP2D6 metabolite 4-OHP is a substrate for UGT1A7, UGT1A8, UGT1A9, and UGT2A1. Therefore, in the current study, diploid fission yeast strains that co-express CYP2D6 with one of four UGTs each (UGT1A7, UGT1A8, UGT1A9, or UGT2A1) were chosen to investigate their mutual activity influences in the presence of propranolol.

In the previous study [136], the activity of CYP2D6 towards a pro-luciferin probe substrate was significantly increased upon co-expression of six UGTs (UGT1A4, 1A9, 1A10, 2A1, 2A3, and 2B10). On the other hand, co-expression of eleven UGTs (UGT1A3, 1A5, 1A6, 1A7, 1A8, 2A2, 2B4, 2B7, 2B15, 2B17, and 2B28) led to activity decreases, while co-expression of the remaining two UGTs (UGT1A1 and 2B11) had no statistically significant effect. The increases of CYP2D6 activities varied between a factor of 1.4 to 4.3, and the reduction was between 1.3-fold to 3.6-fold. The observed positive effect of UGT1A9 on CYP2D6 activity in propranolol hydroxylation is consistent with the increased activity (around 1.8-fold) of CYP2D6 with UGT1A9 co-expression on the metabolism of the pro-luciferin probe substrate [136]. In contrast to the incubation of pro-luciferin as substrates, UGT2A1 has shown no significant influence on the CYP2D6-dependent hydroxylation of propranolol. UGT1A7, UGT1A8, and UGT2A1 showed different tendencies on CYP2D6 activities compared with the previous results [136], indicating that such interactions also depend on the substrate under study.

Based on the expression data obtained from the Human Protein Atlas database [198], CYP2D6 is co-expressed with UGT1A7, UGT1A8, UGT1A9, and UGT2A1 in many human tissues with various expression levels. CYP2D6 is strongly co-expressed with UGT1A9 in the liver and with UGT1A8 in the small intestine. Co-expression of CYP2D6 and UGT1A7 is observed in the colon, cerebellum, and choroid plexus. The cerebellum and choroid plexus also exhibit co-expression of CYP2D6 and UGT2A1, with exclusive co-expression of these enzymes in the pituitary gland. These findings suggest that the observed influence of UGT on CYP2D6 in *in vitro* experiments may have relevance to the tissues where they are co-expressed, potentially affecting the metabolism of propranolol in those specific locations.

In the previous study, the effect of CYP co-expression (using CYP2C9, CYP2D6, and CYP4Z1) on the activities of five UGTs (UGT1A4, 1A9, 2A3, 2B7, and 2B28) was monitored [136]. The activities of UGT1A1, UGT1A9, and UGT2B28 were found to be reduced by all three CYPs, while the activity of UGT2B7 was not influenced at all. Co-expression of CYP4Z1 suppressed the activity of UGT2A3, while no effect was found in the CYP2C9 and CYP2D6 co-expressing strains. In the current study, neither propranolol glucuronides nor hydroxypropranolol glucuronides were observed in the

CYP2D6-UGT co-expression samples, suggesting the suppression of CYP2D6 co-expression on the activity of UGT1A7, UGT1A8, UGT1A9 and UGT2A1. Overall, neither in the previous study [136] nor in the present work, a positive influence of any CYP on the activity of any UGTs was ever observed. If there was an influence, it was always detrimental.

Multiple studies have shown that the polymorphisms of UGTs may influence the enzymatic activity towards different substrates. For example, UGT1A6\*2 has been found to metabolize 3-O-methyl-dopa and methyl-salicylate at 41-74% of the wild-type level, while the metabolism of 1-naphthol, 3-iodopenol, 7-hydroxycoumarin, and 7-hydroxy-4-methylcoumarin remains normal [208]. Additionally, serotonin, 5-hydroxytryptophol, 4-nitrophenol, acetaminophen, and valproic acid were found to have 2-fold higher glucuronidation by UGT1A6\*2 [209]. Another example is UGT1A9\*3, which shows a dramatically decreased glucuronidation activity towards SN-38 with only 3.8% of the wild-type level [210]. In the current study, the influence on the activity of the UGT by co-expression with CYPs was discovered. This kind of influence may be as potent as the influence of polymorphism. The conformation of the UGT and the substrate, or their position in the membrane, might be changed due to interactions with CYPs. The similarity is that in both cases, activities of the UGTs are changed depending on the substrate. The negative effects on UGTs observed in the current study are the strongest I ever seen in any UGT catalyzed reactions.

Additionally, it is worth noting that propranolol glucuronides and 4-OHPG have been previously [164, 211, 212] and currently detected in human urine, indicating the complexity of CYP-UGT interactions under *in vivo* conditions due to the involvement of multiple CYP and UGT isoforms. As such, the suppressed activity of UGTs towards propranolol and hydroxypropranolol glucuronidation observed in the current study might be restored or increased by other CYP isoforms, as seen with the increased activity of UGT2B7 on morphine glucuronidation by CYP3A4 [74]. Therefore, the enzyme bags method with diploid CYP-UGT co-expression yeast strains is an ideal model for investigating individual protein-protein interaction without interference from other isoforms.

## 5 Summary and Outlook

An ADMET study is a comprehensive assessment of the absorption, distribution, metabolism, excretion and toxicity of a drug or drug candidate. It evaluates the safety and efficiency of the drug candidates in the early stage and decides if further clinical investment should be performed. The investigations on DMEs are undoubtedly the most important part during the evaluation of drug metabolism process. This thesis specifically focuses on the metabolic profile of propranolol within the field of ADMET research. Despite being an old drug, propranolol has found new applications [152, 156, 157], prompting investigations into its metabolism and phase I metabolites, namely 4-, 5-, and 7-OHP. Through these studies, novel insights have been gained concerning enzymatic specificity, protein-protein interactions, as well as stereo- and regioselectivity.

In this thesis, a comprehensive reaction phenotyping was conducted to explore the glucuronidation of propranolol and its hydroxypropranolol metabolites (4-, 5-, and 7-OHP) using 19 human members of the UGT1 and UGT2 enzyme families. The results revealed that UGT1A7, UGT1A9, and UGT1A10 exhibited a preference for using (S)-propranolol as a substrate, while UGT2A1 displayed opposite stereoselectivity. *In silico* investigations suggested that the observed stereoselectivity could be attributed to the charge-charge interactions between specific amino acid residues in the UGT enzymes, affecting their binding conditions to the reaction site of propranolol.

Studies on the metabolism of 4-, 5- and 7-OHP have focused on their regioselective glucuronidation using two strategies: pre-glucuronidation derivatization and post-glucuronidation derivatization. The results suggested that although the aliphatic hydroxy group of hydroxypropranolol is, in principle, amenable to being glucuronidated, it is less favored than aromatic-linked glucuronidation under *in vivo* conditions after propranolol administration. However, *in vitro* studies using high concentrations of hydroxypropranolol and extended incubation time have demonstrated the potential for aliphatic-linked glucuronidation. Overall, in a physiological environment, aromatic-linked glucuronidation is the preferred route of glucuronic elimination for hydroxypropranolols.

In addition, the glucosidation of propranolol with UDP-glucose as a cofactor was also explored in this thesis. The four UGTs that were found active in glucuronidation (UGT1A7, UGT1A9, UGT1A10, and UGT2A1) were also observed to be active in the glucosidation of propranolol. It is possible to speculate that in tissues with limited availability of UDPGA but with the four UGTs highly expressed, these UGTs may utilize

UDP-glucose as an alternative metabolic pathway and catalyze the glucosidation of propranolol.

Apart from studying glucuronidation catalyzed by UGTs, the mutual modulation between CYP and UGT enzymes during the metabolism of propranolol was investigated. A diploid yeast system co-expressing CYP2D6 and each of the four UGTs (UGT1A7, UGT1A8, UGT1A9, and UGT2A1) was utilized for this study. The results revealed that UGT1A7, UGT1A8, and UGT1A9 significantly enhanced the activity of CYP2D6, whereas UGT2A1 had no influence. Conversely, the glucuronidation process catalyzed by the four UGTs was markedly suppressed by CYP2D6. The use of propranolol as substrate, which is a widely prescribed drug, provides significant practical implications for the study of CYP and UGT interactions in drug metabolism. In addition, the functional interaction between CYP2D6 and UGT1A subfamilies was observed in this study for the first time.

Throughout the project, the artificial biotransformation system using permeabilized recombinant fission yeast (enzyme bags) was employed. As the project progressed, continuous optimization of the enzyme bags method led to establishing a standardized procedure for studying drug metabolism. This standardized protocol demonstrated great potential in ADMET studies and provided valuable evidence for its efficacy in drug research.

Based on the findings of this project, there are several potential areas for future research. Firstly, identifying and characterizing the additional hydroxypropranolol glucuronide (apart from 4-, 5-, and 7-OHPG) observed in urine samples warrants further investigation to determine whether it corresponds to 2-OHP or another unidentified metabolite.

Secondly, although propranolol glucosides were not detected in urine samples in this study, it would be valuable to explore their presence in other biological samples such as bile, feces, or other tissues. Investigating the presence of glucosides in these samples may provide additional insights into the metabolic pathways and fate of propranolol in the body.

Lastly, obtaining data from patients with CYP2D6 deficiency who are undergoing propranolol treatment could offer physiological insights into the specific effects of CYP2D6 deficiency on propranolol metabolism and its interaction with UGTs. Additionally, genetically modified animal models with deficient CYP2D6 could serve as suitable alternatives for investigating these interactions under physiological conditions, providing further understanding of the underlying mechanisms involved.

## 6 Zusammenfassung

Eine ADMET-Studie ist eine umfassende Bewertung der Absorption, der Distribution, des Metabolismus, der Ausscheidung (Excretion auf Englisch) und der Toxizität eines Arzneimittels oder Arzneimittelkandidaten. Sie bewertet die Sicherheit und Wirksamkeit von Arzneimittelkandidaten im Frühstadium und entscheidet, ob weitere klinische Untersuchungen getätigt werden sollten. Die Untersuchungen der DMEs sind zweifellos der wichtigste Teil bei der Bewertung des Arzneimittelstoffwechsels. Diese Arbeit konzentriert sich speziell auf das metabolische Profil von Propranolol im Bereich der ADMET-Forschung. Obwohl es sich bei Propranolol um ein altes Medikament handelt, hat es neue Anwendungen gefunden[152, 156, 157], was Anlass zu Untersuchungen seines Metabolismus und seiner Phase-I-Metaboliten, nämlich 4-, 5- und 7-OHP, gibt. Durch diese Studien wurden neue Erkenntnisse über die enzymatische Spezifität, die Protein-Protein-Wechselwirkungen sowie die Stereo- und Regioselektivität gewonnen.

In dieser Arbeit wurde eine umfassende Reaktionsphänotypisierung durchgeführt, um die Glucuronidierung von Propranolol und seinen Hydroxypropranolol-Metaboliten (4-, 5- und 7-OHP) mit 19 menschlichen Enzymen der UGT1- und UGT2-Enzymfamilien zu untersuchen. Die Ergebnisse zeigen, dass UGT1A7, UGT1A9 und UGT1A10 eine Präferenz für die Verwendung von (S)-Propranolol als Substrat haben, während UGT2A1 eine entgegengesetzte Stereoselektivität aufweist. *In silico* Untersuchungen legen nahe, dass die beobachtete Stereoselektivität auf die Ladungswechselwirkungen zwischen spezifischen Aminosäureresten in den UGT-Enzymen zurückgeführt werden könnte, die die Bedingungen ihrer Bindung an die Reaktionsstelle von Propranolol beeinflussen.

Studien zum Metabolismus von 4-, 5- und 7-OHP konzentrierten sich auf deren regioselektive Glucuronidierung unter Anwendung zweier Strategien: Derivatisierung vor der Glucuronidierung und Derivatisierung nach der Glucuronidierung. Die Ergebnisse deuten darauf hin, dass die aliphatische Hydroxygruppe von Hydroxypropranolol zwar prinzipiell glucuronidiert werden kann, aber unter *In vivo* Bedingungen nach Verabreichung von Propranolol weniger begünstigt wird als die aromatisch gebundene Glucuronidierung. *In vitro* Studien, bei denen hohe Konzentrationen von Hydroxypropranolol und eine längere Inkubationszeit verwendet wurden, haben jedoch das Potenzial für eine aliphatisch gebundene Glucuronidierung gezeigt. Insgesamt ist in einer physiologischen Umgebung die aromatisch gebundene Glucuronidierung der bevorzugte Weg der Glucuronsäureelimination für Hydroxypropranolole.

Darüber hinaus wurde in dieser Arbeit auch die Glucosidierung von Propranolol mit UDP-Glucose als Cofaktor untersucht. Es wurde festgestellt, dass die vier UGTs, die bei der Glucuronidierung aktiv sind (UGT1A7, UGT1A9, UGT1A10 und UGT2A1), auch bei der Glucosidierung von Propranolol aktiv sind. Es kann spekuliert werden, dass in Geweben mit begrenzter Verfügbarkeit von UDPGA, in denen die vier UGTs jedoch stark exprimiert werden, diese UGTs UDP-Glucose als alternativen Stoffwechselweg nutzen und die Glucosidierung von Propranolol katalysieren.

Neben der Untersuchung der durch UGTs katalysierten Glucuronidierung wurde auch die gegenseitige Modulation zwischen CYP- und UGT-Enzymen während des Metabolismus von Propranolol untersucht. Für diese Studie wurde ein diploides Hefesystem verwendet, das CYP2D6 und jede der vier UGTs (UGT1A7, UGT1A8, UGT1A9 und UGT2A1) gemeinsam exprimiert. Die Ergebnisse zeigen dass UGT1A7, UGT1A8 und UGT1A9 die Aktivität von CYP2D6 deutlich verstärkten, während UGT2A1 keinen Einfluss hatte. Umgekehrt wurde der von den vier UGTs katalysierte Glucuronidierungsprozess durch CYP2D6 deutlich unterdrückt. Die Verwendung von Propranolol als Substrat, einem weit verbreiteten Medikament, hat erhebliche praktische Auswirkungen auf die Untersuchung der Interaktionen zwischen CYP und UGT im Arzneimittelstoffwechsel. Darüber hinaus wurde in dieser Studie zum ersten Mal eine funktionelle Interaktion zwischen den Subfamilien CYP2D6 und UGT1A beobachtet.

Während des gesamten Projekts wurde das künstliche Biotransformationssystem unter Verwendung von permeabilisierter rekombinanter Spaltheife (enzyme bags) eingesetzt. Im Laufe des Projekts führte die kontinuierliche Optimierung der enzyme bag Methode zur Einführung eines standardisierten Verfahrens zur Untersuchung des Arzneimittelstoffwechsels. Dieses standardisierte Protokoll zeigen ein großes Potenzial für ADMET-Studien und liefern wertvolle Beweise für seine Wirksamkeit in der Arzneimittelforschung.

Basierend auf den Ergebnissen dieses Projekts gibt es mehrere potenzielle Bereiche für zukünftige Forschung. Erstens erfordert die Identifizierung und Charakterisierung des zusätzlichen Hydroxypropranololglucuronids (außer 4-, 5- und 7-OHPG), das in Urinproben beobachtet wurde, weitere Untersuchungen, um festzustellen, ob es 2-OHP oder einem anderen nicht identifizierten Metaboliten entspricht.

Zweitens: Obwohl in dieser Studie keine Propranololglukoside in Urinproben nachgewiesen wurden, wäre es wertvoll, ihr Vorhandensein in anderen biologischen Proben wie Galle, Kot oder anderen Geweben zu untersuchen. Die Untersuchung des

Vorhandenseins von Glukosiden in diesen Proben könnte zusätzliche Erkenntnisse über die Stoffwechselwege und den Verbleib von Propranolol im Körper liefern.

Schließlich könnte die Erhebung von Daten von Patienten mit CYP2D6-Mangel, die sich einer Propranolol-Behandlung unterziehen, physiologische Einblicke in die spezifischen Auswirkungen des CYP2D6-Mangels auf den Propranolol-Metabolismus und seine Wechselwirkung mit UGTs liefern. Darüber hinaus könnten gentechnisch veränderte Tiermodelle mit defizientem CYP2D6 als geeignete Alternative zur Untersuchung dieser Wechselwirkungen unter physiologischen Bedingungen dienen und ein tieferes Verständnis der zugrunde liegenden Mechanismen ermöglichen.

**7 CV**

## 8 References

- [1] Hodgson J. ADMET-turning chemicals into drugs. *Nature Biotechnology* 19 (2001) 722-726
- [2] Kramer C, Ting A, Zheng H, Hert J, Schindler T, Stahl M, Robb G, Crawford JJ, Blaney J, Montague S. Learning medicinal chemistry absorption, distribution, metabolism, excretion, and toxicity (ADMET) rules from cross-company matched molecular pairs analysis (MMPA) miniperspective. *Journal of Medicinal Chemistry* 61 (2017) 3277-3292
- [3] Li Y, Meng Q, Yang M, Liu D, Hou X, Tang L, Wang X, Lyu Y, Chen X, Liu K. Current trends in drug metabolism and pharmacokinetics. *Acta Pharmaceutica Sinica B* 9 (2019) 1113-1144
- [4] Iyanagi T. Molecular mechanism of phase I and phase II drug-metabolizing enzymes: implications for detoxification. *International Review of Cytology* 260 (2007) 35-112
- [5] Josephy PD, Guengerich FP, Miners JO. "Phase I and Phase II" drug metabolism: terminology that we should phase out? *Drug Metabolism Reviews* 37 (2005) 575-580
- [6] Meyer UA. Overview of enzymes of drug metabolism. *Journal of Pharmacokinetics and Biopharmaceutics* 24 (1996) 449-459
- [7] Khojasteh SC, Wong H, Hop CE. *Drug metabolism and pharmacokinetics quick guide*, Springer Science & Business Media (2011)
- [8] Jancova P, Anzenbacher P, Anzenbacherova E. Phase II drug metabolizing enzymes. *Biomedical Papers Of The Medical Faculty Of The University Palacky, Olomouc, Czechoslovakia Overview* 154 (2010) 103-116
- [9] Burchell B, Coughtrie MW. UDP-glucuronosyltransferases. *Pharmacology & Therapeutics* 43 (1989) 261-289
- [10] Rowland A, Miners JO, Mackenzie PI. The UDP-glucuronosyltransferases: their role in drug metabolism and detoxification. *The International Journal of Biochemistry & Cell Biology* 45 (2013) 1121-1132
- [11] Garfinkel D. Studies on pig liver microsomes. I. Enzymic and pigment composition of different microsomal fractions. *Archives of Biochemistry and Biophysics* 77 (1958) 493-509
- [12] Klingenberg M. Pigments of rat liver microsomes. *Archives of Biochemistry and Biophysics* 75 (1958) 376-386
- [13] Omura T, Sato R. A new cytochrome in liver microsomes. *Journal of Biological Chemistry* 237 (1962) 1375-1376
- [14] Omura T, Sato R. The carbon monoxide-binding pigment of liver microsomes: II. Solubilization, purification, and properties. *Journal of Biological Chemistry* 239 (1964) 2379-2385

- [15] Nebert DW, Wikvall K, Miller WL. Human cytochromes P450 in health and disease. *Philosophical Transactions of the Royal Society B: Biological Sciences* 368 (2013) 20120431
- [16] The University of Tennessee Health Science Center (UTHSC). Human Cytochrome P450s. <https://drnelson.uthsc.edu/human-p450-table/>
- [17] Guengerich FP. Cytochrome P450s and other enzymes in drug metabolism and toxicity. *The AAPS Journal* 8 (2006) E101-111
- [18] Zanger UM, Schwab M. Cytochrome P450 enzymes in drug metabolism: Regulation of gene expression, enzyme activities, and impact of genetic variation. *Pharmacology and Therapeutics* 138 (2013) 103--141
- [19] Zöllner A, Parr MK, Drăgan C-A, Dräs S, Schlörer N, Peters FT, Maurer HH, Schänzer W, Bureik M. CYP21-catalyzed production of the long-term urinary metandienone metabolite 17 $\beta$ -hydroxymethyl-17 $\alpha$ -methyl-18-norandrost-1, 4, 13-trien-3-one: a contribution to the fight against doping. Vol. 391 (Issue 1), pp. 119-127. (2010)
- [20] Nebert DW, Russell DW. Clinical importance of the cytochromes P450. *Lancet* 360 (2002) 1155-1162
- [21] Achour B, Barber J, Rostami-Hodjegan A. Expression of hepatic drug-metabolizing cytochrome P450 enzymes and their Interrelations: a meta-analysis. *Drug Metabolism and Disposition* 42 (2014) 1349
- [22] Nakamura H, Nakasa H, Ishii I, Ariyoshi N, Igarashi T, Ohmori S, Kitada M. Effects of endogenous steroids on CYP3A4-mediated drug metabolism by human liver microsomes. *Drug Metabolism and Disposition* 30 (2002) 534
- [23] Scott EE, Halpert JR. Structures of cytochrome P450 3A4. *Trends in Biochemical Sciences* 30 (2005) 5-7
- [24] Hendrychová T, Anzenbacherová E, Hudeček J, Skopalík J, Lange R, Hildebrandt P, Otyepka M, Anzenbacher P. Flexibility of human cytochrome P450 enzymes: molecular dynamics and spectroscopy reveal important function-related variations. *Biochimica et Biophysica Acta (BBA) - Proteins and Proteomics* 1814 (2011) 58-68
- [25] Guengerich FP, Cheng Q. Orphans in the human cytochrome P450 superfamily: approaches to discovering functions and relevance in pharmacology. *Pharmacological Reviews* 63 (2011) 684
- [26] Bock KW, Schrenk D, Forster A, Griese E-U, Mörike K, Brockmeier D, Eichelbaum M. The influence of environmental and genetic factors on CYP2D6, CYP1A2 and UDP-glucuronosyltransferases in man using sparteine, caffeine, and paracetamol as probes. *Pharmacogenetics and Genomics* 4 (1994)
- [27] Glaeser H, Drescher S, Eichelbaum M, Fromm MF. Influence of rifampicin on the expression and function of human intestinal cytochrome P450 enzymes. *British Journal of Clinical Pharmacology* 59 (2005) 199-206
- [28] Tirona RG, Kim RB. Chapter 20 - Introduction to clinical pharmacology. in: Robertson D, Williams GH (Eds.) *Clinical and Translational Science (Second Edition)*, Academic Press, (2017) 365-388

- [29] Zanger UM, Raimundo S, Eichelbaum M. Cytochrome P450 2D6: overview and update on pharmacology, genetics, biochemistry. *Naunyn-Schmiedeberg's Archives of Pharmacology* 369 (2004) 23-37
- [30] Stingl JC, Brockmöller J, Viviani R. Genetic variability of drug-metabolizing enzymes: the dual impact on psychiatric therapy and regulation of brain function. *Molecular Psychiatry* 18 (2013) 273-287
- [31] Johnson JA, Herring VL, Wolfe MS, Relling MV. CYP1A2 and CYP2D6 4-hydroxylate propranolol and both reactions exhibit racial differences. *Journal of Pharmacology and Experimental Therapeutics* 294 (2000) 1099-1105
- [32] Ortiz De Montellano PR. Substrate oxidation by cytochrome P450 enzymes. in: *Cytochrome P450: structure, mechanism, and biochemistry* (2015) 111-176
- [33] Meunier B, De Visser SP, Shaik S. Mechanism of oxidation reactions catalyzed by cytochrome P450 enzymes. *Chemical Reviews* 104 (2004) 3947-3980
- [34] Guengerich FP. Mechanisms of cytochrome P450-catalyzed oxidations. *ACS Catalysis* 8 (2018) 10964-10976
- [35] Manikandan P, Nagini S. Cytochrome P450 structure, function and clinical significance: a review. *Current Drug Targets* 19 (2018) 38-54
- [36] Hannemann F, Bichet A, Ewen KM, Bernhardt R. Cytochrome P450 systems-biological variations of electron transport chains. *Biochimica et Biophysica Acta* 1770 (2007) 330-344
- [37] Pandey AV, Flück CE. NADPH P450 oxidoreductase: structure, function, and pathology of diseases. *Pharmacology & Therapeutics* 138 (2013) 229-254
- [38] Danielson PÁ. The cytochrome P450 superfamily: biochemistry, evolution and drug metabolism in humans. *Current Drug Metabolism* 3 (2002) 561-597
- [39] Schenkman JB, Jansson I. The many roles of cytochrome b5. *Pharmacology & Therapeutics* 97 (2003) 139-152
- [40] Tukey RH, Strassburg CP. Human UDP-glucuronosyltransferases: metabolism, expression, and disease. *Annual Review of Pharmacology and Toxicology* 40 (2000) 581-616
- [41] Stingl JC, Bartels H, Viviani R, Lehmann M, Brockmöller J. Relevance of UDP-glucuronosyltransferase polymorphisms for drug dosing: a quantitative systematic review. *Pharmacology & Therapeutics* 141 (2014) 92-116
- [42] Guillemette C, Levesque E, Rouleau M. Pharmacogenomics of human uridine diphospho-glucuronosyltransferases and clinical implications. *Clinical Pharmacology & Therapeutics* 96 (2014) 324-339
- [43] Cerny MA. Prevalence of non-cytochrome P450-mediated metabolism in food and drug administration-approved oral and intravenous drugs: 2006-2015. *Drug Metabolism and Disposition* 44 (2016) 1246-1252
- [44] Brune K, Nürnberg B, Szelenyi I, Vergin H. The enterohepatic circulation of some anti-inflammatory drugs may cause intestinal ulcerations. In: Rainsford KD, Velo GP (Eds.) *Side-Effects of Anti-Inflammatory Drugs: Part Two Studies in Major Organ Systems*, Springer Netherlands, Dordrecht (1987) 29-39

- [45] Miners JO, Mackenzie PI. Drug glucuronidation in humans. *Pharmacology & Therapeutics* 51 (1991) 347-369
- [46] Radomska-Pandya A, Czernik PJ, Little JM, Battaglia E, Mackenzie PI. Structural and functional studies of UDP-glucuronosyltransferases. *Drug Metabolism Reviews* 31 (1999) 817-899
- [47] Mackenzie PI, Bock KW, Burchell B, Guillemette C, Ikushiro S, Iyanagi T, Miners JO, Owens IS, Nebert DW. Nomenclature update for the mammalian UDP glycosyltransferase (UGT) gene superfamily. *Pharmacogenet Genomics* 15 (2005) 677-685
- [48] Court MH, Zhang X, Ding X, Yee KK, Hesse LM, Finel M. Quantitative distribution of mRNAs encoding the 19 human UDP-glucuronosyltransferase enzymes in 26 adult and 3 fetal tissues. *Xenobiotica* 42 (2012) 266-277
- [49] Ohno S, Nakajin S. Determination of mRNA expression of human UDP-glucuronosyltransferases and application for localization in various human tissues by real-time reverse transcriptase-polymerase chain reaction. *Drug Metabolism and Disposition* 37 (2009) 32-40
- [50] Strassburg CP, Kalthoff S, Ehmer U. Variability and function of family 1 Uridine-5'-diphosphate glucuronosyltransferases (UGT1A). *Critical Reviews in Clinical Laboratory Sciences* 45 (2008) 485-530
- [51] Lin J-P, Cupples LA, Wilson PW, Heard-Costa N, O'donnell CJ. Evidence for a gene influencing serum bilirubin on chromosome 2q telomere: a genomewide scan in the Framingham study. *The American Journal of Human Genetics* 72 (2003) 1029-1034
- [52] Bartlett MG, Gourley GR. Assessment of UGT polymorphisms and neonatal jaundice. in: *Seminars in perinatology*, Elsevier (2011) 127-133
- [53] Beutler E, Gelbart T, Demina A. Racial variability in the UDP-glucuronosyltransferase 1 (UGT1A1) promoter: a balanced polymorphism for regulation of bilirubin metabolism? *Proceedings of the National Academy of Sciences* 95 (1998) 8170-8174
- [54] Ma G, Lin J, Cai W, Tan B, Xiang X, Zhang Y, Zhang P. Simultaneous determination of bilirubin and its glucuronides in liver microsomes and recombinant UGT1A1 enzyme incubation systems by HPLC method and its application to bilirubin glucuronidation studies. *Journal of Pharmaceutical and Biomedical Analysis* 92 (2014) 149-159
- [55] Ma G, Wu B, Gao S, Yang Z, Ma Y, Hu M. Mutual regioselective inhibition of human UGT1A1-mediated glucuronidation of four flavonoids. *Molecular Pharmaceutics* 10 (2013) 2891-2903
- [56] King C, Tang W, Ngui J, Tephly T, Braun M. Characterization of rat and human UDP-glucuronosyltransferases responsible for the *in vitro* glucuronidation of diclofenac. *Toxicological Sciences* 61 (2001) 49-53
- [57] Coffman BL, Rios GR, King CD, Tephly TR. Human UGT2B7 catalyzes morphine glucuronidation. *Drug Metabolism and Disposition* 25 (1997) 1-4

- [58] Turgeon D, Carrier J-SB, Lévesque ER, Hum DW, BéLanger A. Relative enzymatic activity, protein stability, and tissue distribution of human steroid-metabolizing UGT2B subfamily members. *Endocrinology* 142 (2001) 778-787
- [59] Nadeau G, Bellemare J, Audet-Walsh É, Flageole C, Huang S-P, Bao B-Y, Douville P, Caron P, Fradet Y, Lacombe L, Guillemette C, Lévesque E. Deletions of the androgen-metabolizing UGT2B genes have an effect on circulating steroid levels and biochemical recurrence after radical prostatectomy in localized prostate cancer. *The Journal of Clinical Endocrinology & Metabolism* 96 (2011) E1550-E1557
- [60] Sneitz N, Court MH, Zhang X, Laajanen K, Yee KK, Dalton P, Ding X, Finel M. Human UDP-glucuronosyltransferase UGT2A2: cDNA construction, expression, and functional characterization in comparison with UGT2A1 and UGT2A3. *Pharmacogenetics and Genomics* 19 (2009) 923
- [61] Burchell B, Brierley CH, Monaghan G, Clarke DJ. The Structure and Function of the UDP-Glucuronosyltransferase Gene Family. In: Goldstein DS, Eisenhofer G, Mccarty R (Eds.) *Advances in Pharmacology*, Academic Press (1997) 335-338
- [62] Neiers F, Jarriault D, Menetrier F, Briand L, Heydel J-M. The odorant metabolizing enzyme UGT2A1: Immunolocalization and impact of the modulation of its activity on the olfactory response. *PLoS One* 16 (2021) e0249029
- [63] Mackenzie PI, Rogers A, Treloar J, Jorgensen BR, Miners JO, Meech R. Identification of UDP glycosyltransferase 3A1 as a UDP *N*-acetylglucosaminyltransferase *Journal of Biological Chemistry* 283 (2008) 36205-36210
- [64] Mackenzie PI, Rogers A, Elliot DJ, Chau N, Hulin JA, Miners JO, Meech R. The novel UDP glycosyltransferase 3A2: cloning, catalytic properties, and tissue distribution. *Molecular Pharmacology* 79 (2011) 472-478
- [65] Meech R, Mackenzie PI. UGT3A: novel UDP-glycosyltransferases of the UGT superfamily. *Drug Metabolism Reviews* 42 (2010) 45-54
- [66] Meech R, Mubarakah N, Shivasami A, Rogers A, Nair PC, Hu DG, Mckinnon RA, Mackenzie PI. A Novel function for UDP glycosyltransferase 8: galactosidation of bile acids. *Molecular Pharmacology* 87 (2015) 442
- [67] Black SD. Membrane topology of the mammalian P450 cytochromes. *The FASEB Journal* 6 (1992) 680-685
- [68] Bock KW, Köhle C. Topological aspects of oligomeric UDP-glucuronosyltransferases in endoplasmic reticulum membranes: advances and open questions. *Biochemical Pharmacology* 77 (2009) 1458-1465
- [69] Vergères G, Waskell L. Cytochrome b5, its functions, structure and membrane topology. *Biochimie* 77 (1995) 604-620
- [70] Ishii Y, Takeda S, Yamada H. Modulation of UDP-glucuronosyltransferase activity by protein-protein association. *Drug Metabolism Reviews* 42 (2010) 145-158
- [71] Taura KI, Yamada H, Hagino Y, Ishii Y, Mori MA, Oguri K. Interaction between cytochrome P450 and other drug-metabolizing enzymes: evidence for an association of CYP1A1 with microsomal epoxide hydrolase and UDP-

- glucuronosyltransferase. *Biochemical and Biophysical Research Communications* 273 (2000) 1048-1052
- [72] Taura K, Naito E, Ishii Y, Mori MA, Oguri K, Yamada H. Cytochrome P450 1A1 (CYP1A1) inhibitor alpha-naphthoflavone interferes with UDP-glucuronosyltransferase (UGT) activity in intact but not in permeabilized hepatic microsomes from 3-methylcholanthrene-treated rats: possible involvement of UGT-P450 interactions. *Biological and Pharmaceutical Bulletin* 27 (2004) 56-60
- [73] Fremont JJ, Wang RW, King CD. Coimmunoprecipitation of UDP-glucuronosyltransferase isoforms and cytochrome P450 3A4. *Molecular Pharmacology* 67 (2005) 260-262
- [74] Takeda S, Ishii Y, Iwanaga M, Mackenzie PI, Nagata K, Yamazoe Y, Oguri K, Yamada H. Modulation of UDP-glucuronosyltransferase function by cytochrome P450: evidence for the alteration of UGT2B7-catalyzed glucuronidation of morphine by CYP3A4. *Molecular Pharmacology* 67 (2005) 665-672
- [75] Takeda S, Ishii Y, Iwanaga M, Nurrochmad A, Ito Y, Mackenzie PI, Nagata K, Yamazoe Y, Oguri K, Yamada H. Interaction of cytochrome P450 3A4 and UDP-glucuronosyltransferase 2B7: evidence for protein-protein association and possible involvement of CYP3A4 J-helix in the interaction. *Molecular Pharmacology* 75 (2009) 956-964
- [76] Ishii Y, Koba H, Kinoshita K, Oizaki T, Iwamoto Y, Takeda S, Miyauchi Y, Nishimura Y, Egoshi N, Taura F, Morimoto S, Ikushiro S, Nagata K, Yamazoe Y, Mackenzie PI, Yamada H. Alteration of the function of the UDP-glucuronosyltransferase 1A subfamily by cytochrome P450 3A4: different susceptibility for UGT isoforms and UGT1A1/7 variants. *Drug Metabolism and Disposition* 42 (2014) 229-238
- [77] Miyauchi Y, Nagata K, Yamazoe Y, Mackenzie PI, Yamada H, Ishii Y. Suppression of cytochrome P450 3A4 function by UDP-glucuronosyltransferase 2B7 through a protein-protein interaction: cooperative roles of the cytosolic carboxyl-terminal domain and the luminal anchoring region. *Molecular Pharmacology* 88 (2015) 800-812
- [78] Miyauchi Y, Tanaka Y, Nagata K, Yamazoe Y, Mackenzie PI, Yamada H, Ishii Y. UDP-glucuronosyltransferase (UGT)-mediated attenuations of cytochrome P450 3A4 activity: UGT isoform-dependent mechanism of suppression. *British Journal of Pharmacology* 177 (2020) 1077-1089
- [79] Yang F, Sharma SS, Bureik M, Parr MK. Mutual modulation of the activities of human CYP2D6 and four UGTs during the metabolism of propranolol. *Current Issues in Molecular Biology* 45 (2023) 7130-7146
- [80] Ishii Y, Iwanaga M, Nishimura Y, Takeda S, Ikushiro S, Nagata K, Yamazoe Y, Mackenzie PI, Yamada H. Protein-protein interactions between rat hepatic cytochromes P450 (P450s) and UDP-glucuronosyltransferases (UGTs): evidence for the functionally active UGT in P450-UGT complex. *Drug Metabolism and Pharmacokinetics*. 22 (2007) 367-376.
- [81] Nakamura T, Yamaguchi N, Miyauchi Y, Takeda T, Yamazoe Y, Nagata K, Mackenzie PI, Yamada H, Ishii Y. Introduction of an N-glycosylation site into UDP-glucuronosyltransferase 2B3 alters its sensitivity to cytochrome P450 3A1-dependent modulation. *Frontiers in Pharmacology* 7 (2016)

- [82] Kummer O, Hammann F, Haschke M, Krahenbuhl S. Reduction of hyperbilirubinemia with hypericum extract (St. John's Wort) in a patient with Crigler-Najjar syndrome type II. *British Journal of Clinical Pharmacology* 81 (2016) 1002-1004
- [83] Fevery J, Van De Vijver M, Michiels R, Heirwegh KPM. Comparison in different species of biliary bilirubin-IX  $\alpha$  conjugates with the activities of hepatic and renal bilirubin-IX  $\alpha$ -uridine diphosphate glycosyltransferases. *Biochemical Journal* 164 (1977) 737-746
- [84] Senafi SB, Clarke DJ, Burchell B. Investigation of the substrate specificity of a cloned expressed human bilirubin UDP-glucuronosyltransferase: UDP-sugar specificity and involvement in steroid and xenobiotic glucuronidation. *Biochemical Journal* 303 (1994) 233-240
- [85] Radomska A, Little J, Pyrek JS, Drake RR, Igari Y, Fournel-Gigleux S, Magdalou J, Burchell B, Elbein AD, Siest G. A novel UDP-Glc-specific glucosyltransferase catalyzing the biosynthesis of 6-O-glucosides of bile acids in human liver microsomes. *Journal of Biological Chemistry* 268 (1993) 15127-15135
- [86] Mackenzie P, Little JM, Radomska-Pandya A. Glucosidation of hyodeoxycholic acid by UDP-glucuronosyltransferase 2B7. *Biochemical pharmacology* 65 (2003) 417-421
- [87] Shipkova M, Strassburg C, Braun F, Streit F, Gröne HJ, Armstrong V, Tukey R, Oellerich M, Wieland E. Glucuronide and glucoside conjugation of mycophenolic acid by human liver, kidney and intestinal microsomes. *British Journal of Pharmacology* 132 (2001) 1027-1034
- [88] Picard N, Ratanasavanh D, Prémaud A, Le Meur Y, Marquet P. Identification of the UDP-glucuronosyltransferase isoforms involved in mycophenolic acid phase II metabolism. *Drug metabolism and disposition* 33 (2005) 139-146
- [89] Chen X, Zhao L, Zhong D. A novel metabolic pathway of morphine: formation of morphine glucosides in cancer patients. *British Journal of Clinical Pharmacology* 55 (2003) 570-578
- [90] Chau N, Elliot DJ, Lewis BC, Burns K, Johnston MR, Mackenzie PI, Miners JO. Morphine glucuronidation and glucosidation represent complementary metabolic pathways that are both catalyzed by UDP-glucuronosyltransferase 2B7: kinetic, inhibition, and molecular modeling studies. *Journal of Pharmacology and Experimental Therapeutics* 349 (2014) 126-137
- [91] Buchheit D, Dragan CA, Schmitt EI, Bureik M. Production of Ibuprofen Acyl Glucosides by Human UGT2B7. *Drug Metabolism and Disposition* 39 (2011) 2174-2181
- [92] Nakazawa T, Miyata K, Omura K, Iwanaga T, Nagata O. Metabolic profile of FYX-051 (4-(5-pyridin-4-yl-1h-[1, 2, 4] triazol-3-yl) pyridine-2-carbonitrile) in the rat, dog, monkey, and human: identification of *N*-glucuronides and *N*-glucosides. *Drug Metabolism and Disposition* 34 (2006) 1880-1886
- [93] Toide K, Terauchi Y, Fujii T, Yamazaki H, Kamataki T. Uridine diphosphate sugar-selective conjugation of an aldose reductase inhibitor (AS-3201) by UDP-glucuronosyltransferase 2B subfamily in human liver microsomes. *Biochemical Pharmacology* 67 (2004) 1269-1278

- [94] Nandi V, Soine WH. HPLC analysis for amobarbital *N*-glycosides in urine. *Journal of Pharmaceutical and Biomedical Analysis* 15 (1997) 1187-1195
- [95] Tang BK, Kalow W, Grey AA. Metabolic fate of phenobarbital in man. *N*-Glucoside formation. *Drug Metabolism and Disposition* 7 (1979) 315-318
- [96] Bosio A, Binczek E, Le Beau MM, Fernald AA, Stoffel W. The human gene CGT encoding the UDP-galactose ceramide galactosyl transferase (cerebroside synthase): cloning, characterization, and assignment to human chromosome 4, band q26. *Genomics* 34 (1996) 69-75
- [97] Nair PC, Meech R, Mackenzie PI, Mckinnon RA, Miners JO. Insights into the UDP-sugar selectivities of human UDP-glycosyltransferases (UGT): a molecular modeling perspective. *Drug Metabolism Reviews* 47 (2015) 335-345
- [98] Dowden H, Munro J. Trends in clinical success rates and therapeutic focus. *Nature Reviews Drug Discovery* 18 (2019) 495-496
- [99] Asha S, Vidyavathi M. Role of human liver microsomes in *in vitro* metabolism of drugs—a review. *Applied Biochemistry and Biotechnology* 160 (2010) 1699-1722
- [100] Brandon EF, Raap CD, Meijerman I, Beijnen JH, Schellens JH. An update on *in vitro* test methods in human hepatic drug biotransformation research: pros and cons. *Toxicology and Applied Pharmacology* 189 (2003) 233-246
- [101] Zhang Q-Y, Dunbar D, Ostrowska A, Zeisloft S, Yang J, Kaminsky LS. Characterization of human small intestinal cytochromes P-450. *Drug Metabolism and Disposition* 27 (1999) 804-809
- [102] Järvinen E, Deng F, Kiander W, Sinokki A, Kidron H, Sjöstedt N. The role of uptake and efflux transporters in the disposition of glucuronide and sulfate conjugates. *Frontiers in Pharmacology* 12 (2022) 802539
- [103] Soars MG, Mcginnity DF, Grime K, Riley RJ. The pivotal role of hepatocytes in drug discovery. *Chemico-biological Interactions* 168 (2007) 2-15
- [104] Gomez-Lechon M, Donato M, Lahoz A, Castell J. Cell lines: a tool for *in vitro* drug metabolism studies. *Current Drug Metabolism* 9 (2008) 1-11
- [105] Radominska-Pandya A, Bratton S, Little JM. A historical overview of the heterologous expression of mammalian UDP-glucuronosyltransferase isoforms over the past twenty years. *Current Drug Metabolism* 6 (2005) 141-160
- [106] Simula A, Crichton M, Black SM, Pemble S, Bligh H, Beggs J, Wolf C. Heterologous expression of drug-metabolizing enzymes in cellular and whole animal models. *Toxicology* 82 (1993) 3-20
- [107] Muruganandan S, Sinal C. Mice as clinically relevant models for the study of cytochrome P450-dependent metabolism. *Clinical Pharmacology & Therapeutics* 83 (2008) 818-828
- [108] Bogaards J, Bertrand M, Jackson P, Oudshoorn M, Weaver R, Van Bladeren P, Walther B. Determining the best animal model for human cytochrome P450 activities: a comparison of mouse, rat, rabbit, dog, micropig, monkey and man. *Xenobiotica* 30 (2000) 1131-1152

- [109] Gonzalez FJ, Kimura S. Study of P450 function using gene knockout and transgenic mice. *Archives of Biochemistry and Biophysics* 409 (2003) 153-158
- [110] Gonzalez FJ, Yu A-M. Cytochrome P450 and xenobiotic receptor humanized mice. *Annual Review of Pharmacology and Toxicology* 46 (2006) 41-64
- [111] Uchida T, Imamura M, Kan H, Hiraga N, Hayes CN, Tsuge M, Abe-Chayama H, Aikata H, Makokha GN, Miki D, Ochi H, Ishida Y, Tateno C, Chayama K. Usefulness of humanized cDNA-uPA/SCID mice for the study of hepatitis B virus and hepatitis C virus virology. *Journal of General Virology* 98 (2017) 1040-1047
- [112] Meuleman P, Leroux-Roels G. The human liver-uPA-SCID mouse: a model for the evaluation of antiviral compounds against HBV and HCV. *Antiviral Research* 80 (2008) 231-238
- [113] Russell WMS, Burch RL. *The principles of humane experimental technique*, Methuen (1959)
- [114] Rusche B. The 3Rs and animal welfare-conflict or the way forward? *ALTEX-Alternatives to animal experimentation* 20 (2003) 63-76
- [115] Kola I. The state of innovation in drug development. *Clinical Pharmacology & Therapeutics* 83 (2008) 227-230
- [116] Zöllner A, Buchheit D, Meyer MR, Maurer HH, Peters FT, Bureik M. Production of human phase 1 and 2 metabolites by whole-cell biotransformation with recombinant microbes. *Bioanalysis* 2 (2010) 1277-1290
- [117] Mattanovich D, Branduardi P, Dato L, Gasser B, Sauer M, Porro D. Recombinant protein production in yeasts. *Recombinant Gene Expression* (2012) 329-358
- [118] Vieira Gomes AM, Souza Carmo T, Silva Carvalho L, Mendonça Bahia F, Parachin NS. Comparison of yeasts as hosts for recombinant protein production. *Microorganisms* 6 (2018) 38
- [119] Forsburg SL, Rhind N. Basic methods for fission yeast. *Yeast* 23 (2006) 173-183
- [120] Dragan CA, Buchheit D, Bischoff D, Ebner T, Bureik M. Glucuronide production by whole-cell biotransformation using genetically engineered fission yeast *Schizosaccharomyces pombe*. *Drug Metabolism and Disposition* 38 (2010) 509-515
- [121] Buchheit D, Schmitt EI, Bischoff D, Ebner T, Bureik M. S-Glucuronidation of 7-mercapto-4-methylcoumarin by human UDP glycosyltransferases in genetically engineered fission yeast cells. *Biological Chemistry* 392 (2011) 1089-1095
- [122] Sun Y, Machalz D, Wolber G, Parr MK, Bureik M. Functional expression of all human sulfotransferases in fission yeast, assay development, and structural models for isoforms SULT4A1 and SULT6B1. *Biomolecules* 10 (2020) 1517
- [123] Peters FT, Bureik M, Maurer HH. Biotechnological synthesis of drug metabolites using human cytochrome P450 isozymes heterologously expressed in fission yeast. *Bioanalysis* 1 (2009) 821-830

- [124] Peters FT, Dragan C-A, Wilde DR, Meyer MR, Zapp J, Bureik M, Maurer HH. Biotechnological synthesis of drug metabolites using human cytochrome P450 2D6 heterologously expressed in fission yeast exemplified for the designer drug metabolite 4'-hydroxymethyl- $\alpha$ -pyrrolidinobutyrophenone. *Biochemical Pharmacology* 74 (2007) 511-520
- [125] Peters FT, Dragan C-A, Schwaninger AE, Sauer C, Zapp J, Bureik M, Maurer HH. Use of fission yeast heterologously expressing human cytochrome P450 2B6 in biotechnological synthesis of the designer drug metabolite *N*-(1-phenylcyclohexyl)-2-hydroxyethanamine. *Forensic Science International* 184 (2009) 69-73
- [126] Yang F, Liu S, Wolber G, Bureik M, Parr MK. Complete reaction phenotyping of propranolol and 4-hydroxypropranolol with the 19 enzymes of the human UGT1 and UGT2 Families. *International Journal of Molecular Sciences* 23 (2022)
- [127] Stoll A, Loke S, Joseph JF, Machalz D, De La Torre X, Botre F, Wolber G, Bureik M, Parr MK. Fine-mapping of the substrate specificity of human steroid 21-hydroxylase (CYP21A2). *The Journal of Steroid Biochemistry and Molecular Biology* 194 (2019) 105446
- [128] Loke S, Stoll A, Machalz D, Botrè F, Wolber G, Bureik M, Parr MK. Corticosteroid biosynthesis revisited: No direct hydroxylation of pregnenolone by steroid 21-hydroxylase. *Frontiers in Endocrinology* 12 (2021) 633785
- [129] Liu J, Chen L, Joseph JF, Naß A, Stoll A, De La Torre X, Botrè F, Wolber G, Parr MK, Bureik M. Combined chemical and biotechnological production of 20 $\beta$ OH-NorDHCMT, a long-term metabolite of Oral-Turinabol (DHCMT). *Journal of Inorganic Biochemistry* 183 (2018) 165-171
- [130] Yang F, Machalz D, Wang S, Li Z, Wolber G, Bureik M. A common polymorphic variant of UGT1A5 displays increased activity due to optimized cofactor binding. *FEBS Letters* 592 (2018) 1837-1846
- [131] Tanaka N, Konomi M, Osumi M, Takegawa K. Characterization of a *Schizosaccharomyces pombe* mutant deficient in UDP-galactose transport activity. *Yeast* 18 (2001) 903-914
- [132] Weyler C, Bureik M, Heinzle E. Selective oxidation of UDP-glucose to UDP-glucuronic acid using permeabilized *Schizosaccharomyces pombe* expressing human UDP-glucose 6-dehydrogenase. *Biotechnology Letters* 38 (2016) 477-481
- [133] Sun Y, Harps LC, Bureik M, Parr MK. Human sulfotransferase assays with PAPS production in situ. *Frontiers in Molecular Biosciences* 9 (2022) 827638
- [134] Sharma S, Durairaj P, Bureik M. Rapid and convenient biotransformation procedure for human drug metabolizing enzymes using permeabilized fission yeast cells. *Analytical Biochemistry* 607 (2020)
- [135] Yan Q, Machalz D, Zollner A, Sorensen EJ, Wolber G, Bureik M. Efficient substrate screening and inhibitor testing of human CYP4Z1 using permeabilized recombinant fission yeast. *Biochemical Pharmacology* 146 (2017) 174-187
- [136] Sharma SS, Sharma S, Zhao J, Bureik M. Mutual influence of human cytochrome P450 enzymes and UDP-glucuronosyltransferases on their

- respective activities in recombinant fission yeast. *Biomedicines* 11(2) (2023) 281
- [137] Hsieh Y. HPLC-MS/MS in drug metabolism and pharmacokinetic screening. *Expert Opinion on Drug Metabolism & Toxicology* 4 (2008) 93-101
- [138] Hao C, Zhao X, Yang P. GC-MS and HPLC-MS analysis of bioactive pharmaceuticals and personal-care products in environmental matrices. *Trends in Analytical Chemistry* 26 (2007) 569-580
- [139] Awad H, Khamis MM, El-Aneed A. Mass spectrometry, review of the basics: ionization. *Applied Spectroscopy Reviews* 50 (2015) 158-175
- [140] Krone N, Hughes BA, Lavery GG, Stewart PM, Arlt W, Shackleton CHL. Gas chromatography/mass spectrometry (GC/MS) remains a pre-eminent discovery tool in clinical steroid investigations even in the era of fast liquid chromatography tandem mass spectrometry (LC/MS/MS). *The Journal of Steroid Biochemistry and Molecular Biology* 121 (2010) 496-504
- [141] Joseph JF, Parr MK. Application of SFC for bioanalysis. In: *Identification and quantification of drugs, metabolites, drug metabolizing enzymes, and transporters*, Elsevier (2020) 151-183
- [142] Vinaixa M, Schymanski EL, Neumann S, Navarro M, Salek RM, Yanes O. Mass spectral databases for LC/MS- and GC/MS-based metabolomics: state of the field and future prospects. *Trends in Analytical Chemistry* 78 (2016) 23-35
- [143] Kazmi SR, Jun R, Yu M-S, Jung C, Na D. *In silico* approaches and tools for the prediction of drug metabolism and fate: a review. *Computers in Biology and Medicine* 106 (2019) 54-64
- [144] Du W, Machalz D, Yan Q, Sorensen EJ, Wolber G, Bureik M. Importance of asparagine-381 and arginine-487 for substrate recognition in CYP4Z1. *Biochemical Pharmacology* 174 (2020) 113850
- [145] Alqahtani S. *In silico* ADME-Tox modeling: progress and prospects. *Expert Opinion on Drug Metabolism & Toxicology* 13 (2017) 1147-1158
- [146] Schuster D, Steindl MT, Langer T. Predicting drug metabolism induction *in silico*. *Current Topics in Medicinal Chemistry* 6 (2006) 1627-1640
- [147] Al-Majed AA, Bakheit AHH, Abdel Aziz HA, Alajmi FM, Alrabiah H. Chapter six - Propranolol. In: Brittain HG (Ed.) *Profiles of drug substances, excipients and related methodology*, Academic Press (2017) 287-338
- [148] Shand DG. Propranolol. *New England journal of medicine* 293 (1975) 280-285
- [149] Routledge PA, Shand DG. Clinical pharmacokinetics of propranolol. *Clinical Pharmacokinetics* 4 (1979) 73-90
- [150] Steenen SA, Van Wijk AJ, Van Der Heijden GJ, Van Westrhenen R, De Lange J, De Jongh A. Propranolol for the treatment of anxiety disorders: systematic review and meta-analysis. *Journal of Psychopharmacology* 30 (2016) 128-139
- [151] Baldwin DS, Anderson IM, Nutt DJ, Allgulander C, Bandelow B, Den Boer JA, Christmas DM, Davies S, Fineberg N, Lidbetter N. Evidence-based pharmacological treatment of anxiety disorders, post-traumatic stress disorder and obsessive-compulsive disorder: a revision of the 2005 guidelines from the

- British Association for Psychopharmacology. *Journal of Psychopharmacology* 28 (2014) 403-439
- [152] Finnie PS, Nader K. The role of metaplasticity mechanisms in regulating memory destabilization and reconsolidation. *Neuroscience & Biobehavioral reviews* 36 (2012) 1667-1707
- [153] Giles J. Beta-blockers tackle memories of horror. *Nature* 436 (2005) 448-450
- [154] Kindt M, Soeter M, Vervliet B. Beyond extinction: erasing human fear responses and preventing the return of fear. *Nature Neuroscience* 12 (2009) 256-258
- [155] Léauté-Labrèze C, De La Roque ED, Hubiche T, Boralevi F, Thambo J-B, Taïeb A. Propranolol for severe hemangiomas of infancy. *New England journal of Medicine* 358 (2008) 2649-2651
- [156] McDonald J, Bayrak-Toydemir P, Pyeritz RE. Hereditary hemorrhagic telangiectasia: an overview of diagnosis, management, and pathogenesis. *Genetics in Medicine* 13 (2011) 607-616
- [157] Horne MA, Flemming KD, Su I-C, Stapf C, Jeon JP, Li D, Maxwell SS, White P, Christianson TJ, Agid R. Clinical course of untreated cerebral cavernous malformations: a meta-analysis of individual patient data. *The Lancet Neurology* 15 (2016) 166-173
- [158] Fitch K. Proscribed drugs at the Olympic Games: permitted use and misuse (doping) by athletes. *Clinical Medicine* 12 (2012) 257
- [159] Kruse P, Ladefoged J, Nielsen U, Paulev P, Sorensen J. Beta-blockade used in precision sports: effect on pistol shooting performance. *Journal of Applied Physiology* 61 (1986) 417-420
- [160] Davis E, Loiacono R, Summers RJ. The rush to adrenaline: drugs in sport acting on the  $\beta$ -adrenergic system. *British Journal of Pharmacology* 154 (2008) 584-597
- [161] Reilly T. Alcohol, anti-anxiety drugs and sport. In: *Drugs in sport*. London (2003) 266-295
- [162] World Anti-Doping Agency. Anti-doping testing figures reports. <https://www.wada-ama.org/en/resources/anti-doping-stats/anti-doping-testing-figures-report>
- [163] Walle T, Conradi EC, Walle UK, Fagan TC, Gaffney TE. The predictable relationship between plasma levels and dose during chronic propranolol therapy. *Clinical Pharmacology & Therapeutics* 24 (1978) 668-677
- [164] Walle T, Walle UK, Olanoff LS. Quantitative account of propranolol metabolism in urine of normal man. *Drug Metabolism and Disposition* 13 (1985) 204-209
- [165] Yoshimoto K, Echizen H, Chiba K, Tani M, Ishizaki T. Identification of human CYP isoforms involved in the metabolism of propranolol enantiomers-*N*-desisopropylation is mediated mainly by CYP1A2. *British Journal of Clinical Pharmacology* 39 (1995) 421-431

- [166] Walle T, Gaffney TE. *N*-dealkylation and oxidative deamination of propranolol in the cardio-pulmonary circuit of dogs. in: *Volunteer presentations, Fifth International Congress on Pharmacology, San Francisco* (1972)
- [167] Goldszer F, Tindell G, Walle U, Walle T. Chemical trapping of labile aldehyde intermediates in the metabolism of propranolol and oxprenolol. *Research Communications in Chemical Pathology and Pharmacology* 34 (1981) 193-205
- [168] Harps LC, Schipperges S, Bredendiek F, Wuest B, Borowiak A, Parr MK. Two dimensional chromatography mass spectrometry: Quantitation of chiral shifts in metabolism of propranolol in bioanalysis. *Journal of Chromatography A* 1617 (2020) 460828
- [169] Lampinen Salomonsson M, Bondesson U, Hedeland M. *In vitro* formation of phase I and II metabolites of propranolol and determination of their structures using chemical derivatization and liquid chromatography–tandem mass spectrometry. *Journal of Mass Spectrometry* 44 (2009) 742-754
- [170] Bichara N, Ching MS, Blake CL, Ghabrial H, Smallwood RA. Propranolol hydroxylation and *N*-desisopropylation by cytochrome P4502D6: studies using the yeast-expressed enzyme and NADPH/O<sub>2</sub> and cumene hydroperoxide-supported reactions. *Drug Metabolism and Disposition* 24 (1996) 112-118
- [171] Masubuchi Y, Hosokawa S, Horie T, Suzuki T, Ohmori S, Kitada M, Narimatsu S. Cytochrome P450 isozymes involved in propranolol metabolism in human liver microsomes. The role of CYP2D6 as ring-hydroxylase and CYP1A2 as *N*-desisopropylase. *Drug Metabolism and Disposition* 22 (1994) 909–915
- [172] Masubuchi Y, Kagimoto N, Narimatsu S, Fujita S, Suzuki T. Regioselective contribution of the cytochrome P-450 2D subfamily to propranolol metabolism in rat liver microsomes. *Drug Metabolism and Disposition* 21 (1993) 1012-1016
- [173] Walle T, Oatis JE, Walle UK, Knapp DR. New ring-hydroxylated metabolites of propranolol: species differences and stereospecific 7-hydroxylation. *Drug Metabolism and Disposition* 10 (1982) 122–127
- [174] Walle T, Gaffney TE. Propranolol metabolism in man and dog: mass spectrometric identification of six new metabolites. *Journal of Pharmacology and experimental Therapeutics* 182 (1972) 83-92
- [175] Saelens DA, Walle T, Gaffney TE, Privitera PJ. Studies on the contribution of active metabolites to the anticonvulsant effects of propranolol. *European Journal of Pharmacology* 42 (1977) 39-46
- [176] Fitzgerald J, O'donnell SR. Pharmacology of 4-hydroxypropranolol, a metabolite of propranolol. *British Journal of Pharmacology* 43 (1971) 222-235
- [177] Ram N, Bauer EW, Hesse UC, Heilman RD. Cardiovascular effects of 5-hydroxypropranolol (ORF 12592) in dogs. *Archives internationales de pharmacodynamie et de therapie* 228 (1977) 118-125
- [178] Silber B, Holford NH, Riegelman S. Stereoselective disposition and glucuronidation of propranolol in humans. *Journal of pharmaceutical sciences* 71 (1982) 699-704
- [179] Barrett A, Cullum VA. The biological properties of the optical isomers of propranolol and their effects on cardiac arrhythmias. *British journal of pharmacology* 34 (1968) 43-55

- [180] Cleaveland CR, Shand DG. Effect of route of administration on the relationship between beta-adrenergic blockade and plasma propranolol level. *Clinical Pharmacology & Therapeutics* 13 (1972) 181-185
- [181] Partani P, Modhave Y, Gurule S, Khuroo A, Monif T. Simultaneous determination of propranolol and 4-hydroxy propranolol in human plasma by solid phase extraction and liquid chromatography/electrospray tandem mass spectrometry. *Journal of Pharmaceutical and Biomedical Analysis* 50 (2009) 966-976
- [182] Brown AK, Wong CS. Simultaneous quantification of propranolol and sulfamethoxazole and major human metabolite conjugates 4-hydroxypropranolol sulfate and sulfamethoxazole- $\beta$ -glucuronide in municipal wastewater—A framework for multiple classes of drugs and conjugates. *Journal of Chromatography A* 1471 (2016) 34-44
- [183] Walle T, Walle UK, Shwed JA, Thornburg KR, Mathis CE, Pesola GR. Human phenolsulfotransferases: chiral substrates and expression in Hep G2 cells. *Chemico-biological Interactions* 92 (1994) 47-55
- [184] Thompson JA, Hull JE, Norris KJ. Glucuronidation of propranolol and 4'-hydroxypropranolol. Substrate specificity and stereoselectivity of rat liver microsomal glucuronyltransferases. *Drug Metabolism and Disposition* 9 (1981) 466-471
- [185] Alfa C, Fantes P, Hyams J, McLeod M, Warbrick E. *Experiments with fission yeast. A laboratory course manual*, Cold Spring Harbor Press, Cold Spring Harbor, NY (1993)
- [186] Oatis Jr JE, Russell MP, Knapp DR, Walle T. Ring-hydroxylated propranolol: synthesis and beta-receptor antagonist and vasodilating activities of the seven isomers. *Journal of Medicinal Chemistry* 24 (1981) 309-314
- [187] Salomonsson ML, Bondesson U, Hedeland M. Structural evaluation of the glucuronides of morphine and formoterol using chemical derivatization with 1, 2-dimethylimidazole-4-sulfonyl chloride and liquid chromatography/ion trap mass spectrometry. *Rapid Communications in Mass Spectrometry: An International Journal Devoted to the Rapid Dissemination of Up-to-the-Minute Research in Mass Spectrometry* 22 (2008) 2685-2697
- [188] Xu L, Spink DC. 1, 2-Dimethylimidazole-4-sulfonyl chloride, a novel derivatization reagent for the analysis of phenolic compounds by liquid chromatography electrospray tandem mass spectrometry: application to 1-hydroxypyrene in human urine. *Journal of Chromatography B* 855 (2007) 159-165
- [189] Maas A, Maier C, Michel-Lauter B, Madea B, Hess C. 1,2-Dimethylimidazole-4-sulfonyl chloride (DMISC), a novel derivatization strategy for the analysis of propofol by LC-ESI-MS/MS. *Analytical and Bioanalytical Chemistry* 409 (2017) 1547-1554
- [190] Beaudry F, Yves Le Blanc J, Coutu M, Ramier I, Moreau JP, Brown NK. Metabolite profiling study of propranolol in rat using LC/MS/MS analysis. *Biomedical Chromatography* 13 (1999) 363-369

- [191] Luan L-J, Shao Q, Ma J-Y, Zeng S. Stereoselective urinary excretion of S-(-)- and R-(+)-propranolol glucuronide following oral administration of RS-propranolol in Chinese Han subjects. *World Journal of Gastroenterology: WJG* 11 (2005) 1822
- [192] Sten T, Qvisen S, Uutela P, Luukkanen L, Kostianen R, Finel M. Prominent but reverse stereoselectivity in propranolol glucuronidation by human UDP-glucuronosyltransferases 1A9 and 1A10. *Drug Metabolism and Disposition* 34 (2006) 1488-1494
- [193] Kantharaj E, Tuytelaars A, Proost PE, Ongel Z, Van Assouw HP, Gilissen RA. Simultaneous measurement of drug metabolic stability and identification of metabolites using ion-trap mass spectrometry. *Rapid Communications in Mass Spectrometry* 17 (2003) 2661-2668
- [194] Otton S, Gillam E, Lennard M, Tucker G, Woods H. Propranolol oxidation by human liver microsomes-the use of cumene hydroperoxide to probe isoenzyme specificity and regio- and stereoselectivity. *British Journal of Clinical Pharmacology* 30 (1990) 751-760
- [195] Dorp ELV, Morariu A, Dahan A. Morphine-6-glucuronide: potency and safety compared with morphine. *Expert Opinion on Pharmacotherapy* 9 (2008) 1955-1961
- [196] Proctor LD, Warr AJ. Development of a Continuous Process for the Industrial Generation of Diazomethane<sup>1</sup>. *Organic Process Research & Development* 6 (2002) 884-892
- [197] Spicer AP, Kaback LA, Smith TJ, Seldin MF. Molecular cloning and characterization of the human and mouse UDP-glucose dehydrogenase genes. *Journal of Biological Chemistry* 273 (1998) 25117-25124
- [198] Human Protein Atlas database. <https://www.proteinatlas.org/>
- [199] Yamashita T, Nishimura I, Nakamura T, Fukami T. A system for LogD screening of new drug candidates using a water-plug injection method and automated liquid handler. *Journal of the Association for Laboratory Automation* 14 (2009) 76-81
- [200] Herring VL, Johnson JA. Direct high-performance liquid chromatographic determination in urine of the enantiomers of propranolol and its major basic metabolite 4-hydroxypropranolol. *Journal of Chromatography B: Biomedical Sciences and Applications* 612 (1993) 215-221
- [201] Pritchard JF, Schneck DW, Hayes Jr AH. Determination of propranolol and six metabolites in human urine by high-pressure liquid chromatography. *Journal of Chromatography B: Biomedical Sciences and Applications* 162 (1979) 47-58
- [202] Di L, Kerns EH. *Drug-like properties: concepts, structure design and methods from ADME to toxicity optimization*, Academic Press, (2016)
- [203] Taylor C, Crosby I, Yip V, Maguire P, Pirmohamed M, Turner RM. A review of the important role of CYP2D6 in pharmacogenomics. *Genes* 11 (2020) 1295
- [204] Durairaj P, Fan L, Du W, Ahmad S, Mebrahtu D, Sharma S, Ashraf RA, Liu J, Liu Q, Bureik M. Functional expression and activity screening of all human cytochrome P450 enzymes in fission yeast. *FEBS Letters* 593 (2019) 1372-1380

- [205] Bureik M, Schiffler B, Hiraoka Y, Vogel F, Bernhardt R. Functional expression of human mitochondrial CYP11B2 in fission yeast and identification of a new internal electron transfer protein, etp1. *Biochemistry* 41 (2002) 2311-2321
- [206] Ikushiro S-I, Sahara M, Emi Y, Yabusaki Y, Iyanagi T. Functional co-expression of xenobiotic metabolizing enzymes, rat cytochrome P450 1A1 and UDP-glucuronosyltransferase 1A6, in yeast microsomes. *Biochimica et Biophysica Acta - General Subjects* 1672 (2004) 86-92
- [207] Distlerath LM, Reilly PE, Martin MV, Davis GG, Wilkinson GR, Guengerich FP. Purification and characterization of the human liver cytochromes P-450 involved in debrisoquine 4-hydroxylation and phenacetin O-deethylation, two prototypes for genetic polymorphism in oxidative drug metabolism. *Journal of Biological Chemistry* 260 (1985) 9057-9067
- [208] Ciotti M, Marrone A, Potter C, Owens IS. Genetic polymorphism in the human UGT1A6 (planar phenol) UDP-glucuronosyltransferase: pharmacological implications. *Pharmacogenetics* 7 (1997) 485-495
- [209] Krishnaswamy S, Hao Q, Al-Rohaimi A, Hesse LM, Von Moltke LL, Greenblatt DJ, Court MH. UDP glucuronosyltransferase (UGT) 1A6 pharmacogenetics: II. Functional impact of the three most common nonsynonymous UGT1A6 polymorphisms (S7A, T181A, and R184S). *Journal of Pharmacology and Experimental Therapeutics* 313 (2005) 1340-1346
- [210] Villeneuve L, Girard H, Fortier LC, Gagne JF, Guillemette C. Novel functional polymorphisms in the UGT1A7 and UGT1A9 glucuronidating enzymes in Caucasian and African-American subjects and their impact on the metabolism of 7-ethyl-10-hydroxycamptothecin and flavopiridol anticancer drugs. *Journal of Pharmacology and Experimental Therapeutics* 307 (2003) 117-128
- [211] Bai SA, Walle T. Isolation, purification, and structure identification of glucuronic acid conjugates of propranolol and alprenolol and their ring-hydroxylated metabolites. *Drug Metabolism and Disposition* 12 (1984) 749-754
- [212] Walle T, Conradi EC, Walle UK, Fagan TC, Gaffney TE. 4-Hydroxypropranolol and its glucuronide after single and long-term doses of propranolol. *Clinical Pharmacology & Therapeutics* 27 (1980) 22-31

## 9 List of figures

### 9.1 List of figures in main text

- Figure 1. Pie chart of weighted mean abundances of CYPs in livers of adult caucasians, adapted from [21]. Others (0.9 %) include CYP3A43 (0.5 %), CYP2J2 (0.3 %) and CYP2C18 (0.1 %). . . . . 3
- Figure 2. Simplified scheme of the catalytic circle of CYPs, adapted from [35]. . . . . 5
- Figure 3. Scheme of glucuronidation reaction, adapted from [42]. UDPGA, uridine 5'-diphosphoglucuronic acid; X could be O, S, N or C for different functional groups. . . . 6
- Figure 4. Phylogenetic tree of human UGT isoforms, adapted from [10]. . . . . 7
- Figure 5. Proposed scheme showing the approximate position of UGTs in the smooth endoplasmic reticulum (SER) in relation to that of CYPs, adapted from [79]. . . . . 9
- Figure 6. Proposed metabolic pathways of propranolol from *in vitro* studies, adapted from [126, 164, 168, 169]. GA, glucuronic acid. . . . . 17
- Figure 7. Chromatograms (LC-QQQ-MS/MS) of (R)-propranolol glucuronide and (S)-propranolol glucuronide obtained from UGT-dependent enzyme bag samples. Ion transition  $m/z$  436→116 is monitored. (R)-PG, (R)-propranolol glucuronide, retention time 12.7 min. (S)-PG, (S)-propranolol glucuronide, retention time 13.1 min. (A) UGT1A7. (B) UGT1A9. (C) UGT1A10. (D) UGT2A1. This figure is adapted from my published paper [126]. . . . . 31
- Figure 8. Chromatograms (LC-QQQ-MS/MS) of (R)-propranolol glucuronide obtained from UGT-dependent enzyme bag samples using (R)-propranolol as the substrate. Ion transition  $m/z$  436→116 is monitored. (R)-PG, (R)-propranolol glucuronide, retention time 12.7 min. (A) UGT1A7. (B) UGT1A9. (C) UGT1A10. (D) UGT2A1. This figure is adapted from my published paper [126]. . . . . 32
- Figure 9. Product ion spectra (LC-QTOF-MS/MS) of propranolol glucuronide obtained by UGT-dependent biotransformation. Propranolol glucuronide,  $C_{22}H_{29}NO_8$ ,  $[M+H]^+$  theor. = 436.1971,  $[M+H]^+$  exp. = 436.1961,  $\Delta m/z$  = -2.29 ppm; collision energy, 30 eV. This figure is adapted from my published paper [126]. . . . . 33
- Figure 10. Chromatograms of 4-, 5- and 7-hydroxypropranolol diastereomeric glucuronides in urine sample and HLMs incubations. The displayed ion transitions are  $m/z$  452→116 (4-OHPG), 452→98 (5-OHPG) and 452→276 (7-OHPG). OHPG, hydroxypropranolol glucuronide. (a), (d) and (g) refer to the analysis of urine sample (collected 17.6 h post administration). (b), (e) and (h) are from incubation of HLMs with ( $\pm$ )-4-hydroxypropranolol, ( $\pm$ )-5-hydroxypropranolol and ( $\pm$ )-7-hydroxypropranolol, respectively. (c), (f) and (i) were from HLMs incubated with (R)-propranolol, UDPGA and NADPH. . . . . 35
- Figure 11. Product ion spectra (LC-QTOF-MS/MS) of (R)-5-hydroxypropranolol glucuronide obtained from HLMs incubations. (R)-5-hydroxypropranolol glucuronide,  $C_{22}H_{29}NO_9$ ,  $[M+H]^+$  theor. = 452.1915,  $[M+H]^+$  exp. = 452.1913,  $\Delta m/z$  = -0.44 ppm; collision energy 20 eV . . . . . 36
- Figure 12. Chromatograms (LC-QQQ-MS/MS) of diastereomeric glucuronides of 4-, 5- and 7-hydroxypropranolol obtained from UGT-dependent enzyme bag samples. Ion

transitions  $m/z$  452→116 (4-OHPG),  $m/z$  452→98 (5-OHPG) and  $m/z$  452→276 (7-OHPG) were monitored. (a1) (b1) (c1) were from UGT1A7 enzyme bags samples. (a2) (b2) (c2) were from UGT1A8 enzyme bags samples. (a3) (b3) (c3) were from UGT1A9 enzyme bags samples. (a4) (b4) (c4) were from UGT2A1 enzyme bags samples.....37

Figure 13. GC/MS analysis of O-TMS-derivative of 4-methoxypropranolol. (A) Total ion chromatogram, retention time 8.27 min; (B) MS spectra,  $M^{+\bullet} = m/z$  361.3.....40

Figure 14. Chromatograms (LC-QQQ-MS/MS) of 4-, 5- and 7-methoxypropranolol glucuronic diastereomers obtained from UGT1A9 enzyme bag samples. The displayed ion transitions are  $m/z$  466→72 (A, 4-MeOPG),  $m/z$  466→290 (B, 5-MeOPG), and  $m/z$  466→116 (C, 7-MeOPG). 4-/5-/7-MeOPG, 4-/5-/7-methoxypropranolol glucuronide.....41

Figure 15. Product ion spectra (LC-QTOF-MS/MS) of 5-methoxypropranolol glucuronide obtained from UGT1A9 enzyme bag incubations. 5-methoxypropranolol glucuronide,  $C_{23}H_{31}NO_9$ ,  $[M+H]^+$  theor. = 466.2072,  $[M+H]^+$  exp. = 466.2061,  $\Delta m/z = -2.36$  ppm; collision energy 20 eV.....42

Figure 16. Extracted ion chromatograms obtained from MS full-scan analysis (LC-QTOF-MS) of DMISC derivatives of propranolol and 5-hydroxypropranolol. (A) (R)-P-DMIS,  $[M+H]^+$   $m/z$  418, single-DMISC-derivatized (R)-propranolol. (B) 5-OHP-DMIS,  $[M+H]^+$   $m/z$  434, single DMISC-derivatized 5-hydroxypropranolol. (C) 5-OHP-2DMIS,  $[M+H]^+$   $m/z$  592, double DMISC-derivatized 5-hydroxypropranolol. OHP, hydroxypropranolol.....44

Figure 17. Product ion spectra of (R)-propranolol and 5-hydroxypropranolol DMISC derivatives. (A) (R)-propranolol-DMIS,  $C_{21}H_{27}N_3O_4S$ , corresponding to the peak in Figure 16A, collision energy 20 eV. (B) 5-hydroxypropranolol-DMIS,  $C_{21}H_{27}N_3O_5S$ , corresponding to the peak in Figure 16B, collision energy 20 eV. (C) 5-hydroxypropranolol-2DMIS,  $C_{26}H_{33}N_5O_7S_2$ , corresponding to the peak in Figure 16C, collision energy 30 eV. DMIS, dimethylimidazole-4-sulfonyl.....45

Figure 18. Extracted ion chromatograms from MS full-scan (LC-QTOF-MS) of HLMs-generated 5- and 7-hydroxypropranolol derivatized with DMISC. (A)  $[M+H]^+$   $m/z$  610, 5-hydroxypropranolol glucuronide DMISC derivatives; (B)  $[M+H]^+$   $m/z$  610, 7-hydroxypropranolol glucuronide DMISC derivatives.....48

Figure 19. Product ion spectra of 5-hydroxypropranolol glucuronides DMISC derivatives obtained from HLMs samples after derivatization. (A) 5-hydroxypropranolol glucuronide-DMIS I,  $C_{27}H_{35}N_3O_{11}S$ ,  $[M+H]^+$  theor. = 610.2065,  $[M+H]^+$  exp. = 610.2077,  $\Delta m/z = 1.97$  ppm, collision energy 30 eV, (B) 5-hydroxypropranolol glucuronide-DMIS III,  $C_{27}H_{35}N_3O_{11}S$ ,  $[M+H]^+$  theor. = 610.2065,  $[M+H]^+$  exp. = 610.2090,  $\Delta m/z = 4.10$  ppm, collision energy, 30 eV.....49

Figure 20. Chromatograms (LC-QQQ-MS/MS) of (S)- and (R)-propranolol glucoside from HLMs incubations. (A) HLMs incubation with racemic propranolol; (B) HLMs incubated with (R)-propranolol. The displayed ion transition is  $m/z$  422→260.....53

Figure 21. Chromatograms (LC-QQQ-MS/MS) of (S)- and (R)-propranolol glucoside from enzyme bag samples. (A) obtained from UGT1A7 enzyme bag samples. (B) obtained from UGT1A9 enzyme bag samples. (C) obtained from UGT1A10 enzyme bag samples. (D) obtained from UGT2A1 enzyme bag samples. The displayed ion transition is  $m/z$  422→260.....54

Figure 22. Product ion spectra (LC-QTOF-MS) of (R)-propranolol glucoside obtained from HLMs incubations. (R)-propranolol glucoside,  $C_{22}H_{31}NO_7$ ,  $[M+H]^+$  theor. = 422.2173,  $[M+H]^+$  exp. = 422.2163,  $\Delta m/z = -2.37$  ppm; collision energy, 30 eV.....55

Figure 23. (A) Extraction efficiency of propranolol (P), 4-hydroxypropranolol (4-OHP), and 4-methoxypropranolol (4-MeOP) at different pH values as indicated; (B) Comparison of the activity of freshly made SAN308 enzyme bags and those stored in a deep freezer (-80 °C) for the times indicated. All reactions were done in triplicates. This figure is adapted from my published paper [79].....57

Figure 24. (A) Yield of hydroxypropranolol isomers and glucuronic acid conjugates at different reaction times (2h, 4h, 8h, 16h and 24h). Ratio of peak area is the ratio of peak area of 4- or 5-OHP divided by the peak area of 4-MeOP; OHP-G, hydroxypropranolol glucuronides. (B) Chromatogram (LC-QQQ-MS/MS) of hydroxypropranolol isomers obtained from SAN308-dependent biotransformation of propranolol. Ion transition  $m/z$  276→58 was monitored for 4-hydroxypropranolol (4-OHP) and 5-hydroxypropranolol (5-OHP). All reactions were done in triplicates. This figure is adapted from my published paper [79].....59

Figure 25. Degradation assay of 4-hydroxypropranolol in  $NH_4HCO_3$  buffer. The amounts of 4-hydroxypropranolol left at six time points (0 h, 2 h, 4 h, 8 h, 16 h and 24 h) were analyzed and normalized to values at  $T_0 = 0$  h. All reactions were done in triplicates. This figure is adapted from my published paper [79].....60

Figure 26. Comparison of the production of 4-hydroxypropranolol (A) and 5-hydroxypropranolol (B) in CYP2D6-UGTs co-expression yeast samples with the control CYP2D6 strain. All reactions were done in triplicates. All the enzyme bags used were stored within 3 months. \*  $p < 0.05$ , \*\*  $p < 0.01$ , \*\*\*  $p < 0.005$ , \*\*\*\*  $p < 0.0001$ . This figure is adapted from my published paper [79].....61

Figure 27. Comparison of the production of 4-hydroxypropranolol (A) and 5-hydroxypropranolol (B) in mixed samples of control CYP2D6 samples (SAN300) and four UGT single-expression yeast strains (DB24, DB25, CAD200, and DB3). All reactions were done in triplicates. All the enzyme bags used were stored within 3 months. This figure is adapted from my published paper [79].....62

Figure 28. Yield of (S)-propranolol glucuronide at different reaction times (A) and chromatogram (LC-QQQ-MS/MS) of propranolol glucuronides (B) produced by UGT1A9 enzyme bags samples. Ion transition 436→116 was monitored for (R)-propranolol glucuronide (R-PG) and (S)-propranolol glucuronide (S-PG). This figure is adapted from my published paper [79].....63

## 9.2 List of supplementary figures

- Supplementary Figure 1. Product ion spectra (LC-QTOF-MS/MS) of (R)-4-hydroxypropranolol glucuronide (A) and (R)-7-hydroxypropranolol glucuronide (B) obtained from HLMs incubations. (R)-4-hydroxypropranolol glucuronide,  $C_{22}H_{29}NO_9$ ,  $[M+H]^+$  theor. = 452.1915,  $[M+H]^+$  exp. = 452.1895,  $\Delta m/z = -4.42$  ppm, collision energy 30 eV; (R)-7-hydroxypropranolol glucuronide,  $C_{22}H_{29}NO_9$ ,  $[M+H]^+$  theor. = 452.1915,  $[M+H]^+$  exp. = 452.1918,  $\Delta m/z = 0.66$  ppm, collision energy 30 eV.....95
- Supplementary Figure 2. Product ion spectra (LC-QTOF-MS/MS) of the peak at 16.9 min in Figure 10g, obtained from urine samples.  $C_{22}H_{29}NO_9$ ,  $[M+H]^+$  theor. = 452.1915,  $[M+H]^+$  exp. = 452.1911,  $\Delta m/z = -0.88$  ppm, collision energy 30 eV.....96
- Supplementary Figure 3. Product ion spectra (LC-QTOF-MS/MS) of 4-methoxypropranolol glucuronide (A) and 7-methoxypropranolol glucuronide (B) obtained from UGT1A9 enzyme bag incubations. 4-methoxypropranolol glucuronide,  $C_{23}H_{31}NO_9$ ,  $[M+H]^+$  theor. = 466.2072,  $[M+H]^+$  exp. = 466.2061,  $\Delta m/z = -2.36$  ppm; collision energy 30 eV. 7-methoxypropranolol glucuronide,  $C_{23}H_{31}NO_9$ ,  $[M+H]^+$  theor. = 466.2072,  $[M+H]^+$  exp. = 466.2058,  $\Delta m/z = -3.00$  ppm, collision energy 30 eV.....96
- Supplementary Figure 4. Extracted ion chromatograms (LC-QTOF-MS) of DMISC derivatives of 4-hydroxypropranolol. (A) 4-OHP-DMIS, single-DMISC-derivatized 4-hydroxypropranolol,  $[M+H]^+$  m/z 434. (B) 4-OHP-2DMIS, double-DMISC-derivatized 4-hydroxypropranolol,  $[M+H]^+$  m/z 592.....97
- Supplementary Figure 5. Product ion spectra (LC-QTOF-MS/MS) of 4-hydroxypropranolol DMISC derivatives obtained from HLMs samples after derivatization. (A) 4-hydroxypropranolol-DMIS,  $C_{21}H_{27}N_3O_5S$ , corresponding to the peak in Supplementary Figure 4A,  $[M+H]^+$  theor. = 434.1744,  $[M+H]^+$  exp. = 434.1750,  $\Delta m/z = 1.38$  ppm, collision energy 30 eV. (B) 4-hydroxypropranolol-2DMIS,  $C_{26}H_{33}N_5O_7S_2$ , corresponding to the peak in Supplementary Figure 4B,  $[M+H]^+$  theor. = 592.1894,  $[M+H]^+$  exp. = 592.1889,  $\Delta m/z = -0.84$  ppm, collision energy 30 eV. DMIS, dimethylimidazole-4-sulfonyl.....97
- Supplementary Figure 6. Extracted ion chromatograms obtained from MS full-scan analysis (LC-QTOF-MS) of DMISC derivatives of 7-hydroxypropranolol. (A) 7-OHP-DMIS, single-DMISC-derivatized 7-hydroxypropranolol,  $[M+H]^+$  m/z 434; (B) 7-OHP-2DMIS, double-DMISC-derivatized 7-hydroxypropranolol,  $[M+H]^+$  m/z 592.....98
- Supplementary Figure 7. Product ion spectra (LC-QTOF-MS/MS) of 7-hydroxypropranolol DMISC derivatives obtained from HLMs samples after derivatization. (A) 7-hydroxypropranolol-DMIS,  $C_{21}H_{27}N_3O_5S$ , corresponding to the peak in Supplementary Figure 6A,  $[M+H]^+$  theor. = 434.1744,  $[M+H]^+$  exp. = 434.1745,  $\Delta m/z = 0.23$  ppm, collision energy 20 eV. (B) 7-hydroxypropranolol-2DMIS,  $C_{26}H_{33}N_5O_7S_2$ , corresponding to the peak in Supplementary Figure 6B,  $[M+H]^+$  theor. = 592.1894,  $[M+H]^+$  exp. = 592.1877,  $\Delta m/z = -2.87$  ppm, collision energy 30 eV. DMIS, dimethylimidazole-4-sulfonyl.....99
- Supplementary Figure 8. Chromatograms (LC-QQQ-MS/MS) of additional 5-hydroxypropranolol glucuronides in 24-hours HLMs incubations. The displayed ion transition is  $m/z 452 \rightarrow 72$ .....100

- Supplementary Figure 9. Product ion spectra (LC-QTOF-MS/MS) of the additional 5-hydroxypropranolol glucuronides in 24-hours HLMs incubations.  $C_{22}H_{29}NO_9$ ,  $[M+H]^+$  theor. = 452.1915,  $[M+H]^+$  exp. = 452.1947,  $\Delta m/z$  = 7.08 ppm, collision energy 40 eV.....100
- Supplementary Figure 10. Product ion spectra of DMISC derivatives of 7-hydroxypropranolol glucuronides obtained from HLMs samples after derivatization. 7-hydroxypropranolol glucuronide DMIS,  $C_{27}H_{35}N_3O_{11}S$ ,  $[M+H]^+$  theor. = 610.2075,  $[M+H]^+$  exp. = 610.2076,  $\Delta m/z$  = 0.16 ppm; collision energy, 30 eV.....101
- Supplementary Figure 11. Extracted ion chromatogram ( $[M+H]^+$  m/z 610) from MS full-scan (LC-QTOF-MS) of HLMs-generated (S)-4-hydroxypropranolol glucuronides derivatized with DMISC. (S)-4OHPG DMIS I and II, DMISC derivative of (S)-4-hydroxypropranolol glucuronide I and II.....101
- Supplementary Figure 12. Product ion spectra of DMISC derivatives of (S)-4-hydroxypropranolol glucuronides obtained from HLMs samples after derivatization. (A) corresponding to (S)-4-OHPG DMIS I in Supplementary Figure 11,  $C_{27}H_{35}N_3O_{11}S$ ,  $[M+H]^+$  theor. = 610.2075,  $[M+H]^+$  exp. = 610.2051,  $\Delta m/z$  = -3.93 ppm; collision energy, 30 eV. (B) corresponding to (S)-4-OHPG DMIS II in Supplementary Figure 11,  $C_{27}H_{35}N_3O_{11}S$ ,  $[M+H]^+$  theor. = 610.2075,  $[M+H]^+$  exp. = 610.2062,  $\Delta m/z$  = -2.13 ppm, collision energy, 30 eV.....102

## 10 List of tables

### 10.1 List of tables in main text

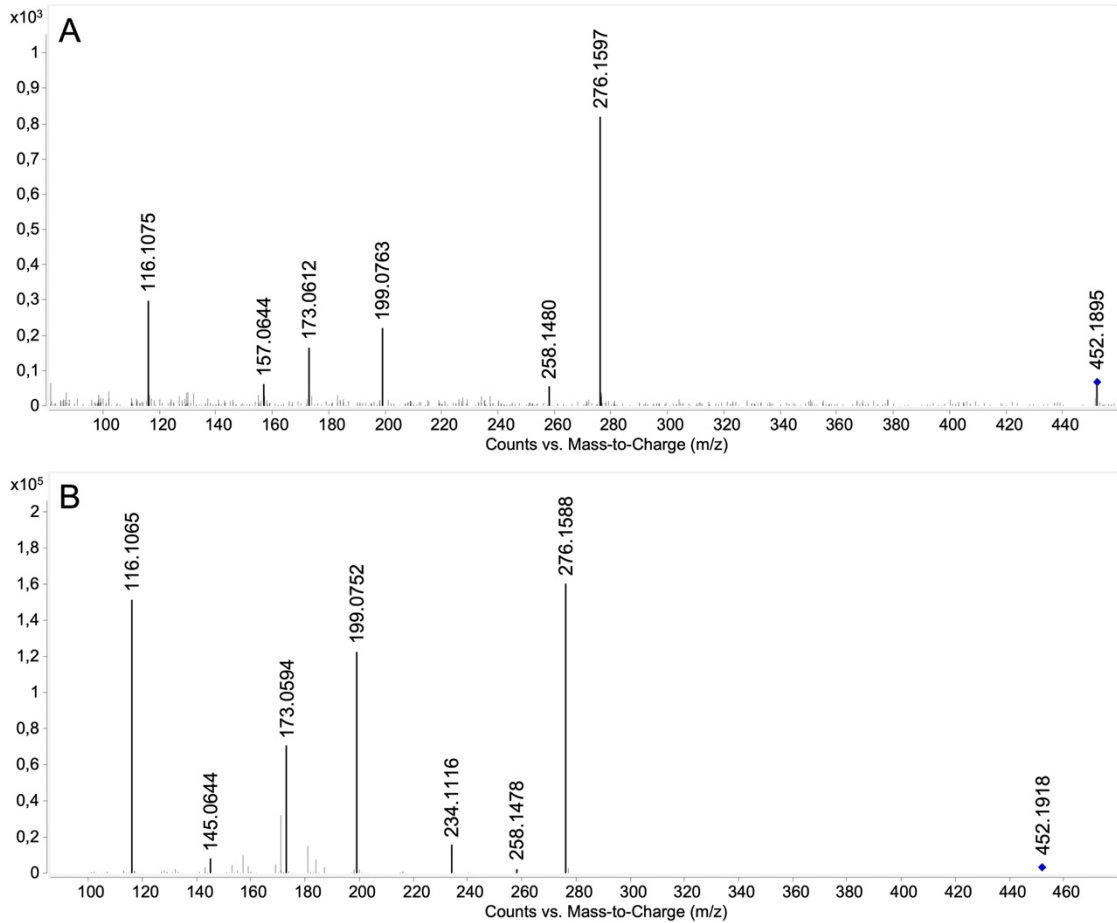
<i>Table 1. Substrates and cofactors.....</i>	<i>20</i>
<i>Table 2. Materials, reagents and solvents.....</i>	<i>20</i>
<i>Table 3. Fission yeast strains used in this study.....</i>	<i>22</i>
<i>Table 4. Transitions and retention time for all analytes in MRM.....</i>	<i>28</i>
<i>Table 5. Postulated fragments, elementary composition, their theoretical mass, observed mass, and the resulting mass differences for (R)-propranolol DMIS, corresponding to Figure 17A.....</i>	<i>44</i>
<i>Table 6. Postulated fragments, elementary composition, their theoretical mass, observed mass, and the resulting mass differences for single-DMIS-derivatized 5-hydroxypropranolol, corresponding to Figure 17B.....</i>	<i>46</i>
<i>Table 7. Postulated fragments, elementary composition, their theoretical mass, observed mass, and the resulting mass differences for double-DMIS-derivatized 5-hydroxypropranolol, corresponding to Figure 17C.....</i>	<i>47</i>

### 10.2 List of supplementary tables

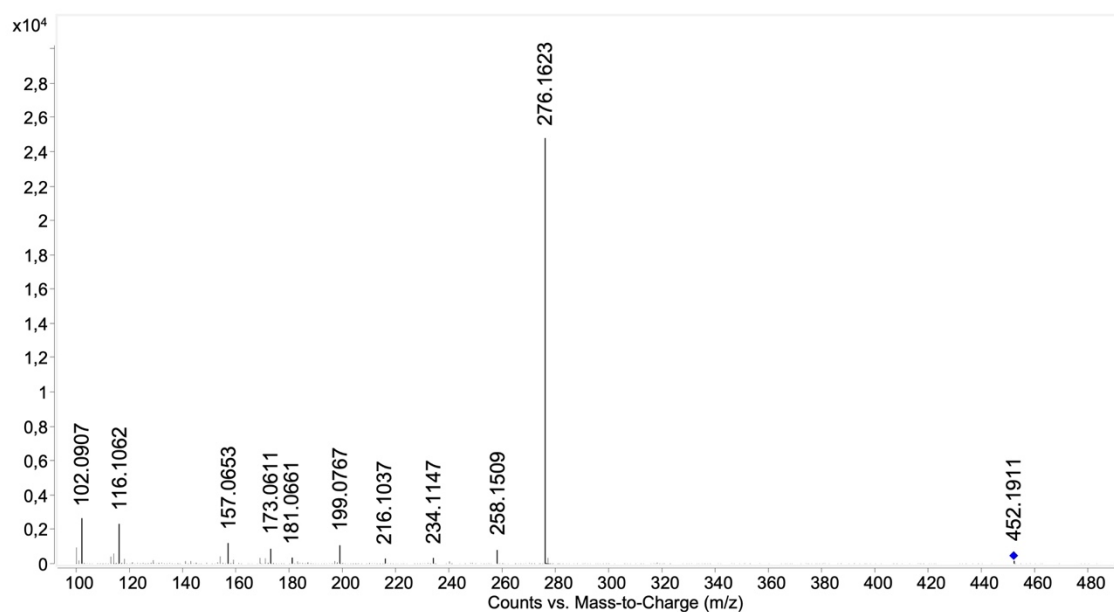
<i>Supplementary Table 1. The abundant of 4-,5- and 7-hydroxypropranolol glucuronides observed in urine samples. The presented peak areas were provided by transitions of the highest intensity as indicated in Figure 10.....</i>	<i>103</i>
<i>Supplementary Table 2. The activity of 19 human UGTs on racemic propranolol.....</i>	<i>104</i>
<i>Supplementary Table 3. The activity of 19 UGTs on racemic 4-, 5- and 7-hydroxypropranolol.....</i>	<i>105</i>
<i>Supplementary Table 4. The activity of UGTs on racemic 4-, 5- and 7-methoxypropranolol.....</i>	<i>106</i>
<i>Supplementary Table 5. Postulated structures of fragments in Table 5 (P-DMIS).....</i>	<i>107</i>
<i>Supplementary Table 6. Postulated structures of fragments in Table 6 (5-OHP-DMIS).....</i>	<i>108</i>
<i>Supplementary Table 7. Postulated structures of fragments in Table 7 (5-OHP-2DMIS).....</i>	<i>109</i>

# 11 Appendix

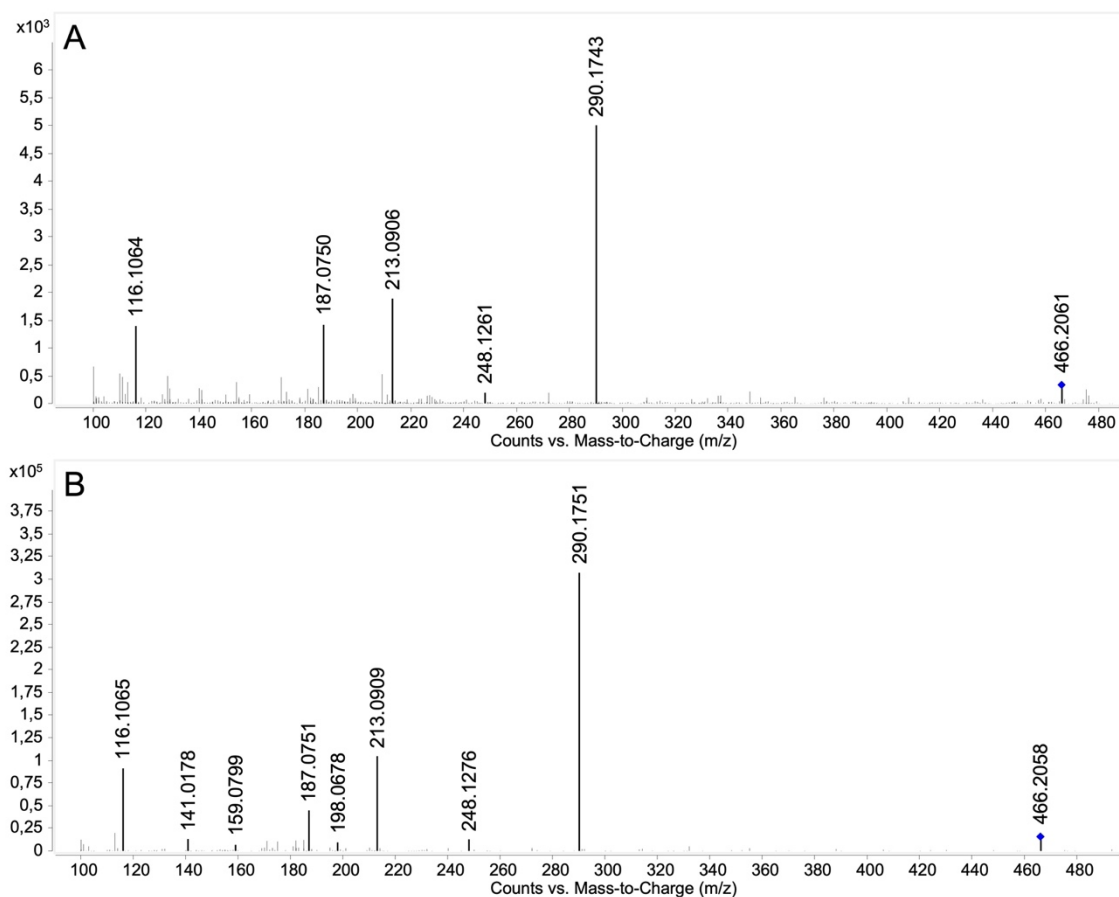
## 11.1 Supplementary figures



Supplementary Figure 1. Product ion spectra (LC-QTOF-MS/MS) of (R)-4-hydroxypropranolol glucuronide (A) and (R)-7-hydroxypropranolol glucuronide (B) obtained from HLMs incubations. (R)-4-hydroxypropranolol glucuronide,  $C_{22}H_{29}NO_9$ ,  $[M+H]^+$  theor. = 452.1915,  $[M+H]^+$  exp. = 452.1895,  $\Delta m/z = -4.42$  ppm, collision energy 30 eV; (R)-7-hydroxypropranolol glucuronide,  $C_{22}H_{29}NO_9$ ,  $[M+H]^+$  theor. = 452.1915,  $[M+H]^+$  exp. = 452.1918,  $\Delta m/z = 0.66$  ppm, collision energy 30 eV.

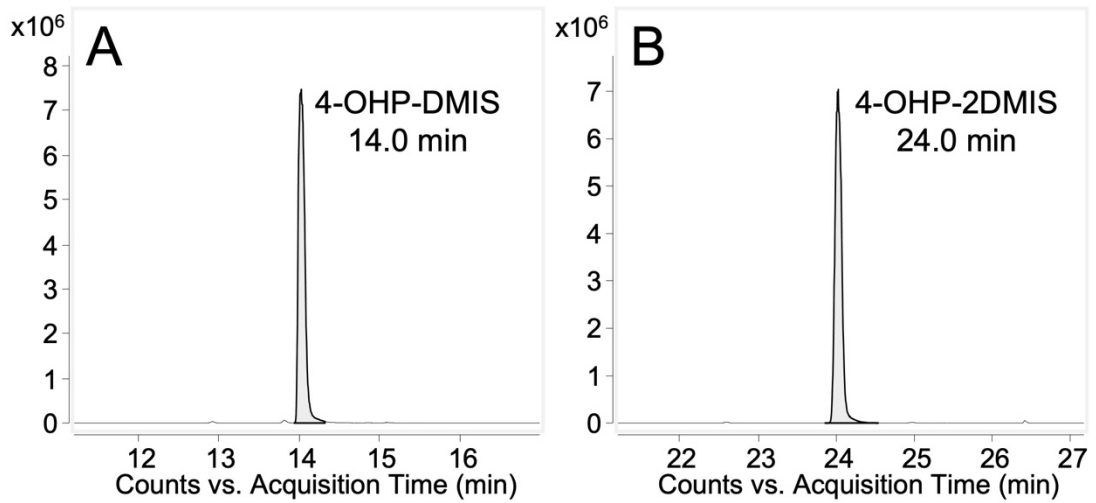


Supplementary Figure 2. Product ion spectra (LC-QTOF-MS/MS) of the peak at 16.9 min in Figure 10g, obtained from urine samples.  $C_{22}H_{29}NO_9$ ,  $[M+H]^+$  theor. = 452.1915,  $[M+H]^+$  exp. = 452.1911,  $\Delta m/z = -0.88$  ppm, collision energy 30 eV.

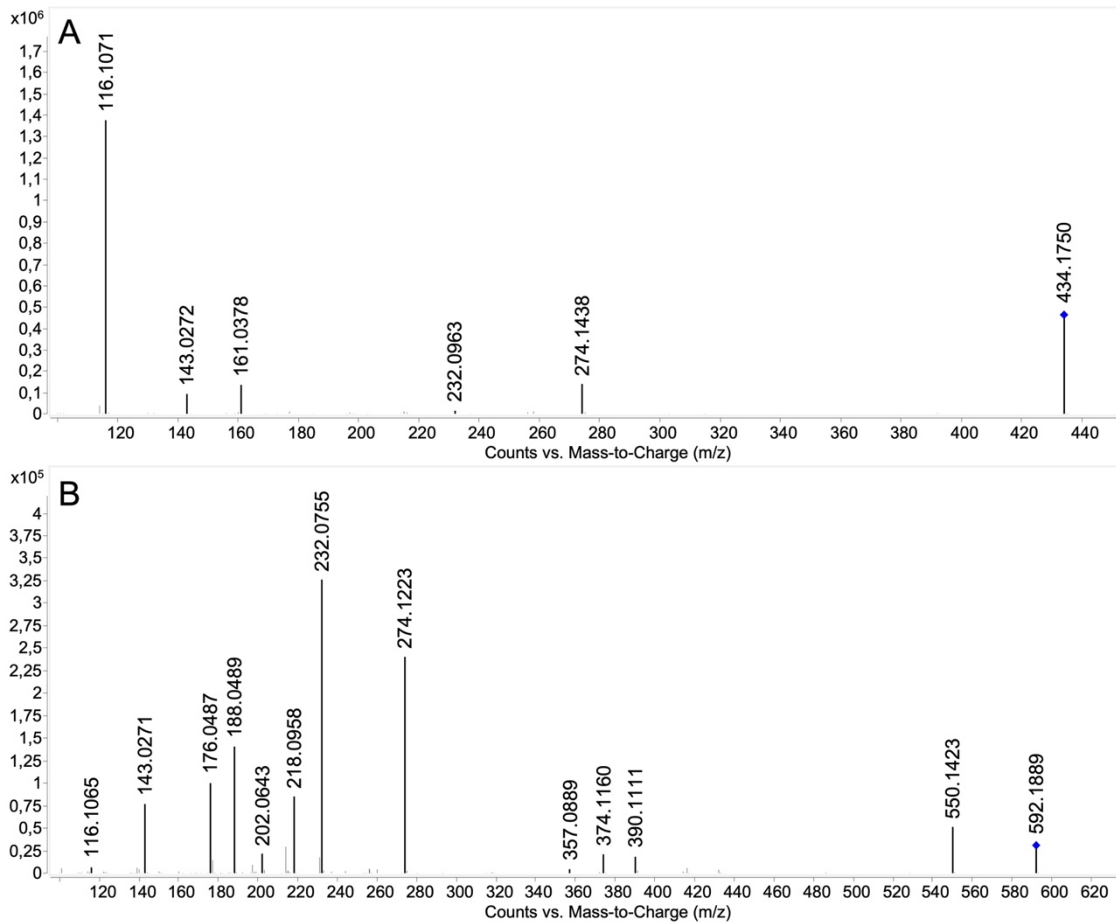


Supplementary Figure 3. Product ion spectra (LC-QTOF-MS/MS) of 4-methoxypropranolol glucuronide (A) and 7-methoxypropranolol glucuronide (B) obtained from UGT1A9 enzyme bag incubations. 4-methoxypropranolol glucuronide,  $C_{23}H_{31}NO_9$ ,  $[M+H]^+$  theor. = 466.2072,  $[M+H]^+$  exp. = 466.2061,  $\Delta m/z = -2.36$  ppm; collision energy 30 eV. 7-methoxypropranolol glucuronide,

$C_{23}H_{31}NO_9$ ,  $[M+H]^+$  theor. = 466.2072,  $[M+H]^+$  exp. = 466.2058,  $\Delta m/z = -3.00$  ppm, collision energy 30 eV.

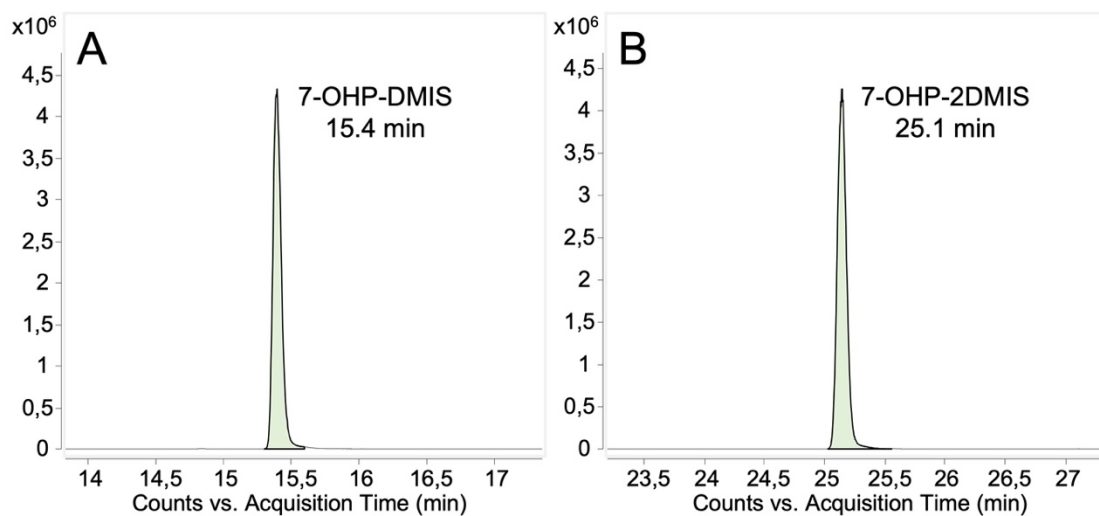


Supplementary Figure 4. Extracted ion chromatograms (LC-QTOF-MS) of DMISC derivatives of 4-hydroxypropranolol. (A) 4-OHP-DMIS, single-DMISC-derivatized 4-hydroxypropranolol,  $[M+H]^+$   $m/z$  434. (B) 4-OHP-2DMIS, double-DMISC-derivatized 4-hydroxypropranolol,  $[M+H]^+$   $m/z$  592.

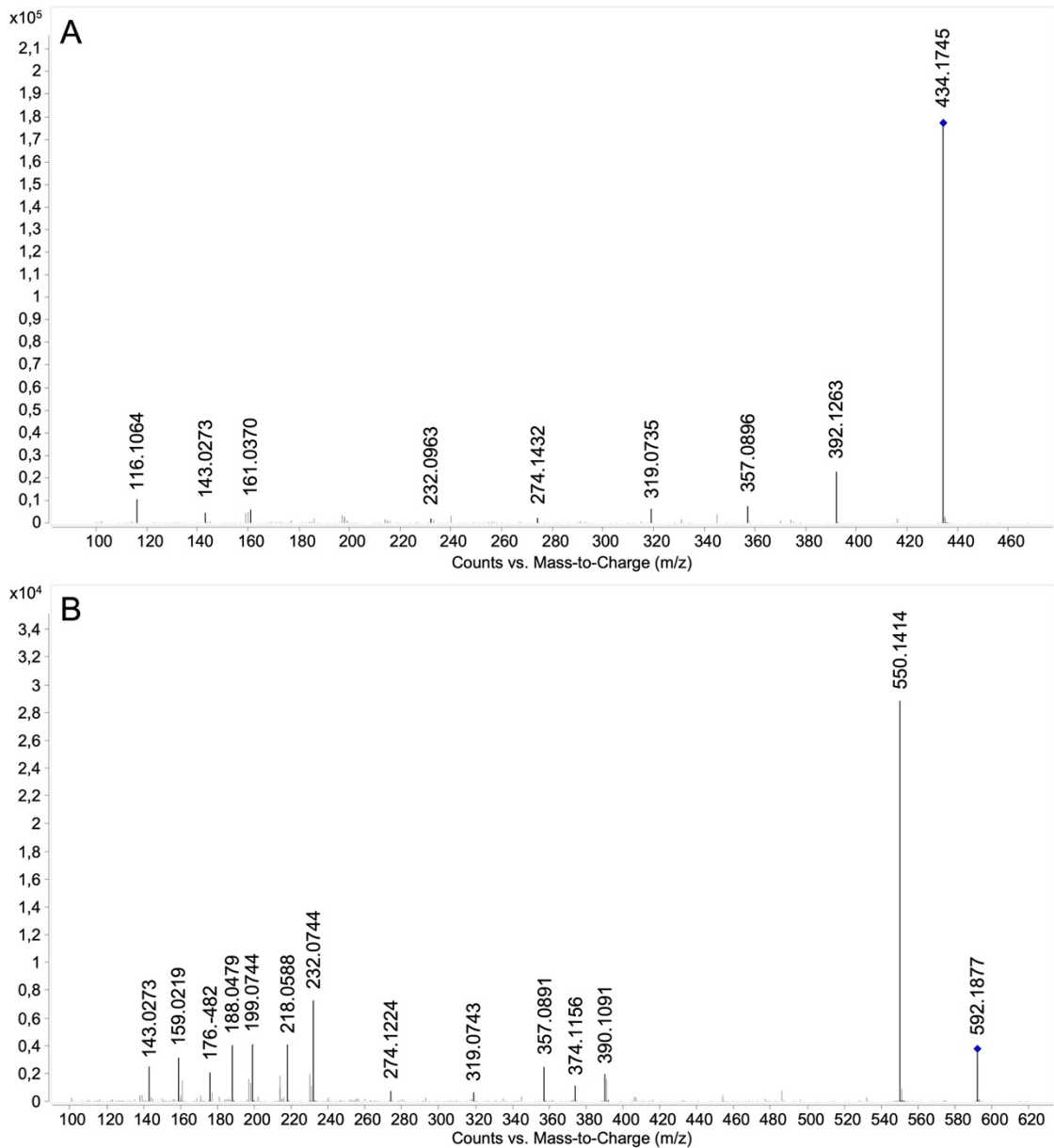


Supplementary Figure 5. Product ion spectra (LC-QTOF-MS/MS) of 4-hydroxypropranolol DMISC derivatives obtained from HLMs samples after derivatization. (A) 4-hydroxypropranolol-DMIS,  $C_{21}H_{27}N_3O_5S$ , corresponding to the peak in Supplementary Figure 4A,  $[M+H]^+$  theor. = 434.1744,  $[M+H]^+$  exp. = 434.1750,  $\Delta m/z = 1.38$  ppm, collision energy 30 eV. (B) 4-hydroxypropranolol-2DMIS,  $C_{26}H_{33}N_5O_7S_2$ , corresponding to the peak in Supplementary

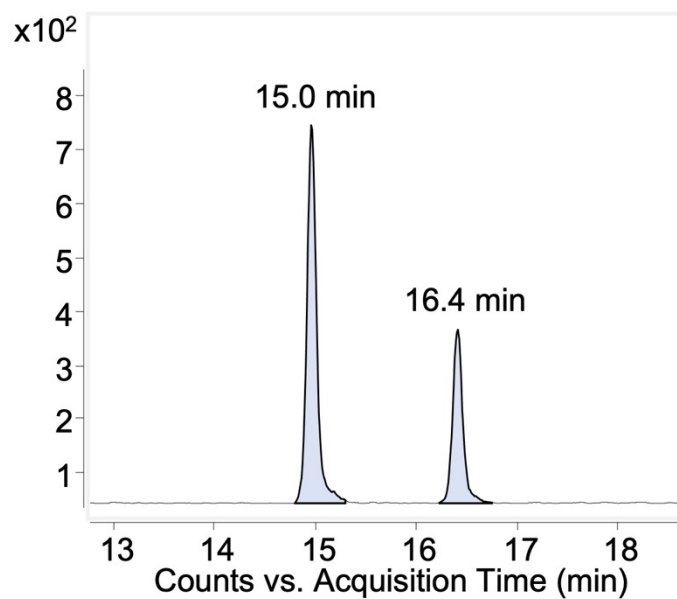
Figure 4B,  $[M+H]^+$  theor. = 592.1894,  $[M+H]^+$  exp. = 592.1889,  $\Delta m/z = -0.84$  ppm, collision energy 30 eV. DMIS, dimethylimidazole-4-sulfonyl.



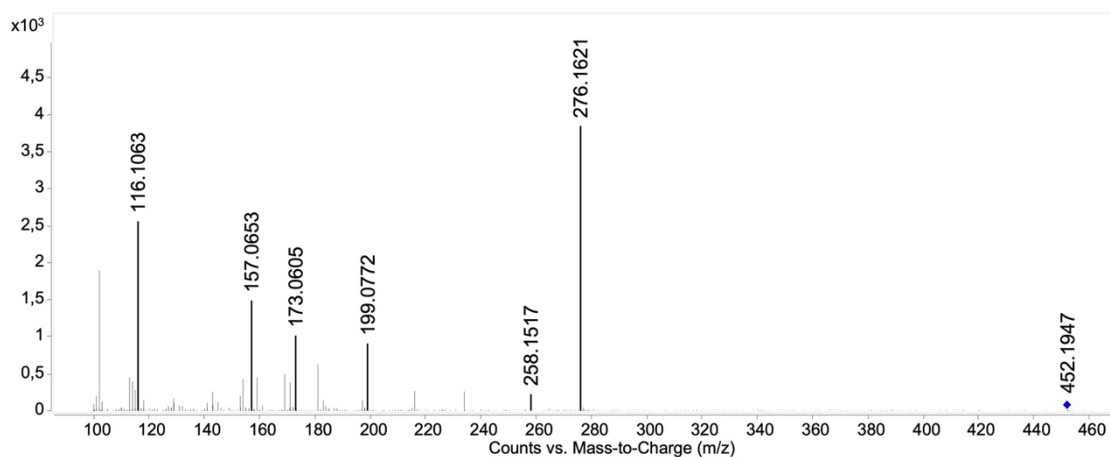
Supplementary Figure 6. Extracted ion chromatograms obtained from MS full-scan analysis (LC-QTOF-MS) of DMISC derivatives of 7-hydroxypropranolol. (A) 7-OHP-DMIS, single-DMISC-derivatized 7-hydroxypropranolol,  $[M+H]^+$  m/z 434; (B) 7-OHP-2DMIS, double-DMISC-derivatized 7-hydroxypropranolol,  $[M+H]^+$  m/z 592.



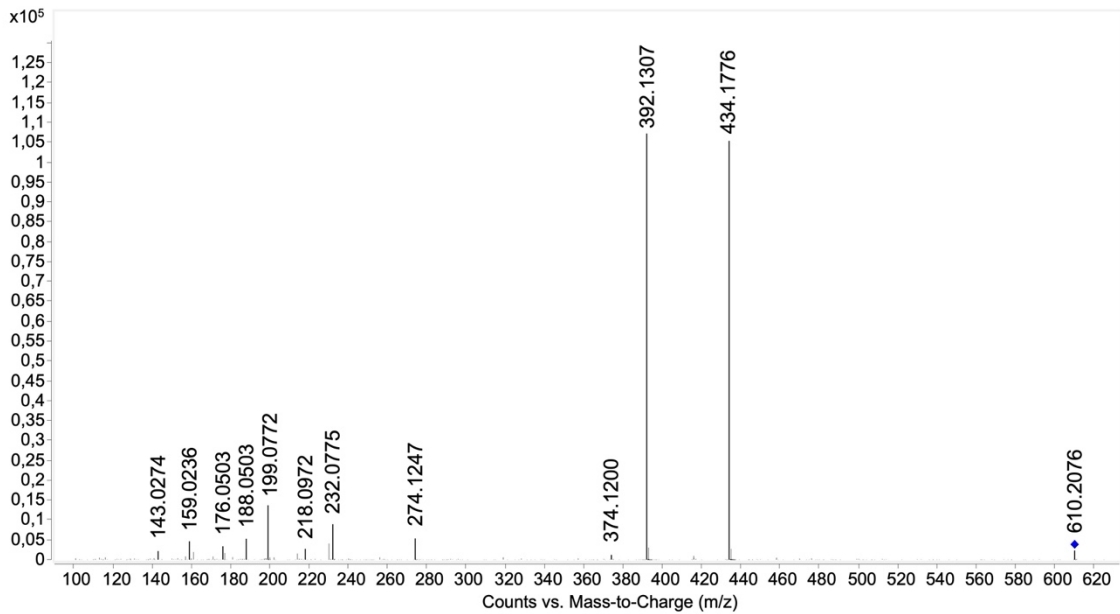
Supplementary Figure 7. Product ion spectra (LC-QTOF-MS/MS) of 7-hydroxypropranolol DMIS derivatives obtained from HLMs samples after derivatization. (A) 7-hydroxypropranolol-DMIS,  $C_{21}H_{27}N_3O_5S$ , corresponding to the peak in Supplementary Figure 6A,  $[M+H]^+$  theor. = 434.1744,  $[M+H]^+$  exp. = 434.1745,  $\Delta m/z = 0.23$  ppm, collision energy 20 eV. (B) 7-hydroxypropranolol-2DMIS,  $C_{26}H_{33}N_5O_7S_2$ , corresponding to the peak in Supplementary Figure 6B,  $[M+H]^+$  theor. = 592.1894,  $[M+H]^+$  exp. = 592.1877,  $\Delta m/z = -2.87$  ppm, collision energy 30 eV. DMIS, dimethylimidazole-4-sulfonyl.



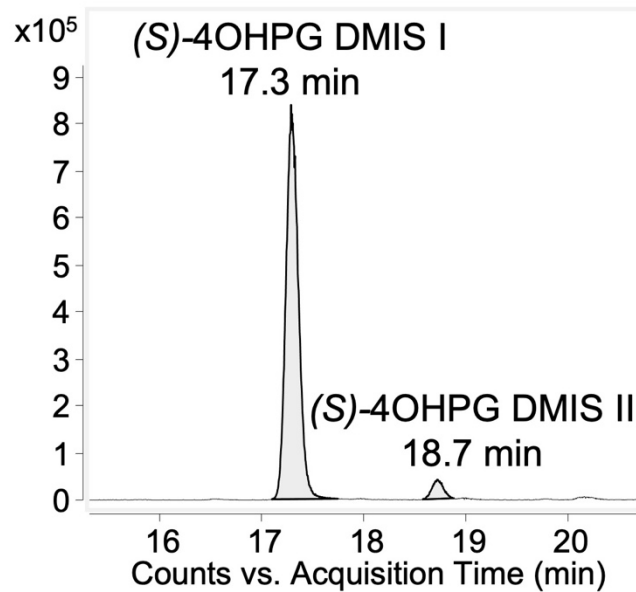
Supplementary Figure 8. Chromatograms (LC-QQQ-MS/MS) of additional 5-hydroxypropranolol glucuronides in 24-hours HLMs incubations. The displayed ion transition is  $m/z$  452→72.



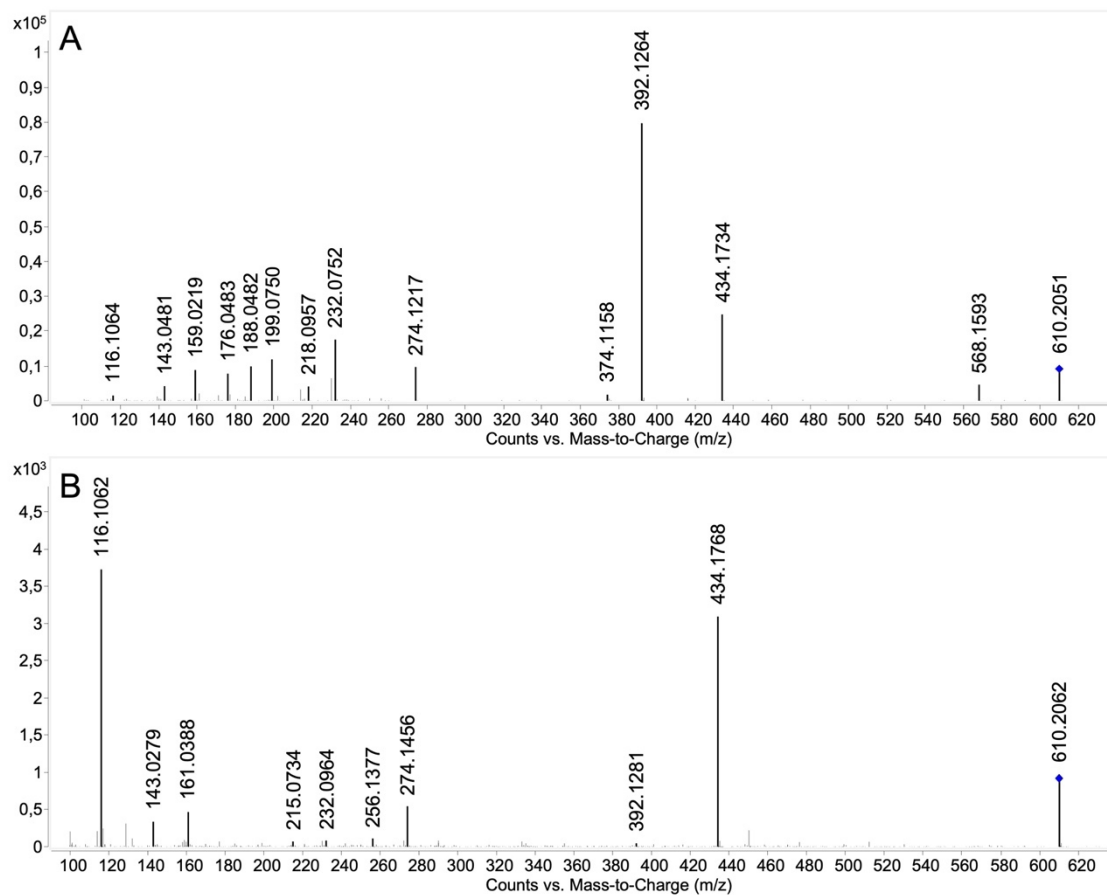
Supplementary Figure 9. Product ion spectra (LC-QTOF-MS/MS) of the additional 5-hydroxypropranolol glucuronides in 24-hours HLMs incubations.  $C_{22}H_{29}NO_9$ ,  $[M+H]^+$  theor. = 452.1915,  $[M+H]^+$  exp. = 452.1947,  $\Delta m/z = 7.08$  ppm, collision energy 40 eV.



Supplementary Figure 10. Product ion spectra of DMISC derivatives of 7-hydroxypropranolol glucuronides obtained from HLMs samples after derivatization. 7-hydroxypropranolol glucuronide DMIS,  $C_{27}H_{35}N_3O_{11}S$ ,  $[M+H]^+$  theor. = 610.2075,  $[M+H]^+$  exp. = 610.2076,  $\Delta m/z = 0.16$  ppm; collision energy, 30 eV.



Supplementary Figure 11. Extracted ion chromatogram ( $[M+H]^+$   $m/z$  610) from MS full-scan (LC-QTOF-MS) of HLMs-generated (S)-4-hydroxypropranolol glucuronides derivatized with DMISC. (S)-4OHPG DMIS I and II, DMISC derivative of (S)-4-hydroxypropranolol glucuronide I and II.



Supplementary Figure 12. Product ion spectra of DMISC derivatives of (S)-4-hydroxypropranolol glucuronides obtained from HLMs samples after derivatization. (A) corresponding to (S)-4-OHPG DMIS I in Supplementary Figure 11,  $C_{27}H_{35}N_3O_{11}S$ ,  $[M+H]^+$  theor. = 610.2075,  $[M+H]^+$  exp. = 610.2051,  $\Delta m/z = -3.93$  ppm; collision energy, 30 eV. (B) corresponding to (S)-4-OHPG DMIS II in Supplementary Figure 11,  $C_{27}H_{35}N_3O_{11}S$ ,  $[M+H]^+$  theor. = 610.2075,  $[M+H]^+$  exp. = 610.2062,  $\Delta m/z = -2.13$  ppm, collision energy, 30 eV.

## 11.2 Supplementary tables

Supplementary Table 1. The abundance of 4-,5- and 7-hydroxypropranolol glucuronides observed in urine samples. The presented peak areas were provided by transitions of the highest intensity as indicated in Figure 10.

Collected post administration (h)	(S)-4-OHPG	(R)-4-OHPG	(S)-5-OHPG	(R)-5-OHPG	(S)-7-OHPG	(R)-7-OHPG
0.7	-	-	-	-	-	-
2.4	++++	++	-	+	++	++
5.1	++++	++	-	+	++	++
7.3	++++	++	-	+	++	+++
8.2	++++	++	-	+	++	+++
9.5	++++	++	-	+	++	+++
13.3	+++++	+++	-	++	++	+++
17.6	+++++	+++	-	++	++	++++
20.6	++++	+++	-	+	+	++
23.0	++++	++	-	+	+	++
38.8	++	+	-	-	-	++
61.6	+	+	-	-	-	++
87.5	+	+	-	-	-	++
98.3	-	-	-	-	-	+
167.9	-	-	-	-	-	+

“+” for peak area < 1000; “++” for peak area 1000 – 10000; “+++” for peak area 10000 – 25000; “++++” for peak area 25000 – 40000; “+++++” for peak area > 40000, “-” not detected. (S)- or (R)-4-/5-/7-OHPG, (S)- or (R)-4-/5-/7-hydroxypropranolol glucuronide.

Supplementary Table 2. The activity of 19 human UGTs on racemic propranolol.

UGTs	(R)-PG	(S)-PG
UGT1A1	-	-
UGT1A3	-	-
UGT1A4	-	-
UGT1A5	-	-
UGT1A6	-	-
UGT1A7	++	+++
UGT1A8	-	-
UGT1A9	+++	++++
UGT1A10	++	+
UGT2A1	+++	++++
UGT2A2	-	-
UGT2A3	-	-
UGT2B4	-	-
UGT2B7	-	-
UGT2B10	-	-
UGT2B11	-	-
UGT2B15	-	-
UGT2B17	-	-
UGT2B28	-	-

“+” for peak area < 100; “++” for peak area 100–500; “+++” for peak area 500 – 2500; “++++” for peak area > 2500, “-” not detected; (R)- or (S)-PG, (R)- or (S)-propranolol glucuronide.

Supplementary Table 3. The activity of 19 UGTs on racemic 4-, 5- and 7-hydroxypropranolol.

UGTs	(S)-4-OHPG	(R)-4-OHPG	(S)-5-OHPG	(R)-5-OHPG	(S)-7-OHPG	(R)-7-OHPG
UGT1A1	-	-	+	+	+	+
UGT1A3	-	-	+	+	+	+
UGT1A4	-	-	-	-	-	-
UGT1A5	-	-	-	-	-	-
UGT1A6	-	-	-	-	+	+
UGT1A7	+++	++	++++	++++	+++++	++++
UGT1A8	++	++	++	+	+	+
UGT1A9	++	+++	++++	+++	+++++	++++
UGT1A10	-	-	+	+	+	+
UGT2A1	+	+	+++	+++	++++	++
UGT2A2	-	-	+	+	+	+
UGT2A3	-	-	-	-	-	-
UGT2B4	-	-	-	-	-	-
UGT2B7	-	-	-	-	-	-
UGT2B10	-	-	-	-	-	-
UGT2B11	-	-	-	-	-	-
UGT2B15	-	-	-	-	-	-
UGT2B17	-	-	-	-	-	-
UGT2B28	-	-	-	-	-	-

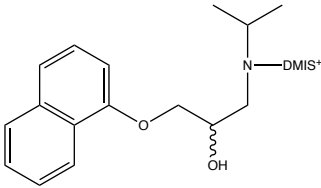
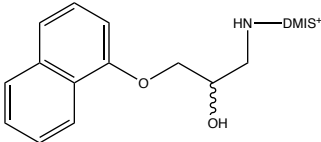
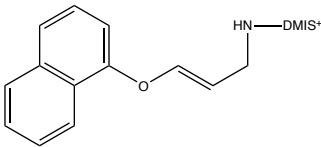
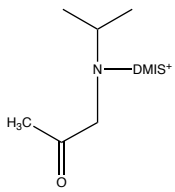
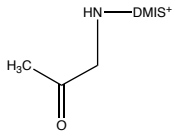
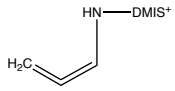
“+” for peak area < 5000; “++” for peak area 5,000 – 20,000; “+++” for peak area 20,000 – 50,000; “++++” for peak area 50,000 – 250,000; “+++++” for peak area > 250,000; “-” not detected; (S)- or (R)-4-/5-/7-OHPG, (S)- or (R)-4-/5-/7-hydroxypropranolol glucuronide.

Supplementary Table 4. The activity of UGTs on racemic 4-, 5- and 7-methoxypropranolol.

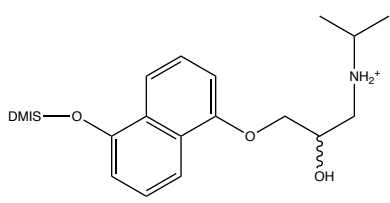
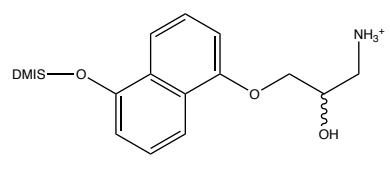
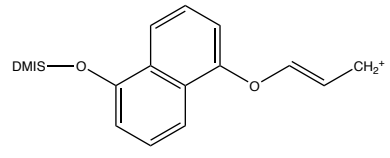
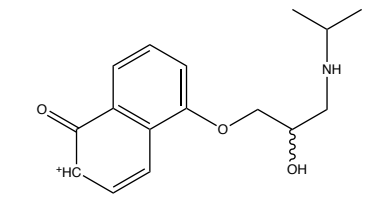
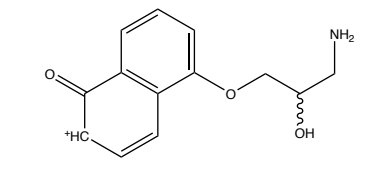
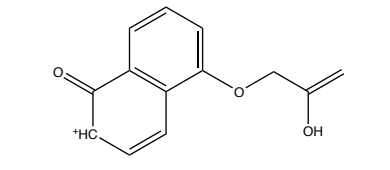
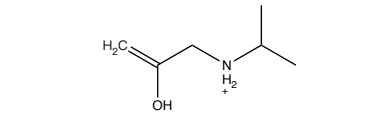
UGTs	4-MeOPG I	4-MeOPG II	5-MeOPG I	5-MeOPG II	7-MeOPG I	7-MeOPG II
UGT1A1	**	**	++	++	+	++
UGT1A3	**	**	++	++	++	++
UGT1A6	**	**	**	**	-	-
UGT1A7	-	-	+++	++++	+++	++++
UGT1A8	-	-	-	-	-	-
UGT1A9	+++	++++	+++	++++	+++	++++
UGT1A10	**	**	+++	+	++	+
UGT2A1	+++	++++	+++	++++	+++	++++
UGT2A2	**	**	-	-	-	-

“+” for peak area < 100; “++” for peak area 100 – 1,000; “+++” for peak area 1,000 – 10,000; “++++” for peak area > 10,000; “\*\*” The substrate was not tested by respective UGT; “-” not detected; 4-/5-/7-MeOPG, 4-/5-/7-methoxypropranolol glucuronide.

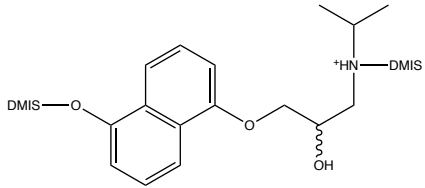
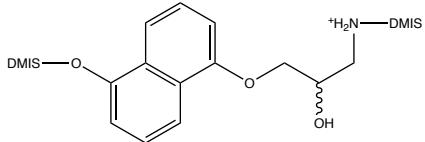
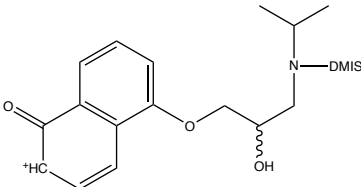
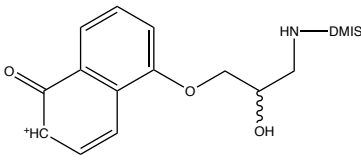
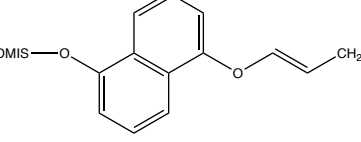
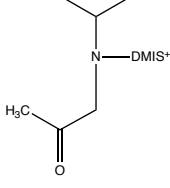
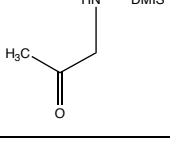
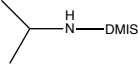
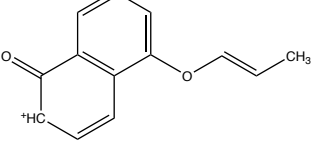
Supplementary Table 5. Postulated structures of fragments in Table 5 (P-DMIS).

Postulated fragment	Elementary composition	Postulated structure
$[M+H]^+$	$[C_{21}H_{28}N_3O_4S]^+$	
$[M+H-C_3H_6]^+$	$[C_{18}H_{22}N_3O_4S]^+$	
$[M+H-C_3H_6-H_2O]^+$	$[C_{18}H_{20}N_3O_3S]^+$	
$[M+H-C_{10}H_8O]^+$	$[C_{11}H_{20}N_3O_3S]^+$	
$[M+H-C_{10}H_8O-C_3H_6]^+$	$[C_8H_{14}N_3O_3S]^+$	
$[M+H-C_{10}H_8O-C_3H_6-H_2O]^+$	$[C_8H_{12}N_3O_2S]^+$	
$[DMIS-NCH_2+H]^+$	$[C_6H_{10}N_3O_2S]^+$	$H_2C=N-DMIS^+$
$[DMIS-NH_2+H]^+$	$[C_5H_{10}N_3O_2S]^+$	$H_2N-DMIS^+$

Supplementary Table 6. Postulated structures of fragments in Table 6 (5-OHP-DMIS).

Postulated fragment	Elementary composition	Postulated structure
$[M+H]^+$	$[C_{21}H_{28}N_3O_5S]^+$	
$[M+H-C_3H_6]^+$	$[C_{18}H_{22}N_3O_5S]^+$	
$[M+H-C_3H_9N-H_2O]^+$	$[C_{18}H_{17}N_2O_4S]^+$	
$[M+H-DMIS]^+$	$[C_{16}H_{20}NO_3]^+$	
$[M+H-DMIS-C_3H_6]^+$	$[C_{13}H_{14}NO_3]^+$	
$[M+H-DMIS-C_3H_9N]^+$	$[C_{13}H_{11}O_3]^+$	
$[M+H-DMIS-C_{10}H_8O]^+$	$[C_6H_{14}NO]^+$	

Supplementary Table 7. Postulated structures of fragments in Table 7 (5-OHP-2DMIS)

Postulated fragment	Elementary composition	Postulated structure
$[M+H]^+$	$[C_{26}H_{34}N_5O_7S_2]^+$	
$[M+H-C_3H_6]^+$	$[C_{23}H_{28}N_5O_7S_2]^+$	
$[M+H-DMIS]^+$	$[C_{21}H_{26}N_3O_5S]^+$	
$[M+H-C_3H_6-DMIS]^+$	$[C_{18}H_{20}N_3O_5S]^+$	
$[M+H-DMIS-C_3H_9N-H_2O]^+$	$[C_{18}H_{17}N_2O_4S]^+$	
$[M+H-DMIS-C_{10}H_8O]^+$	$[C_{11}H_{20}N_3O_3S]^+$	
$[M+H-DMIS-C_{10}H_8O-C_3H_6]^+$	$[C_8H_{14}N_3O_3S]^+$	
$[NH_2-(CH_3)_2-DMIS]^+$	$[C_8H_{16}N_3O_2S]^+$	
$[M+H-2DMIS-C_3H_9N-H_2O]^+$	$[C_{13}H_{11}O_2]^+$	
$[DMIS-NCH_2+H]^+$	$[C_6H_{10}N_3O_2S]^+$	$H_2C=N-DMIS^+$

Postulated fragment	Elementary composition	Postulated structure
$[\text{DMIS-NH}_2]^+$	$[\text{C}_5\text{H}_{10}\text{N}_3\text{O}_2\text{S}]^+$	$\text{H}_2\text{N}-\text{DMIS}^+$